2. STRUCTURAL EVALUATION

The structural evaluation in this addendum examines the incorporation of plutonium metal as a new payload for the PAT-1 package. The Pu metal is packed in an inner container (*T-Ampoule Assembly,*[A] Drawing 2A0261, designated the T-Ampoule) that replaces the inner container (*Can Assembly*, Drawing 1024, designated PC-1) that is carried within the TB-1 *Containment Vessel* (Drawing 1017, designed TB-1). The T-Ampoule and associated Pu metal contents packing configurations are described in Section 1.2.1, and the Pu metal contents are discussed in Section 1.2.2 of this addendum.

2.1 Description of Structural Design

This section describes the structural evaluation of the T-Ampoule and its contents and packing. The T-Ampoule and its loading configurations replace the PC-1 and its contents described in the SAR.[1] In the case of the PAT-1, (1) the aluminum honeycomb (*Spacer, Top,* Drawing 1015, designated Top Spacer) and the PC-1 stainless steel inner container is being replaced by the titanium T-Ampoule, and (2) the PuO_2 content is being replaced by plutonium metals or sample containers containing plutonium metal and composite materials. The primary purpose of this addendum is to demonstrate that the modifications to the TB-1 of replacing the PC-1 and its contents and packing with the T-Ampoule and its contents and packing do not significantly change the design, operating characteristics, or safe performance of the package so that the requirements of 10 CFR 71.19(d) are met.

The T-Ampoule is not a containment boundary, it is similar to the PC-1 in the SAR.[1] Its function is to provide a eutectic prevention barrier between the plutonium metal contents and the stainless steel (*TB-1 Containment Vessel,* Drawing 1017, designated TB-1) throughout normal and accident conditions. The PAT-1 (*Overpack, AQ,* Drawing 1002, designated AQ-1 and TB-1) with the Ti-6Al-4V Grade 5 T-Ampoule is designed to transport bulk plutonium metal in the form of hollow cylinders, as well as various shaped plutonium metal contents packed in sample containers. The plutonium metal may be in alloyed or pure form.

The Pu hollow cylinders (Electro-Refined [ER] material is analyzed, see Section 1.2.2) are cast in two weights – 831 g (6.350 cm [2.500 in.] OD, 5.801 cm [2.284 in.] ID × 8.054 cm [3.171 in.] length) and 731 g (6.350 cm [2.500 in.] OD, 5.801 cm [2.284 in.] ID × 7.087 cm [2.790 in.] length).* Two sizes of Ti-6Al-4V Grade 5 sample containers (SC-1 or SC-2) provide for two- and three-sample-container stacked configurations nested within a Ti-6Al-4V Grade 5 Inner Cradle, which is installed inside of the T-Ampoule. Pure and alloyed plutonium metal sample contents in the form of disks, cylinders, and assorted shapes can be carried, weighing a maximum of 174 g in each SC-1 or 338 g in each SC-2. For the bounding analysis of the Pu contents in SC-1 and SC-2, solid Pu cylinders of 2.23 cm (0.88 in. dia.) × 2.23 cm (0.88 in.) height and 2.79 cm (1.1 in.) dia. × 2.79 cm (1.1 in.) height were analyzed respectively. Pu/Be composite samples in the form of disks, cylinders and assorted shapes can be carried, weighing a

[A] The drawing titles are in italics and are used interchangeably with the designated names in this addendum. See Section 1.3.2 in this addendum and Chapter 9 in the SAR[1] for drawing number, title, and revision.

* These are the general dimensions provided without tolerances.

maximum of 60 g in SC-1 or SC-2. For the bounding analysis of the Pu/Be contents in the SC-1 and SC-2, solid Pu cylinders of 0.663 in. dia. × 0.663 in. height (60 g in each SC) were analyzed.

Optional Packing materials in the form of tantalum foil and copper foam are used within the sample containers to pack the Pu contents. The Pu hollow metal cylinders are wrapped with tantalum foil to prevent contamination and for packing.

See Table 2-1 for the mass limits of the Pu contents for four loading configurations, the weights of the various components within the TB-1, and the weight allowances for the packing material, assuming loading of the maximum Pu content weight for each configuration. Detailed descriptions of the T-Ampoule and sample containers are presented in Section 1 of this addendum. The AQ-1 and TB-1 are described in Chapter 1 of the PAT-1 Safety Analysis Report (SAR).[1] The maximum bounding activity of the contents is 897 Ci (3000 A_2), as discussed in Section 1.2.2 for 831 g of plutonium metal hollow cylinders (excluding Pu-241 decay).

As described in the following sections, the analysis and testing documented herein demonstrates that the T-Ampoule maintains its integrity as a eutectics prevention barrier under plutonium air transport accident conditions, thus demonstrating that the TB-1 maintains its integrity and provides containment of its contents under normal conditions of transport (NCT), hypothetical accident conditions (HAC), and plutonium air transport accident conditions.

Table 2-1. Weight of Plutonium Metal Contents and T-Ampoule and Packing for Six Loading Configurations.

Component	831 g Pu Hollow Cylinder[a] (g)	731 g Pu Hollow Cylinder[b] (g)	Three Stack SC-1, Solid Pu Cylinders (Bounding) (g)	Two Stack SC-2, Solid Pu Cylinders (Bounding) (g)	Three Stack SC-1, Composite Contents (Bounding) (g)	Two Stack SC-2, Composite Contents (Bounding) (g)
Total Weight Allowance Inside TB-1	2100	2100	2100	2100	2100	2100
Titanium Filler Ring[k]	65	65	65	65	65	65
Titanium Ampoule[k]	571	571	571	571	571	571
Sample Containers (Total Weight)[k]	NA	NA	454[c]	391[d]	454[c]	391[d]
Inner Cradle[g]	NA[h]	NA	364	356	364	356
Plutonium Contents	831	731	523[e]	676[f]	180[i]	120[i]
Maximum Weight Allowance for	633	733	123	41	466	597

Component	831 g Pu Hollow Cylinder[a] (g)	731 g Pu Hollow Cylinder[b] (g)	Three Stack SC-1, Solid Pu Cylinders (Bounding) (g)	Two Stack SC-2, Solid Pu Cylinders (Bounding) (g)	Three Stack SC-1, Composite Contents (Bounding) (g)	Two Stack SC-2, Composite Contents (Bounding) (g)
Tantalum Foil and Copper Foam Packing						

[a] Dimensions of the 831 g. Pu hollow cylinder: 6.350 cm (2.500 in.) OD, 5.801 cm (2.284 in.) ID x 8.054 cm (3.171 in.) length. The bounding dimensions for the structural analysis are 6.375 cm (2.510 in.) OD x 5.801 cm (2.274 in.) ID x 7.374 cm (2.903) in. length.

[b] Dimensions of the 731 g Pu hollow cylinder: 6.350 cm (2.500 in.) OD, 5.801 cm (2.284 in.) ID x 7.087 cm (2.790 in.) length. The bounding dimensions for the structural analysis are 6.375 cm (2.510 in.) OD x 5.776 cm (2.274 in.) ID x 6.490 cm (2.555 in.) length bounding dimensions.

[c] 3 SC-1 Sample Containers, 151 g each.

[d] 2 SC-2 Sample Containers, 196 g each.

[e] 174 g Pu content per container. A Pu metal cylinder of 2.23 cm (0.88 in). dia. x 2.23 cm (0.88 in.) height is used as the bounding configuration for the structural analysis. See Section 1 for other forms.

[f] 338 g Pu content per container. A Pu metal cylinder of 2.79 cm (1.1 in. dia.) x 2.79 cm (1.1 in.) height is used as the bounding configuration for the structural analysis. See Section 1 for other forms.

[g] Inner cradle part weights: Leg, Body, each 50.49 g; Leg, Lid, each 12.00 g; Dish, each 37.16 g; Ring, each 6.42 g, Spacer, SC-1, each 13.52 g; Spacer, SC-2, each 18.33 g. Calculated weight from SolidWorks. (http://www.solidworks.com/)

[h] Not Applicable.

[i] 60 g composite sample per container.

[j] 60 g composite sample per container.

[k] Calculated weight from ProENGINEER (http://www.ptc.com/products/proengineer/).

2.1.1 Discussion

Several tests on the PAT-1 package are prescribed in 10 CFR 71, Subpart F (from 1978); the results of these tests are described in the SAR.[1] The PAT-1 package meets the containment criteria for NCT, HAC, and plutonium air transport accident conditions. Conditions for meeting these criteria are described in the following sections:

- Section 2.6 of the SAR[1] describes the response of the PAT-1 package design to the NCT performance tests specified in 10 CFR 71.71.
- Section 2.7 of the SAR[1] describes the response of the PAT-1 package design to the HAC performance tests prescribed in 10 CFR 71.73.
- Section 2.8 of the SAR[1] describes the response of five specimen PAT-1 packages to the sequential tests prescribed in 10 CFR 71.74(a), as well as the response of a TB-1 containment vessel to the 600 psi immersion test prescribed in 10 CFR 71.74(c).

Structural calculations described in Section 2.12.2 were performed to model and benchmark the response of the PAT-1 package to end-on, side-on, and center-of-gravity-over-corner (CGOC) high-speed impact tests. These analyses were used to determine the response of the TB-1 containment vessel and T-Ampoule eutectic barrier for NCT, HAC, and plutonium air transport accident conditions.

The TB-1 was also analyzed under the HAC dynamic crush condition since it was not considered during the performance tests conducted for the SAR.[1] In addition, the differences in the contents from the original package lead to different internal pressures and are therefore analyzed in this addendum. These analyses were used to verify that the TB-1 is within design limits (see Sections 2.6 and 2.7).

2.1.2 Design Criteria

A general description of the PAT-1 package was provided in Chapter 1 of the SAR.[1] Additional structural design descriptions of the AQ-1 and TB-1 are provided in Chapter 2 of the SAR.[1] This section of the addendum focuses on the structural design criteria for the TB-1 in areas not addressed in the SAR[1] or affected by changes in the package. The addendum also includes structural analyses of the T-Ampoule during the air transport accident conditions to ensure that a eutectic barrier is maintained.

The design criteria for the TB-1 containment vessel for NCT and HAC are described in Section 2.1.2.1 below. The design criteria for the TB-1 for the aircraft accident conditions are that the average through-wall stresses remain elastic and the forces on the closure joint do not exceed the aggregate bolt preload force.

The design criterion for the T-Ampoule eutectic prevention barrier under NCT is that it remains fully elastic. The design criteria for the T-Ampoule eutectic prevention barrier under HAC are described in Section 2.1.2.1 below. The design criteria for the T-Ampoule eutectic prevention barrier under aircraft accident conditions are described in Section 2.1.2.2 of this addendum.

2.1.2.1 NCT and HAC

The design criterion for the T-Ampoule under HAC environments is that the eutectic prevention barrier maintains structural integrity, i.e., avoiding even the initiation of a ductile tear. This is proven by analytically demonstrating that all 580,000 finite elements representing the T-Ampoule remain within a tested stress-triaxiality-versus-equivalent-plastic-strain locus, and below an empirically-based failure criterion that would indicate initiation of ductile tearing if exceeded.

For the assessment of the stainless steel TB-1 containment vessel under the NCT and HAC, Regulatory Guides 7.6[2] and 7.8[3] and 10 CFR 71.71 and 71.73 were used to determine the appropriate allowable stress values and load combinations. Acceptance criteria for the PAT-1 package are defined in 10 CFR 71.73 for Type-B dynamic crush hypothetical accident conditions as the containment boundary remaining essentially elastic (through-thickness stresses below ASME allowables), as well as maintaining containment to a release of less than 1 A_2 in a week.

Table 2-2 summarizes the load combinations for the NCT and HAC as given in Regulatory Guide 7.8. The "Crush" condition for the HAC was added to the table based on 10 CFR 71.73. The TB-1 containment vessel was heat treated to the H1075 condition after forging, thus minimizing fabrication stresses which were not examined in the analyses. In addition, the majority of load combinations in Table 2-2 were analyzed during the testing performed for the SAR.[1] Replacement of the PC-1 with the T-Ampoule and the associated contents require additional NCT and HAC analysis of the load combinations that affect the TB-1. Checks for NCT are performed on the TB-1 to determine if the change in contents causes any internal pressure effects or

differential thermal expansion/contraction interaction with the T-Ampoule (Hot Environment and Cold Environment). For the HAC, the dynamic crush analysis is included as well as a discussion on the potential effects from thermal fire. All other load combinations for the NCT and HAC are bounded by the testing and analysis performed in support of the SAR[1] and the results of the air transport accident analyses described in Sections 2.1.2.2, 2.8, 2.12.2, and 2.12.5. Specifically, the original tests did not show any effect on the TB-1 from the 4-foot or 30-foot drops for the NCT or HAC. Since there are now different contents within the TB-1, the results of the air transport accident analyses performed for this addendum are used for comparison. In these analyses, the T-Ampoule remains intact and the TB-1 remains essentially elastic, excepting minimal localized denting from the solid metal contents. Since the impact velocity for the air transport accident of 422 ft/s is substantially greater that the 44 ft/s for the HAC and the 16 ft/s for the NCT, the HAC and NCT free-drops will not threaten the integrity of the TB-1.

Table 2-2. Load Combinations for NCT and HAC

	Applicable Initial Condition								
	Ambient Temperature[1]		Insolation		Decay Heat		Internal Pressure[2]		Fabrication Stresses[3]
	100°F	-20°F	Max[1]	Zero	Max	Zero	Max	Min	
NORMAL CONDITIONS (Analyze Separately)									
Hot environment: 100°F ambient temp.			X		X		X		X
Cold environment: -40°F ambient temp.				X		X		X	X
Increased external pressure: 20 psia		X		X		X		X	X
Minimum external pressure: 3.5 psia	X		X		X		X		X
Vibration and shock[4] (normally incident to the mode of transport)	X		X		X		X		X
		X		X		X		X	X
Free-drop: 4-foot drop	X		X		X		X		X
		X		X		X		X	X
ACCIDENT CONDITIONS (Apply sequentially)									
Free drop: 30-foot drop	X		X		X		X		X
		X		X		X		X	X
Crush:[6] 1100 lb drop from 30 ft	X		X		X		X		X
		X		X		X		X	X
Puncture: Drop onto bar	X		X		X		X		X
		X		X		X		X	X
Thermal[5]: Fire accident	X		X		X		X		X

This table is from Regulatory Guide 7.8[3]
X designates the initial conditions included for a given load combination.

[1] See Regulatory Position 1.1. For this addendum, Section 2.8.5.1 Cold Ambient Temperature Tests and Section 2.8.5.2 High Ambient Temperature Tests in the SAR[1] indicate that the PAT-1 that testing at -40°F and 130°F ambient temperature (higher than the current regulation of 100°F) would have no significant adverse effect on the PAT-1 package. The NCT, HAC, and accident conditions for air transport of plutonium were evaluated at room temperature.

[2] See Regulatory Positions 1.3 and 1.4. The MNOP gage pressure calculated in Section 2.6.1.1 of this addendum of 19.2 psig is negligible when one considers that the TB-1 withstands a pressure of 1110 psia during the accident conditions for air transport of plutonium fire test evaluated in Section 3.6.4 in the SAR[1]. Internal pressure was not included in the structural calculations of NCT, HAC, and accident conditions for air transport of plutonium in this addendum.

[3] See Regulatory Position 1.5. The T-Ampoule is machined from a block of solid titanium stock procured to PAT-1040 in this addendum. Since the T-Ampoule is machined and heat treated, there are no fabrication stresses.

[4] See Regulatory Position 2.5. The shock and vibration loads encompassing road, rail, and air transportation are negligible compared to the impact loads associated with the NCT drop test [ref: NUREG/CR-0030[15]], for which a detailed analysis showed elastic response for both the T-Ampoule and TB-1 (see Section 2.12.5.3.2 of this addendum).

[5] Evaluations should be made 30 minutes after start of fire and at postfire steady-state conditions.

[6] Sequential application of crush test described in 10 CFR 71.73(c)(2) and 10 CFR 71.55(f)(1)(ii).

Regulatory Guide 7.6 states that Section III of the ASME Boiler and Pressure Vessel (B&PV) Code[5] should be used to compute the allowable stress intensity, S_m. The TB-1 was constructed in the 1970s from PH13-8Mo stainless steel with a H1075 heat treat. This material is chemically identical to SA-705, XM-13 as specified in ASME Section II, Part A. Section II, Part A of the B&PV Code defines the yield stress (S_y) as 150 ksi (averaged between H1050 and H1100), and the ultimate or tensile stress (S_u or S_T) as 162 ksi. Note that these values are the same as specified in the Military Handbook.[6] However, in Section II, Part D, the PH13-8Mo material is not listed among materials whose allowable stress intensity is provided. Therefore, Appendix 2 of Section II, Part D was mandatory and used to establish the allowable stress intensity. Based on Appendix 2, S_m is equal to the smaller of 1/3 S_T or 2/3 S_y, establishing the allowable stress intensity, S_m, at 54 ksi.

Table 2-3 lists the primary membrane stress and the primary membrane plus bending stress for both NCT and HAC, and the primary plus secondary stress for the NCT, based on Regulatory Guide 7.6 at room temperature.

Table 2-3. Allowable Stresses for NCT and HAC Based on Regulatory Guide 7.6 (Room Temperature)

	NCT		HAC	
Primary membrane stress	S_m	54 ksi	smaller of 2.4 S_m or 0.7 S_u	113.4 ksi
Primary membrane plus bending stress	1.5 S_m	81 ksi	smaller of 3.6 S_m or S_u	162 ksi
Primary stress plus secondary stress	3 S_m	162 ksi		

The NCT and HAC conditions are not at room temperature. At an increased temperature of 114°C (238°F) (see TB-1 maximum NCT temperatures in Table 3-1 of Section 3) for the NCT, the yield and tensile strength of PH 13-8Mo is determined to be 141 and 152.3 ksi, respectively (Figure 2.6.5.1.1 of the Military Handbook, 94% of room temperature strength[6]). Based on Mandatory Appendix 2 of Section II, Part D, the allowable stress intensity is the smaller of 2/3 S_y and 1/3 S_T, or 50.8 ksi. For the HAC impact analyses at 114°C (238°F), prior to the fire, Mandatory Appendix 2 of Section II, Part D, gives the same allowable stress intensity as for NCT, 50.8 ksi. At an increased temperature of 147°C (296°F) (see TB-1 maximum HAC temperatures in Table 3-1 of Section 3) for the HAC during the fire, the yield and tensile strength of PH 13-8Mo is determined to be 137 and 147 ksi, respectively.[5] Based on Mandatory Appendix 2 of Section II, Part D, the allowable stress intensity is the smaller of 2/3 S_y and 1/3 S_T, or 49 ksi.

Table 2-4 lists the primary membrane stress and the primary membrane plus bending stress for both NCT and HAC (at both 114°C (238°F) and 147°C (296°F), and the primary plus secondary stress for the NCT, based on Mandatory Appendix 2 of Section II, Part D. These stresses will be used to assess the NCT and HAC load conditions.

Table 2-4. Allowable Stresses for NCT and HAC Based on Regulatory Guide 7.6, (Elevated Temperatures)

	NCT (114 °C)		HAC (at 114 °C, 147 °C)	
Primary membrane stress	S_m	50.8 ksi	smaller of 2.4 S_m or 0.7 S_u	106.6 ksi, 102.9 ksi
Primary membrane plus bending stress	1.5 S_m	76.2 ksi	smaller of 3.6 S_m or S_u	152.3 ksi, 147 ksi
Primary stress plus secondary stress	3 S_m	152.4 ksi		

2.1.2.2 Accident Conditions for Air Transport of Pu

The TB-1 was shown in the SAR[1] aircraft impact tests to remain elastic and to maintain containment to a release of less than 1 A_2 in a week. With similar mass contents, similar TB-1 response would be expected, excepting the possibility of minor localized denting due to more dense contents (solid Pu vs. oxide powder). Since there are no stress limits required for the containment vessel during 10 CFR 71.74 air transport accidents (only < A_2/week release rate), demonstrating the avoidance of yielding was conservatively set as the primary goal. Von Mises stress (distortion-energy theory) predicts yielding with the greatest accuracy for all stress states, and thus this stress was conservatively compared against the stress intensity limits for surface transport (10 CFR-71.73) shown in Table 2-4. An acceptance criterion of "below through-thickness yielding" was used to demonstrate similar TB-1 behavior as in the original regulatory testing. This also means zero plasticity in the seal area of the TB-1, ensuring similar containment requirements of < A_2/week release rate performance of the containment vessel.

For the evaluation of the T-Ampoule eutectic prevention barrier in the PAT-1 package subjected to the requirements of 10 CFR 71.74 (Accident conditions for air transport of plutonium), two strain-based criteria are used to ensure that its structural integrity is maintained. The first is a locus in stress triaxiality–equivalent strain space developed from impact tests conducted using

the Sandia National Laboratories (SNL) 18" horizontal actuator, along with a finite element model of these tests. The impact tests are described in Section 2.12.3, along with the detailed development of the strain locus for the titanium material. The second is an empirically-based failure criterion in the form of an evolution integral in plastic strain modified by the stress state called, Tearing Parameter, which is described in Sections 2.12.3.2 and 2.12.3.7.

Although the tested strain locus encompasses most of the stress triaxiality—equivalent plastic strain space needed for the SAR Addendum analyses, velocity limits at the test facility required the use of a second, complimentary criterion to demonstrate that the T-Ampoule integrity would be maintained throughout all regulatory accident environments. Tearing Parameter is a true analytical failure criterion, which is based on material tensile tests to failure, and is valid over the entire range of stress triaxialities. The two strain-based integrity criteria are complimentary in that the two combined provide additional confidence that even the initiation of a ductile tear will be avoided, and thus T-Ampoule structural integrity will be maintained.

A plot of the strain locus is shown in Figure 2-1. It should be noted that this is not a failure locus, since no cracks were formed in the test. However, it does represent regions in strain space where failure does not occur; therefore, the container is safe. In this sense, the data from the component analyses (see Section 2.12.5) can be compared with the locus in Figure 2-1, and a safety margin based on the strain generated in the test can be calculated. For elements exceeding the tested strain locus, Tearing Parameter is integrated over the plastic strain, and is compared to the critical Tearing Parameter value for the Ti-6Al-4V to determine a safety margin.

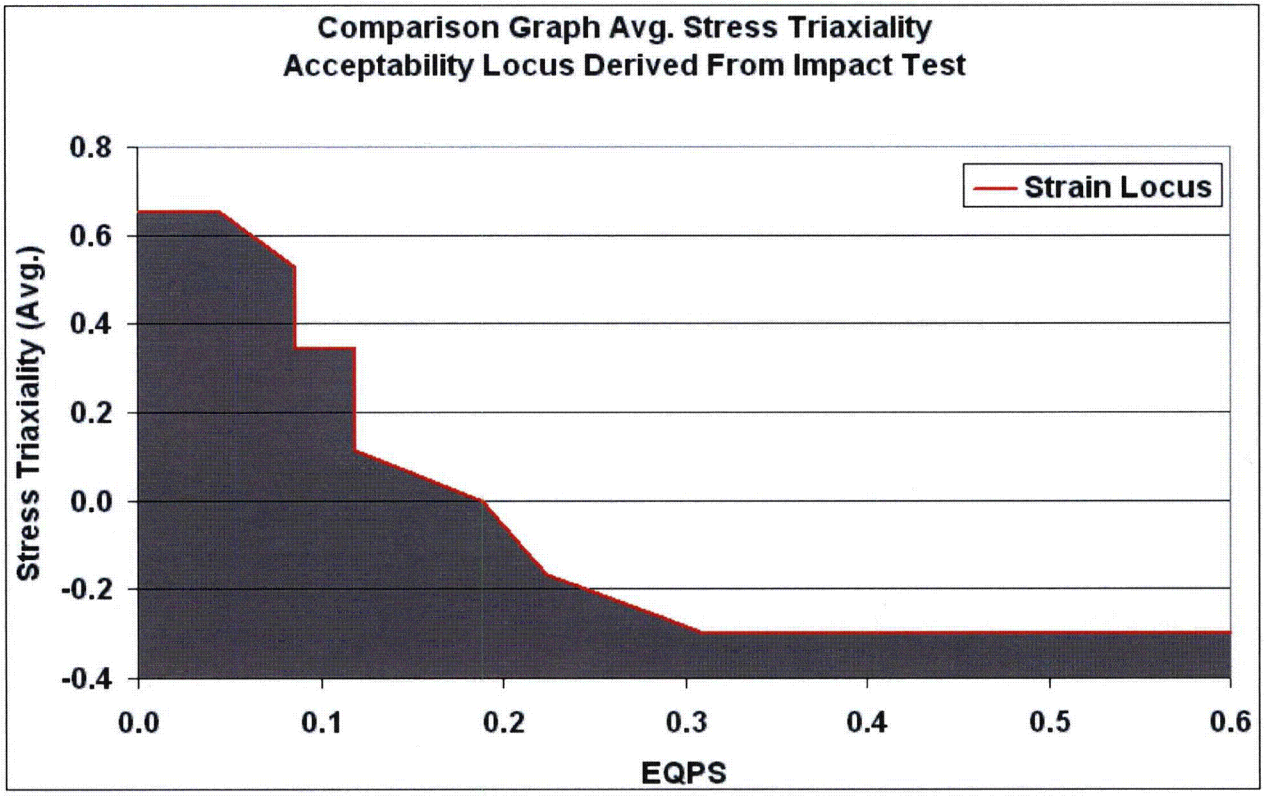

Figure 2-1. Locus in Equivalent Plastic Strain–Stress Triaxiality Space Developed from Titanium Impact Test

2.1.3 Weights and Centers of Gravity

The approximate weights of the three basic components of the PAT-1 package for this addendum are shown in Table 2-5.

Table 2-5. Approximate Weights of PAT-1 Package Components

Component	Weight (kg)	Weight (lb)
AQ-1 Overpack	206[a]	454[a]
TB-1 Containment Vessel[c]	16.8	37
T-Ampoule and its Packing[b]	See Table 2-1	See Table 2-1
Pu Metal Contents[b]	See Table 2-1	See Table 2-1
Total	225	496

[a] The weight of the AQ-1 can vary due to the natural weight variation of kiln-dried redwood as stated in Section 2.2 of the SAR.[1]

[b] The weights of the T-Ampoule and its packing are calculated using ProENGINEER (http://www.ptc.com/products/proengineer/) and SolidWorks (http://www.solidworks.com/) commercial drafting programs. The T-Ampoule and its contents within the TB-1 do not exceed the 2.1 kg weight of the PC-1 and its contents as shown in Section 2.2 of the SAR.[1]

[c] The weight of the TB-1 is from Section 2.2 of the SAR.[1]

The center of gravity (CG) of the PAT-1 package is located along its longitudinal centerline, approximately 20.2 inches from the bottom end (see Figure 2-2). The variation in the CG for the plutonium metal contents within the T-Ampoule and its packing for the Pu hollow cylinder to the sample containers with Pu contents and Inner Cradle is less than ±1/4 inch.

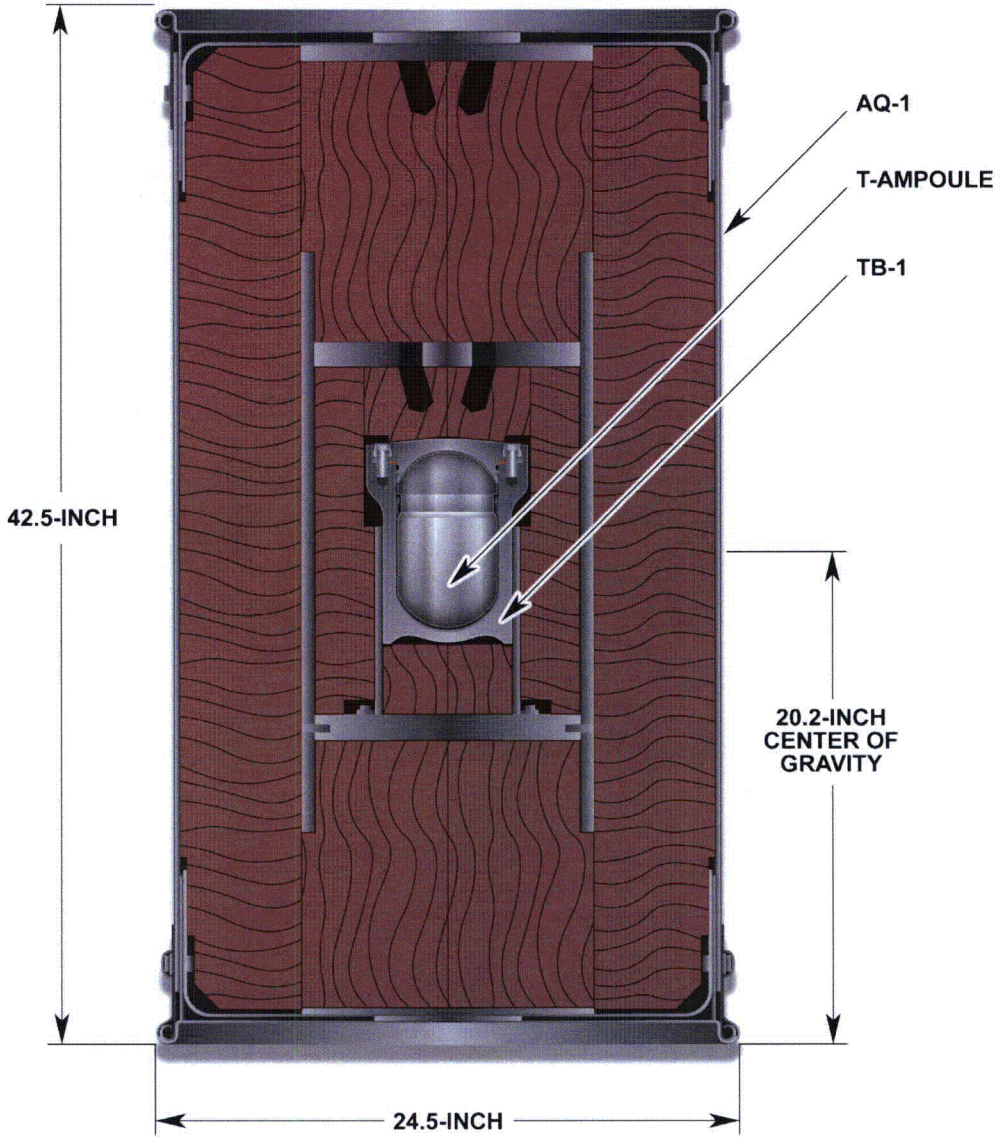

Figure 2-2. Center of Gravity for PAT-1. (Note That the Center of Gravity Varies with the Inclusion of the Support Structure and Could Vary Because of the Natural Weight Variation of the Kiln-Dried Redwood.)

2.1.4 Identification of Codes and Standards for the Package Design

The codes and standards used for design and fabrication of the AQ-1 overpack, TB-1, and PC-1 are the same as those described in the SAR.[1] The TB-1 uses design values derived from ASME B&PV Code for both NCT and HAC. For evaluation of the T-Ampoule eutectic barrier in air transport accident conditions, a strain-based criterion is used based on testing at SNL and on Bao and Wierzbicki[7, 12], as well as a stress-state modified strain-based failure criterion called Tearing Parameter[13, 14]. The T-Ampoule design was evaluated using ASME B&PV Code Section VIII Division I (See Section 2.12.8) and uses fabrication and acceptance criteria from the code as defined in PAT-1040. The titanium components within the TB-1 are procured using ASTM material standards with increased minimums for yield and ultimate strength, elongation at tensile

failure, and reduction in area at failure. For the TB-1 and AQ-1, the codes and standards are provided in Section 9 of the SAR.[1]

2.2 Materials

2.2.1 Material Properties and Specifications

A list of materials used in the finite element models for the structural evaluation of the PAT-1 package is presented in Table 2-6. The table lists the model, the component, and the component material, along with the appendix where the material's reference information, material properties, and constitutive model parameters are listed.

Table 2-6. Listing of Material for Each Component in the Finite Element Models

Model	Component	Material	Appendix
Full Models			
	Redwood Impact Material	Redwood	2.12.4.1
	Load Spreader Cylinder	Aluminum 6061	2.12.4.3
	Load Spreader Top Plate	Aluminum 7075	2.12.4.5
	Load Spreader Lower Plate	Aluminum 7075	2.12.4.5
	Copper Cylinder	Copper	2.12.4.7
	TB-1 Container	Stainless PH13-8-Mo	2.12.4.9
	TB-1 Contents	Elastic Plastic Soft	2.12.4.11
	Can Shell and Flange	Stainless 304	2.12.4.12
	T-Ampoule	Titanium 6Al-4V	2.12.4.14
	Sample Container	Titanium 6Al-4V	2.12.4.14
	Sample Container Cylinder	Plutonium (delta)	2.12.4.18
	ER Cylinders	Plutonium (alpha)	2.12.4.16
	Be Composite Cylinder	Beryllium	2.12.4.24
Impact Test Model			
	Tungsten Ballast	Tungsten	2.12.4.20
	Impact Specimen Brass	Brass UNS C36000	2.12.4.22
	Impact Specimen Titanium	Titanium 6Al-4V	2.12.4.14
	Ampoule Specimen	Titanium 6Al-4V	2.12.4.14
	Hemisphere Fixture	Stainless PH13-8-Mo	2.12.4.9

2.2.2 Chemical, Galvanic, or Other Reactions

The chemical and galvanic reaction evaluations of the AQ-1 and TB-1 are documented in Section 2.4.1 of the SAR.[1] The evaluation concluded that there was no significant potential for chemical or galvanic reactions to occur.

There is no potential for significant chemical or galvanic reactions to occur with the T-Ampoule or materials contained therein under 10 CFR 71.71, 71.73, and 71.74 conditions because containment is maintained by the TB-1 in those environments as demonstrated in Sections 2, 3, and 4 of this addendum. Within the T-Ampoule, contact is made between the plutonium metal surrounded by copper foam (optional packing) and/or tantalum foil (optional packing) and the inside surfaces of the titanium T-Ampoule or sample container (SC-1 or SC-2). These surfaces have no significant potential for corrosion since the atmosphere within the T-Ampoule and sample container(s) (if used) is the same as the glove box atmosphere in which the plutonium metal contents are handled. The standard glove box line atmosphere consists of nitrogen/argon/helium, with an oxygen content not exceeding 0.5% and a water content not exceeding 20 ppm.

If water in flooding is assumed as in the criticality analysis, there is a galvanic potential (assume flowing sea water for the galvanic analysis) between the plutonium metal content and the materials within the T-Ampoule which include beryllium (as part of the content), titanium, copper, tantalum and PH13-8Mo stainless steel material of the TB-1. There is virtually no chance for water in flooding to occur based upon the accident conditions for air transport of plutonium tests in Section 2.8 and Section 3.6 of the SAR,[1] the accident conditions for air transport of plutonium analyses in Section 2.8 of this addendum, and the hypothetical accident conditions for fissile material packages for air transport analyses in Section 3.4.5 of this addendum.

There is possible gas generation from alpha decay of plutonium which yields helium gas. The helium gas is non-reactive with the materials within the TB-1.

Evaluation of the potential for a Pu/Fe eutectic reaction is documented in Section 3.5.2 of the SAR Addendum. The eutectics evaluation of the plutonium metal contents; the titanium materials used for the T-Ampoule, Sample Container-1, Sample Container-2, and Inner Cradle; and the optional tantalum foil and copper foam packing in Section 3.5.2 concluded, by analysis of phase diagrams for all possible binary systems, that no liquid phases are expected in this system at 582°C (1080°F). Furthermore, it is anticipated that the lowest melting point phase that may form within this system is 595°C (1103°F) – the plutonium/beryllium eutectic temperature. This is 13°C (23°F) greater than the highest temperature excursion that occurs in the system. This is not a large margin but the 595°C (1103°F) value is a conservative estimate, thus the system in a transient reaching 582°C (1080°F) is still considered safe. Review of ternary phase diagrams in the literature involving components of this system supports the conclusions drawn from the binary systems, however, the ternary systems are limited and this is a much more complex system than reviewed in binary or ternary systems available in the literature.

2.2.3 Effects of Radiation on Materials

The results provided in Sections 5 and 6 of this addendum indicate that the neutron and gamma radiation from the plutonium metal contents is very low as shown below. Based on the known effects of radiation on various materials, these results indicate that the effects of radiation from the package contents on the titanium T-Ampoule shell, the elastomeric O-rings, the Inner Cradle titanium parts, and the tantalum foil or copper foam will be minimal.

Gamma-ray and neutron source strengths are provided in Table 5-3 and Table 5-4, respectively, in this addendum. For estimating flux or dose, the assumption of a point source configuration is conservative since all the neutrons/photons are concentrated at the same point and there is no intervening shielding which would reduce the flux or dose. The following formula can be used to convert the source S (neutrons/s or photons/s) to a flux (neutrons/s-cm^2 or photons/s-cm^2) or dose (rem/h):

$$\text{Dose} = K*\text{flux} = K*S/(4\pi*R^2)$$

where

K is the flux-to-dose conversion factors in Tables 5-7 and 5-8 in Section 5 of this addendum
R is the minimum distance from the Pu content to the seal

If 16 groups are used for gamma, the gamma dose calculated is 3.38E+06 rad with a 1-cm-source-to-seal separation after a period of one year. For neutrons, the neutron fluence is 4.9E+12 n/cm^2 after one year. From Figure F1, "Tolerance of elastomers to ionizing radiation," in the Handbook of Radiation Effects,[24] the range for which there is no detectable damage is 1E+06 rad to 8E+06 rad. Damage from ionizing radiation would start at 8E+06 rad. The calculated dose to the seal is within the no detectable damage range. For metals, Figure 1 on Page 654 in the Handbook of Accelerator Physics[25] shows no damage to metals at 1.0E+10 Gy or 10^{-17} for titanium in Irradiation Effects on Structural Alloys.[26] In summary, after a one-year exposure to either neutrons or gamma from the plutonium contents, there is virtually no damage to either the Viton elastomer, the titanium in the T-Ampoule, or the steel in the TB-1 containment vessel.

2.3 Fabrication and Examination

PAT-1040 "Titanium and O-ring Materials and Component Fabrication Specification" (see Section 1.3.3 in this addendum) provides for the procurement, fabrication, and examination of the T-Ampoule, Sample Container-1, Sample Container-2, Inner Cradle, and O-rings. Areas described include:

- ASTM materials specifications, minimums are specified for yield strength, ultimate tensile strength, elongation at tensile failure, reduction in area at failure
- SAE AMS O-ring specifications for material and tolerances
- Fabrication – includes requirements for quality assurance, fabrication, inspection and examination, product marking, surface finish, packaging and shipping, and documentation

2.3.1 Fabrication

The fabrication specification for the T-Ampoule and other components is provided in Section 1.3.3, "PAT-1040 Titanium and O-ring Materials and Component Fabrication Specification." Since the T-Ampoule is considered as an "Other Safety Component" of a Category I package (see NUREG/CR-3854[22]), the selected standard for the T-Ampoule is ASME Boiler and Pressure Vessel Code (Section VIII, Division 1[23]). As defined in Section 5.0 within the PAT-1040

specification, the T-Ampoule was designed (see Section 2.12.8) and will be fabricated and inspected to meet the requirements of ASME Boiler and Pressure Vessel Code (Section VIII, Division 1). ASTM standards are used for the procurement of the materials used for fabrication.

2.3.2 Examination

The examination requirements for the T-Ampoule and other components are provided in Section 1.3.3, "PAT-1040 Titanium and O-ring Materials and Component Fabrication Specification." As defined in Section 5.0 in the PAT-1040 specification, the T-Ampoule will be inspected to meet the requirements of ASME Boiler and Pressure Vessel Code (Section VIII, Division 1).

2.4 General Requirements for All Packages

2.4.1 Minimum Package Size

The PAT-1 package measures 62 cm (24 ½ in.) outside diameter (OD) by 108 cm (42 ½ in.) long.

2.4.2 Tamper-Indicating Device

A wire tamper seal is wired to the bolted connection on the lid clamping ring (*Ring, Clamp, Modified* (1006))[1*] on the AQ-1 drum closure.

2.4.3 Positive Closure

No change for the PAT-1. Positive closure of the PAT-1 is described in Section 2.4.2 of the SAR.[1]

2.5 Lifting and Tie-Down Standards for All Packages

2.5.1 Lifting Devices

No change. This analysis for the PAT-1 package is covered in Section 2.4.3 of the SAR.[1]

2.5.2 Tie-Down Devices

No change. This analysis for the PAT-1 package is covered in Section 2.4.3 of the SAR.[1]

2.6 Normal Conditions of Transport

This section evaluates the replacement of the PC-1 and its contents and associated packing with the T-Ampoule and its contents and associated packing. The T-Ampoule replacement has no effect on the NCT structural performance of the TB-1 and AQ-1 overpack as demonstrated in this section. The temperature invariance of titanium alloy, T-Ampoule material properties, is shown in Section 2.12.4.14, vibration is addressed in Section 2.6.5, and free drops from the NCT (see Section 2.12.5.3), HAC (see Section 2.12.5.6) Dynamic Crush, and 30 ft Drop (see Section 2.12.5.7).

The wall structure in the T-Ampoule did not rupture and the TB-1 remains nearly elastic (excepting minimal localized internal "denting" from contents impacts) during the 10 CFR 71.74

* The drawing title names are shown in italics. See Section 1.3.2 for engineering drawings of the components.

air transport accident impact evaluations described in Section 2.8 and Section 2.12.5.4. Since the loads imposed by the T-Ampoule contents in the 10 CFR 71.71 NCT impact test are considerably smaller, they will not threaten the integrity of the T-Ampoule or TB-1. In addition, the original NCT testing performed for the SAR[1] showed no effect on the TB-1. This was verified in Section 2.12.5.3.2 analytically for the NCT side drop, which showed no plasticity in either the T-Ampoule or the TB-1, and TB-1 through-thickness stress intensities below ASME limits in Table 2-4. The only condition examined is the potential for different thermal effects due to the change in contents (e.g., T-Ampoule). Possible deformation of the sample container Inner Cradle was investigated analytically, as well, in order to verify that the initial position of the sample containers was not changed for the HAC and air transport accident environments.

The following sections on the NCT provide a discussion of the NCT tests required by 10 CFR 71.71 and demonstrate that the package meets the acceptance criteria.

2.6.1 Heat

The following section summarizes the stresses induced in the TB-1 under the thermal conditions of NCT.

2.6.1.1 Summary of Pressures and Temperatures

The average internal surface temperature of the T-Ampoule during NCT has been found in Section 3 to be 103.3°C (218°F). This produces a maximum internal pressure in the TB-1 of 18.8 psia due to the temperature difference, with a total internal pressure of 33.9 psia if helium generation (15.1 psia, computed in Section 4) is included. Ignoring any containment by the T-Ampoule and regardless of specific contents, this pressure (33.9 psia, 233.74 kPa; 19.2 psig, 132.4 kPa) defines the maximum normal operating pressure (MNOP) for the TB-1.

2.6.1.2 Differential Thermal Expansion

Since the original testing did not observe any effect of differential thermal expansion on the TB-1, only the potential for the T-Ampoule expanding into contact with the TB-1 will be examined. Differential thermal expansion is evaluated for the NCT temperature of 103°C (218°F), which produces the highest differential thermal expansion between room temperature and the lowest (-40°C (-40°F) and the highest 103°C (218°F) NCT temperature for the TB-1. The Military Handbook[6] reports a coefficient of thermal expansion (α) for the Ti-6Al-4V used for the T-Ampoule of 5.1×10^{-6} in./in./°F in the range of temperatures from 70°F to 312°F (see also Section 2.12.4.14 in this addendum).

A conservative estimate of the maximum expansion of the T-Ampoule can be calculated by assuming the T-Ampoule is a 7.418-in.-long cylinder (the actual T-Ampoule is capped) with an outer diameter of 4.22 in. The T-Ampoule reaches a maximum temperature of 250°F (121°C) as stated in Section 3, Table 3-1. Assuming a temperature increase of 180°F (250°F – 70°F), the expansion produced equals $\alpha \Delta TL$, or 0.0068 in. in the longitudinal direction and 0.0122 in. in circumference (or 0.0039 in. in diameter). Since the gap between the T-Ampoule and the TB-1 is 0.015 in. around the entire perimeter, the expansion is conservatively estimated to be about 13% to 23% of the total gap because the TB-1 would also expand outward, allowing for more expansion of the T-Ampoule. Therefore, no stresses are induced by differential thermal expansion for NCT conditions.

2.6.1.3 Stress Calculations

Since the testing for the SAR[1] documents the adequacy of the TB-1 under pressures exceeding 34.3 psia, the Maximum Normal Operating Pressure (MNOP) for this addendum of 33.9 psia pressure possible for the NCT decay heat and helium generation will also be in compliance. A simple check of the stresses in a cylinder under 33.9 psia pressure, using the outer diameter of the cylindrical section of the TB-1 (5.35 in.) and a thickness of 0.55 in., yields pr/t = 93.4 psi (19.2 psig × 2.675 in./0.55 in.). Since this stress is considerably below the allowable stress, and because of the test results from the SAR,[1] no detailed stress calculation was performed due to thermal effects.

Although the T-Ampoule is only a eutectic barrier, it is useful to show that the stresses due to NCT decay heat and helium generation are low. Using the T-Ampoule outer diameter of 4.220 in. and a minimum thickness of 0.060 in. yields pr/t = 675.2 psi (19.2 psig × 2.11 in./0.060 in.). Since this stress is considerably low (<1 ksi), as well as being considerably below localized contact stresses from impacting contents in accident conditions (shown in subsequent sections), it can be neglected in those detailed structural analyses.

2.6.1.4 Comparison with Allowable Stresses

The first load combination listed under NCT in Table 2-2 consists of a hot environment of 100°F with maximum insolation, maximum decay heat, and maximum internal pressure. In Section 3, the average internal surface temperature obtained from the decay heat in the T-Ampoule was 103.3°C (218°F) for the analysis starting at 38°C (100°F) with maximum insolation as specified in 10 CFR 71.71. These temperatures were used to compute the MNOP at 19.2 psig (33.9 psia), which is extended out to the TB-1 by ignoring any containment by the T-Ampoule. Since the decay heat does not cause the gap between the T-Ampoule and the TB-1 to close, no stresses are induced as a result of thermal expansion due to the change in the package. A simple pr/t estimate of the stress due to the 19.2 psig internal pressure produces a stress of 93.4 psi. This is considerably below the 50,800 psi allowable stress in the TB-1 at 114°C (238°F).

2.6.2 Cold

The second load combination listed under NCT in Table 2-2 consists of a cold environment of -40°F, with no insolation, decay heat, or internal pressure. The assumption of no insolation and no decay heat is conservative since the lowest temperature would produce the large differential temperature. The MNOP gage pressure calculated in Section 2.6.1.1 of this addendum of 19.2 psig is negligible when any expansion of the T-Ampoule or TB-1 due to internal pressure is considered. During the testing for the SAR,[1] the package was cold soaked for 48 hours at –40°F. Only the thermal contraction of the TB-1 vessel into contact with the newly added T-Ampoule could impose different stresses on the TB-1 than those that occurred in the original test. As shown in Section 2.12.4.9, the coefficient of thermal expansion of the stainless steel PH13-8Mo used for the TB-1 is approximately 5.9E-6 in/in/°F. A temperature decrease from 70°F to –40°F produces a 110°F temperature reduction. Assuming the TB-1 to be a cylinder of length 8.68 in. with a 5.35 in. diameter (outer diameter of main TB-1 body) gives a reduction of length equal to $\alpha \Delta TL$, or 0.0056 in. and a decrease in circumference of approximately 0.011 in. (a decrease of 0.0035 in. in diameter). Since the gap between the T-Ampoule and the TB-1 is 0.015 in. around the entire perimeter, the contraction is conservatively estimated to be between 12 and 19% of the total gap. This does not account for the reduction in size of the T-Ampoule.

Therefore, there is no potential for stress induced in the TB-1 due to differential thermal expansion/contraction with the T-Ampoule.

2.6.3 Reduced External Pressure

The PAT-1 package was subjected to and shown capable of withstanding a reduced external pressure of less than 0.5 atmospheres (<7.35 psia) during the SAR[1] testing to show compliance with 10 CFR 71.71. The changes in this addendum will have no effect on these results.

2.6.4 Increased External Pressure

The PAT-1 package was subjected to and shown capable of withstanding an external pressure of 600 psi during the SAR[1] testing. It will therefore, be capable of withstanding the 20 psi absolute pressure required by 10 CFR 71.71. The changes in this addendum will have no effect on these results.

2.6.5 Vibration

Vibration was examined during the testing for the SAR[1] and showed no effect on the package. The shock and vibration loads encompassing road, rail, and air transportation are negligible compared to the impact loads associated with the NCT drop test,[15] for which a detailed analysis showed elastic response for both the T-Ampoule and TB-1 (see Section 2.12.5.3). The changes in this addendum will have no effect on these results.

2.6.6 Water Spray

The water spray test was conducted during the SAR[1] testing and showed no effect.

2.6.7 Free Drop

A series of free drops were conducted during the testing for the SAR.[1] The effects were determined to be "inconsequential" and the package met the acceptance standards specified in 10 CFR 71.71. However, this addendum proposes a change in contents within the TB-1. The air transport accident analyses performed with the new contents (see Section 2.8) show that the TB-1 remains essentially elastic for each of the cases examined. Since the air transport accident will be considerably more severe than the NCT 4-foot drops, the TB-1 will remain elastic for the NCT free drops supported by analyses in Section 2.12.5.3.

2.6.8 Corner Drop

Since the PAT-1 package exceeds 220 lbs, it is not required to be subjected to the corner drop.

2.6.9 Compression

This analysis is covered in Section 2.6.10 of the SAR.[1] The package was unaffected by the compression test. The changes in this addendum will have no effect on these results.

2.6.10 Penetration

This analysis is covered in Section 2.6.9 of the SAR.[1] The TB-1 was unaffected by the penetration test. The changes in this addendum will have no effect on these results.

2.7 Hypothetical Accident Conditions

This section evaluates the replacement of the PC-1 and its contents and associated packing with the T-Ampoule and its contents and associated packing. The T-Ampoule replacement has no effect on the HAC structural performance of the TB-1 and AQ-1 overpack as documented in this section.

The wall structure in the T-Ampoule does not rupture and the TB-1 remains essentially elastic during the 10 CFR 71.74 air transport accident impact evaluations described in Section 2.8 and Section 2.12.5. Since the loads imposed by the T-Ampoule contents in the 10 CFR 71.73 HAC impact test are considerably smaller, they will not threaten the integrity of the T-Ampoule or TB-1. In addition, the original HAC testing performed for the SAR[1] showed no effect on the TB-1. A 30-ft drop analysis in each of the end, side, and corner impact orientations was performed in Section 2.12.5.7 to demonstrate these assumptions and verify acceptable T-Ampoule and TB-1 response. Other conditions examined in this addendum are the potential for different thermal effects due to the change in contents (e.g., T-Ampoule) and the dynamic crush event, which was not examined in the SAR[1] testing.

The dynamic crush event was evaluated using an undamaged package, although a small quantity of overpack crush would have occurred in the 30-ft drop. This assumption is justified because less than 2% of the available redwood in each of the three linear dimensions (for end, side, and CGOC) is crushed in the 30-ft drop. For example, in the CGOC 0.684 inches of lineal diagonal redwood is crushed out of the 36 inches of diagonally available redwood on both sides of the TB-1 (even lower percentages for side and end impacts); thus at least 98% of the lineal redwood is still available for crush in the dynamic crush event. Since the overpack is thick enough and designed to absorb the energy of a 422 ft/sec impact (not just a 44 ft/sec impact, which is only 1% of the kinetic energy), it still has sufficient crush capacity to absorb the subsequent dynamic crush event after a 30 ft drop, and no additional loading would occur to the TB-1 since it remains fully elastic in both cases. Only minimal localized plasticity (0.26%) occurred in the T-Ampoule during the 30-ft side impact (none seen in the other 30 ft drops), so assuming an essentially undamaged package for the subsequent dynamic crush is justified.

The following HAC sections provide a discussion of the HAC tests required by 10 CFR 71.73 and demonstrates that the package meets the acceptance criteria.

2.7.1 Free Drop

Based on the series of analyses performed for the high-speed aircraft impact which showed that the TB-1 remains essentially elastic under that more severe condition, and that the testing for the SAR[1] showed no damage to the TB-1, only three 30-ft drop analyses were performed for this addendum: a side, end, and CG-over-corner drop. The contents for each case were chosen to have the likely highest stresses and/or strains based on extensive aircraft impact analyses.

2.7.1.1 End Drop

One end drop analysis is examined: a lid-end impact with an angled 831 g plutonium metal hollow cylinder.

2.7.1.2 Side Drop

One side drop analyses is examined: a two-sample-container 45-degree-rotated side impact.

2.7.1.3 Corner Drop

One corner drop analyses is examined: a CG-over-corner impact with a straight 831 g plutonium metal hollow cylinder.

2.7.1.4 Oblique Drops

No oblique drop analyses are examined.

2.7.1.5 Summary of Results

In order to verify package response with the different contents from the original SAR,[1] one end, side, and corner drop analysis was performed. As shown in Section 2.12.5.7, TB-1 through-thickness stress intensities remained below allowables in Table 2-4 and the containment vessel response was elastic (excepting small localized outer surface points where contact modeling artifacts exist). The seal and closure area of the TB-1 also remained fully elastic (like the test results from the SAR[1]), so the vessel maintained containment to a release of less than 1 A_2 in a week. The T-Ampoule had only the smallest of plasticity at points where the plutonium metal hollow cylinder impacted it, and thus its seal and structural integrity as a eutectic barrier were maintained.

2.7.2 Crush

The dynamic crush load combination was examined because the PAT-1 overall density fell below 62.4 lb/ft^3 at approximately 50.8 lb/ft^3, and the overall mass of approximately 500 lb fell below 1100 lb (10 CFR 71.73). Therefore, the full model of the PAT-1 (see Figure 2-7 of Section 2.12.2) was subjected to the drop of an 1100 lb steel plate from a height of 30 ft. The PAT-1 was placed in the side position and resting on an unyielding surface. The side position has the least quantity of redwood between the TB-1 and the steel impacting plate, however end and CG-over-corner cases were also analyzed. The 40 in. × 40 in. × 2.4 in. steel plate was oriented in a flat position when dropped, impacting the PAT-1 at 528 in./s. The 831 g and 731 g plutonium metal hollow cylinders (straight and angled), as well as 2 and 3 sample container contents analysis cases were examined in the dynamic crush environment. These analyses are summarized in Section 2.12.5, Subsections 2.12.5.6. The contents models were constructed by conservatively ignoring the optional tantalum foil and copper foam packing and placing the cylinder and sample containers at the bottom of the T-Ampoule (when placed in a side orientation). For the plutonium metal hollow cylinders contents, as well as the sample containers contents dynamic crush analyses, the maximum observed through-thickness stress intensity was less than 23.5 ksi at any time during the event, which is far below the allowable through-thickness primary membrane stress of 106.6 ksi at 238°F (114°C).

The analyses were performed on an undamaged package although the free drop is required to precede the crush. This is justified due to only minor denting of the outer drum observed during the 30-foot free drop testing for the SAR.[1] In addition, the high-speed aircraft accident analyses described in Section 2.12.5 show that the TB-1 remains elastic except for localized deformations in much more severe impacts. Therefore, no damage will occur to the TB-1 during the free drop,

which further demonstrates the acceptability of analyzing the crush with an undamaged package. This is supported by the free drop analyses summarized in Section 2.12.5.7.

2.7.3 Puncture

The original test produced only a minor imprint on the outer drum of the AQ-1; there was no effect on the TB-1.

2.7.4 Thermal

The following section summarizes the stresses induced in the TB-1 under the thermal conditions of HAC.

2.7.4.1 Summary of Pressures and Temperatures

The average internal surface temperature of the T-Ampoule during HAC was found to be 136°C (276°F) as documented in Section 3. As calculated in Section 4, the combination of temperature increase and helium generation produces a maximum internal pressure in the TB-1 for HAC of 36.8 psia.

2.7.4.2 Differential Thermal Expansion

Since the original testing did not observe any effect of differential thermal expansion on the TB-1, only the potential for the T-Ampoule expanding into contact with the TB-1 will be examined. The Military Handbook[6] reports a coefficient of thermal expansion (α) for the Ti-6Al-4V used for the T-Ampoule of 5.1×10^{-6} in./in./°F in the range of temperatures for the HAC.

A conservative estimate of the maximum expansion of the T-Ampoule can be calculated by assuming the T-Ampoule is a 7.418-in.-long cylinder (the actual T-Ampoule is capped) with a diameter of 4.22 in. The T-Ampoule reaches a maximum temperature of 308°F (153°C) as stated in Section 3. Assuming a temperature increase of 238°F (308°F – 70°F), the expansion produced equals $\alpha\Delta TL$, or 0.0090 in. in the longitudinal direction and 0.0161 in. in circumference (or 0.0051 in. in diameter). Since the gap between the T-Ampoule and the TB-1 is 0.015 in. around the entire perimeter, the expansion is conservatively estimated to be about 17% to 30% of the total gap because the TB-1 would also expand outward, allowing for more expansion of the T-Ampoule. Therefore, no stresses are induced by differential thermal expansion for HAC conditions.

2.7.4.3 Stress Calculations

Since the testing for the SAR[1] showed the adequacy of the TB-1 under pressures exceeding 34.2 psig, the 36.8 psia pressure possible for the HAC thermal event will also be in compliance. A simple check of the stresses in a cylinder under 36.8 psia pressure, using the outer diameter or the cylindrical section of the TB-1 (5.35 in.) and a thickness of 0.55 in., yields pr/t = 107.5 psi (22.1 psig × 2.675 in./0.55 in.). Since this stress is considerably below the allowable stress, and because of the test results from the SAR,[1] no detailed stress calculation was performed.

2.7.4.4 Comparison with Allowable Stresses

The thermal fire load combination listed under HAC in Table 2-2 consists of the fire conditions examined in Section 3 with maximum insolation, maximum decay heat, and maximum internal pressure. In Section 3, the average internal surface temperature obtained in the T-Ampoule was

136 °C (277 °F) for the analysis. The internal pressure in the TB-1 increased from the MNOP value of 34.0 psia to 36.8 psig during the fire (ignoring containment by the T-Ampoule). The maximum internal pressure during the fire therefore induces a primary membrane stress of 107.5 psi. Since the decay heat and fire do not cause the gap between the T-Ampoule and the TB-1 to cause compression in the T-Ampoule, no stresses are induced as the result of thermal expansion. Therefore, the total primary membrane stresses induced by the fire load combination for the HAC is 107.5 psi, far below the allowable membrane stress of 102,900 psi at 147°C (296°F).

2.7.5 Immersion – Fissile Material

The TB-1 remained sealed during the immersion test (see Section 2.7.5 of the SAR[1]).

2.7.6 Immersion – All Packages

The TB-1 remained sealed during the immersion test (see Section 2.8.3 of the SAR[1]).

2.7.7 Deep Water Immersion Test (for Type B Packages Containing More than 10^5 A_2)

This test does not apply for Type B packages containing less than 10^5 A_2.

2.7.8 Summary of Damage

Since no damage was observed in the TB-1 during the original 30-foot free drop conducted for the SAR[1] and since the high-speed aircraft accident examined in Section 2.8 shows the TB-1 remaining essentially elastic (excepting minimal localized denting from solid metal contents) under those conditions, only a few free drop analyses were conducted to verify the fully-elastic condition of the TB-1, and to assess overpack deformation before dynamic crush. The dynamic crush event was not examined during the SAR[1] testing and was therefore examined here, in Sections 2.8.4 and 2.12.5.6. The numerous cases examined included side, end, and CG-over-corner impacts with two sizes and orientations of plutonium metal hollow cylinders, as well as 2 and 3 sample container sets of contents. The maximum dynamic crush stresses observed in the TB-1 were those resulting from local impacts of the contents on the T-Ampoule and then to the TB-1. These stresses are not primary membrane stresses, but are conservatively compared with those allowables. Although some localized high stresses exist on the outer TB-1 surface due to minor contact modeling artifacts, neither peak internal denting stresses from impacts of the contents nor peak through-thickness stresses in the containment vessel (all less than 40 ksi) do not approach the allowable 106.6 ksi from Table 2-4.

For the dynamic crush plutonium metal hollow cylinder contents, as well as the sample container contents analyses, the maximum observed through-thickness stress intensity was less than 23.5 ksi at any time during the event which is far below the allowable through-thickness primary membrane stress of 106.6 ksi at 238°F (114°C). The peak TB-1 stress magnitudes (localized, not through-thickness) were higher, but were either due to localized contents impacts or due to small contact issues at the outer corners of the TB-1, and in no way threaten the integrity of the containment boundary.

No examination of the puncture was performed because no damage was observed during the original test. For the fire test, the average temperature of the TB-1 during HAC was found to be

136°C (276°F) as determined in Section 3.4.3. This produces a maximum internal pressure in the TB-1 of 22.1 psig as computed in Section 4.3, ignoring any containment by the T-Ampoule. Using a simple *pr/t* estimate of the stresses in the TB-1, the internal pressure due to the fire induces a primary membrane stress of 107.5 psi. This is far below the allowable membrane stress of 102,900 psi at 153°C (308°F). It was also demonstrated that no stresses will be induced in the TB-1 as the result of differential thermal expansion with the T-Ampoule. Finally, the SAR[1] demonstrated that the TB-1 will not be susceptible to the immersion tests required for HAC. Overall, no damage will be experienced by the TB-1 during the HAC conditions outlined in 10 CFR 71.73. The TB-1 maintained containment during the original testing and will continue to do so here.

2.8 Accident Conditions for Air Transport of Plutonium

2.8.1 Discussion

This section discusses the analyses conducted on the PAT-1 package subjected to the requirements of 10 CFR 71.74 (Accident conditions for air transport of plutonium[4]). The analyses were performed using the SNL-developed, nonlinear finite element code, PRONTO-3D.[10] PRONTO-3D is a structural mechanics code developed specifically for impact analysis. It uses an explicit time-integration algorithm for solving equations of motion and accurately calculating highly nonlinear deformations, including automatically determining buckling response. PRONTO has been used successfully at Sandia National Laboratories for many years to accurately model impact and large-deformation solid mechanics problems.[13, 14, 17, 18, 19, 20]

The primary purpose of these analyses is to show that the inner container, the T-Ampoule, does not rupture during the air transport accident condition. The complete analyses consist of six separate sets of analyses, as shown in the flowchart in Figure 2-3. The first sets of analyses are of the full package assembly (see Section 2.12.2, Full Model Validation Analysis, in this addendum). These consist of a full package model, high-speed impact analysis to simulate the requirements of 10 CFR 71.74, as well as a full package analysis of the low-velocity NCT free drop for determining the positioning of the internals.

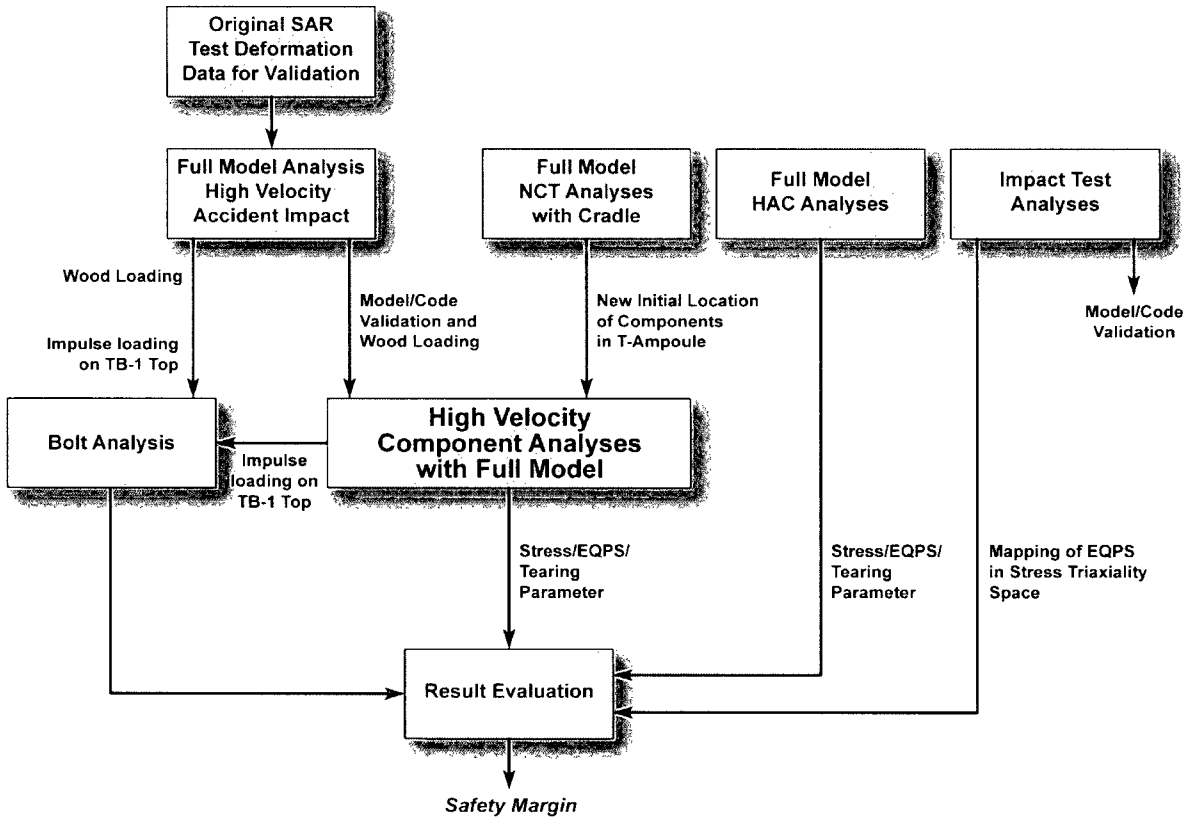

Figure 2-3. Flowchart of PAT-1 Analyses

The original package certification was performed by testing the PAT-1 package assembly. During these tests, neither accelerometers nor strain gages were placed on the package. Therefore, elastic strains and deceleration impulses of the test package are not known. Redwood overpack gross deformations were measured and photographed, and this deformation data from the original certification tests was used to tune the redwood constitutive properties and finally validate the high-speed impact model. This overpack performance evaluation was done with a simplified model of the original PuO_2 powder and at the higher impact velocity of the actual test (445 ft/sec) (see Section 2.12.2.3, Original Certification Test Analysis with the Validation Model, in this addendum).

A "most detailed" model of the package and its various solid metal contents (including the rolled 304 SS outer skin lids on each end, the T-Ampoule, cradle, and sample containers) was used in NCT 4-ft. drop impacts to verify that the Inner Cradle remains essentially elastic, so that position of the sample containers can be verified for subsequent HAC and high speed (air transport) impact analyses (see Section 2.12.2.7, Full Model NCT and HAC, in this addendum). This "most detailed" finite element model was also used for HAC dynamic crush impact analyses, since the outer skin lid deformation provides significant energy absorption in this relatively low-energy event. A slightly less detailed model (no rolled lids on each end of the 304 SS overpack skin) was used for the high-velocity impact analyses where virtually all of the energy absorption occurs in the redwood overpack. The primary outputs from the high-velocity impact analyses are stresses and plastic strains in the T-Ampoule wall and the TB-1. These outputs will be used

to evaluate the integrity of the T-Ampoule and the TB-1. TB-1 wall stress outputs in the HAC dynamic crush cases are used to compare to through-thickness ASME stress allowables, verifying the primary containment boundary's integrity in 10 CFR 71.73 environments.

A series of impact tests (see Section 2.12.3, Impact Test and Material Failure Criterion, in the addendum) were also conducted on the TB-1 component materials.[11] Analysis of these tests served two purposes: (1) to provide additional benchmarking and validation for the analyses and for the finite element code, and (2) to provide data for developing a strain-based locus in stress triaxiality and equivalent strain space. These data, along with the results from the high-velocity impact analyses, are used in the result evaluation step to determine a safety margin on the strength of the T-Ampoule wall. Although the impact tests and full package impact analyses were conducted using room-temperature materials, this is deemed a reasonable approximation because of the constant value of the elongation of titanium shown in Figure 2-60 and the small change in yield strength shown in Figure 2-59 over a temperature range of –20°F to 200°F.

The final analysis (see Section 2.8.5, Bolt Analysis, Section 2.12.6 Bolt Analysis, and Figure 2-506 is a bolt analysis performed on the TB-1 closure bolts. Using the impulse loading determined in the high-velocity TB-1 end impact analyses, along with the loading from the original full model (validation) analyses, an analytical calculation is performed to determine the margin of safety in the TB-1 lid bolts.

2.8.2 Full Package Validation Model

Analyses of the original PAT-1 package certification tests were performed to validate the redwood overpack constitutive model during the high-speed aircraft accident test condition (10 CFR 71.74). A full description of the model and results are presented in Section 2.12.2, Full Model Validation Analyses, in this addendum. The same overpack model is then combined with more detailed models of the new solid metal contents and used in NCT, HAC, and high velocity impact analyses to determine the effect of the internal components on the integrity of the titanium T-Ampoule, which acts as a eutectic barrier between the contents and the stainless-steel TB-1 vessel.

2.8.3 Impact Test and Material Failure

In support of the PAT-1 SAR[1] analysis, a series of impact tests were conducted using the SNL 18" horizontal actuator[10] and the DT-45 drop table.[21] These tests had two main purposes: (1) to provide data for validating the finite element model, and (2) to provide data for developing a strain-based failure locus. A brief summary of the impact tests is given in Section 2.12.3, Impact Test and Material Failure Criterion, in this addendum, along with details of the finite element model used for code validation.

Using the finite element model and the data from the titanium impact tests, a strain locus in stress-triaxiality–equivalent strain space was developed for the titanium material. The resulting locus is shown in Figure 2-4; the development of these curves is presented in Section 2.12.3.3. The curves were developed with data from the titanium impact or and the titanium cup (simulated T-Ampoule). The curves represent highly strained regions of the test specimens, showing their loading path and stress states. It should be noted that this is not a failure locus, since no cracks were formed in the test. The only curve that was taken to failure is the tensile

test specimen, which had a failure strain of 62%. In this sense, the highly strained regions of the T-Ampoule in the high velocity impact analyses (see Section 2.12.5) can be compared with the locus in Figure 2-4, and a safety margin based on comparing the strains generated in the test specimen to the strains generated in the submodel finite element analysis can be calculated based on its location in the locus. For elements exceeding the tested strain locus, a Tearing Parameter is integrated over the plastic strain, and is compared to the critical Tearing Parameter value for the Ti-6Al-4V to determine a safety margin.

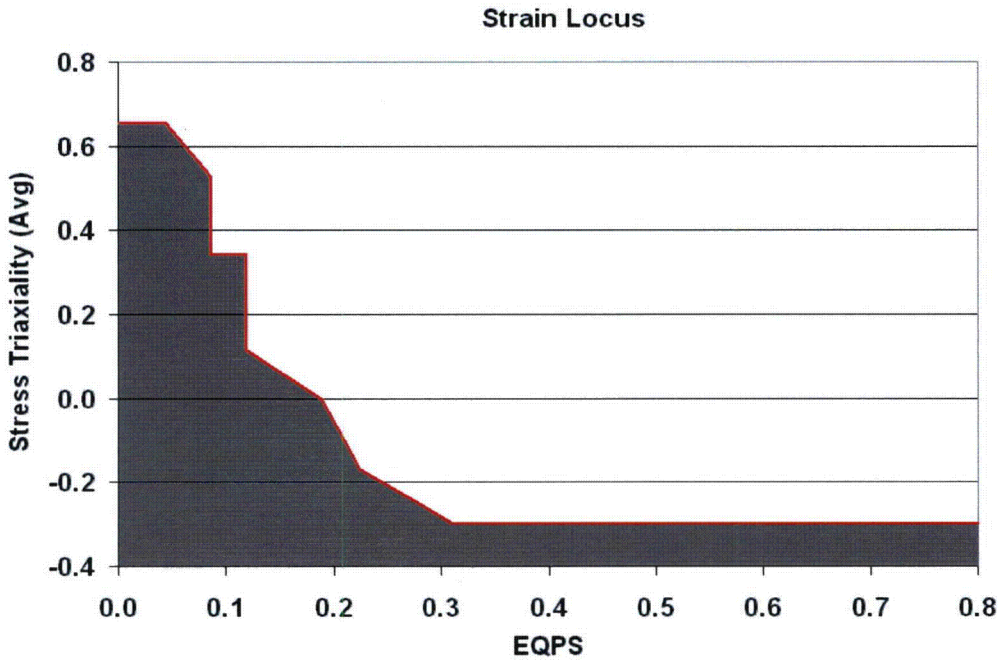

Figure 2-4. Strain Locus Developed from Titanium Experiment and Finite Element Model

2.8.4 NCT, HAC, and High Velocity Impact Analyses

Detailed impact analyses of the PAT-1 package and its components were conducted to determine the response of the TB-1 and T-Ampoule to internal impacts from the contents, as well as external compressive and bending loads from the redwood overpack. As discussed in Section 2.1, the components within the titanium T-Ampoule consist of either cast plutonium metal hollow cylinders with a mass of 831 g or 731 g, or titanium sample containers containing plutonium material (or a Pu/Be composite). A full description of the detailed package models and results are presented in Section 2.12.5, Component Analyses Using Complete Model, in this addendum. Numerous impact cases were analyzed: end, side, CG-over-corner impacts for plutonium metal hollow cylinders, solid delta-phase Pu cylinders inside sample containers, and smaller Pu/Be composite cylinders inside sample containers.

Table 2-7, Table 2-8, Table 2-9, and Table 2-10 list the various NCT, HAC, and High Velocity impact analyses that were conducted for evaluating package performance with the solid metal contents.

Table 2-7. Normal Conditions of Transport (NCT) Impact Analyses (6), Components, and Orientations

Run No.	Component	Submodel Orientation
1	2 SC-2 Sample Containers, delta Pu	Lid end impact
4	3 SC-1 Sample Containers, delta Pu	Lid end impact
2	2 SC-2 Sample Containers, delta Pu	Side impact
3	2 SC-2 Sample Containers, delta Pu	Side impact, 45-degree-rotated
5	3 SC-1 Sample Containers, delta Pu	Side impact
6	3 SC-1 Sample Containers, delta Pu	Side impact, 45-degree-rotated

Table 2-8. Hypothetical Accident Condition (HAC) Dynamic Crush Analyses (20), Components, and Orientations

Run No.	Component	Submodel Orientation
1	2 SC-2 Sample Containers, delta Pu	Lid end impact
2	2 SC-2 Sample Containers, delta Pu	Side impact
3	2 SC-2 Sample Containers, delta Pu	Side impact, 45-degree-rotated
4	2 SC-2 Sample Containers, delta Pu	CGOC impact
5	2 SC-2 Sample Containers, delta Pu	CGOC impact, 45-degree-rotated
6	3 SC-1 Sample Containers, delta Pu	Lid end impact
7	3 SC-1 Sample Containers, delta Pu	Side impact
8	3 SC-1 Sample Containers, delta Pu	Side impact, 45-degree-rotated
9	3 SC-1 Sample Containers, delta Pu	CGOC impact
10	3 SC-1 Sample Containers, delta Pu	CGOC impact, 45-degree-rotated
11	831 g Plutonium Metal Hollow Cylinder, alpha Pu	Lid end impact
12	831 g Plutonium Metal Hollow Cylinder, alpha Pu	Side impact
13	831 g Plutonium Metal Hollow Cylinder, alpha Pu	Lid end impact, angled cylinder
14	831 g Plutonium Metal Hollow Cylinder, alpha Pu	Side impact, angled cylinder
15	831 g Plutonium Metal Hollow Cylinder, alpha Pu	CGOC impact, angled cylinder
16	731 g Plutonium Metal Hollow Cylinder, alpha Pu	Lid end impact
17	731 g Plutonium Metal Hollow Cylinder, alpha Pu	Side impact

Run No.	Component	Submodel Orientation
18	731 g Plutonium Metal Hollow Cylinder, alpha Pu	Lid end impact, angled cylinder
19	731 g Plutonium Metal Hollow Cylinder, alpha Pu	Side impact, angled cylinder
20	731 g Plutonium Metal Hollow Cylinder, alpha Pu	CGOC impact, angled cylinder

Table 2-9. High Velocity (Aircraft) Impact Analyses (27), Components, and Orientations

Run No.	Component	Submodel Orientation
1	831 g Plutonium Metal Hollow Cylinder, alpha Pu	Bottom position, top impact
2	831 g Plutonium Metal Hollow Cylinder, alpha Pu	Bottom position (angled), top impact
3	831 g Plutonium Metal Hollow Cylinder, alpha Pu	Bottom position (angled), CGOC impact
4	831 g Plutonium Metal Hollow Cylinder, alpha Pu	Far side position, side impact
5	831 g Plutonium Metal Hollow Cylinder, alpha Pu	Far side position (angled), side impact
6	731 g Plutonium Metal Hollow Cylinder, alpha Pu	Bottom position, top impact
7	731 g Plutonium Metal Hollow Cylinder, alpha Pu	Bottom position (angled), top impact
8	731 g Plutonium Metal Hollow Cylinder, alpha Pu	Bottom position (angled), CGOC impact
9	731 g Plutonium Metal Hollow Cylinder, alpha Pu	Far side position, side impact
10	731 g Plutonium Metal Hollow Cylinder, alpha Pu	Far side position (angled), side impact
11	SC-1 – Pu	Bottom position, support structure 0°, top impact
12	SC-1 – Pu	Far side position, support structure 0°,side impact
13	SC-1 – Pu	Far side position, support structure 45°, side impact
14	SC-1 – Pu	Bottom position, support structure 0°, CGOC impact
15	SC-1 – Pu	Bottom position, support structure 45°, CGOC impact
16	SC-2 – Pu	Bottom position, support structure 0°, top impact
17	SC-2 – Pu	Far side position, support structure 0°,side impact
18	SC-2 – Pu	Far side position, support structure 45°, side impact
19	SC-2 – Pu	Bottom position, support structure 0°, CGOC impact
20	SC-2 – Pu	Bottom position, support structure 45°, CGOC impact

Run No.	Component	Submodel Orientation
21	SC-1 - Be	Bottom position, angled Be, support structure 0°, top impact
22	SC-1 – Be	Far side position, angled Be, support structure 0°, side impact
23	SC-1 – Be	Far side position, angled Be, support structure 45°, side impact
24	SC-1 – Be	Bottom position, angled Be, support structure 0°, CGOC impact
25	SC-1 – Be	Bottom position, angled Be, support structure 45°, CGOC impact
26	SC-2 – Pu	Far side position, support structure 45°, side impact, friction 0.4
27	SC-2 – Pu	Far side position, support structure 45°, side impact, friction 0.2

Table 2-10. 30-ft Drop Impact Analyses (3), Components, and Orientations

Run No.	Component	Submodel Orientation
1	SC-2 - Pu	Far side position, support structure 45°, side impact
2	831 g Plutonium Metal Hollow Cylinder, alpha Pu	Bottom position (angled), top impact
3	831 g Plutonium Metal Hollow Cylinder, alpha Pu	Bottom position (angled), CGOC impact

Figure 2-5 is a summary plot of the Tearing Parameter versus equivalent plastic strain for the highest-value elements in the T-Ampoule body from 19 of the HAC and High Velocity impact analyses, or at least those that have any elements extending beyond the Bao-Wierzbicki (B-W) strain locus. The purpose of the plot is to assess the margin that exists in the T-Ampoule wall for sites that may initiate ductile tearing. The lowest factor of safety shown in this plot is 1.63 (critical Tearing Parameter is 1.012, divided by peak Tearing Parameter value of 0.62, equals 1.63). It is important to note that some of the element locations within the T-Ampoule body are along the internal closure lip, which would not threaten T-Ampoule integrity even if tear initiation were ever to occur. As detailed in Section 2.12.5, the maximum number of elements exceeding the B-W strain locus in any one impact analysis is 126 (out of 580,000 elements in the T-Ampoule model).

Figure 2-6 is a summary plot of the B-W strain locus for the highest-TP value element in Figure 2-5, for comparison. Note that although all of these elements extend beyond the B-W dashed line locus from test data, they only exceed the tested locus by a relatively small quantity (less than 0.3, and stress triaxiality can theoretically be infinitely positive or negative as perfect hydrostatic tension or compression is approached). A factor of safety cannot be quantified from this B-W strain locus, since points outside the locus do not necessarily indicate failure (they are only outside the tested stress triaxiality—plastic strain region of non-failure). This should give additional confidence that even the elements with the lowest factor of safety (based on Tearing Parameter) are nearly within the tested range of stress-triaxiality versus EQPS that did not fail.

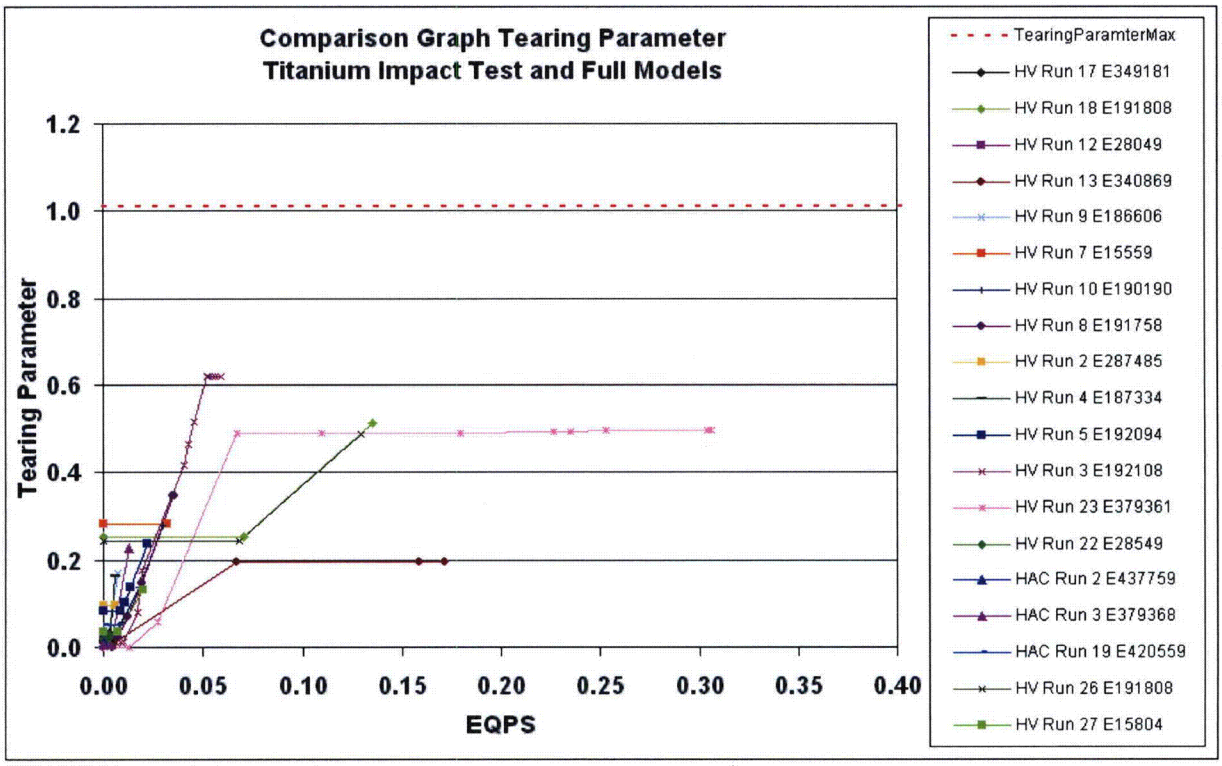

Figure 2-5. Summary of Highest Tearing Parameter versus Plastic Strain Elements for HAC and High Velocity Analyses

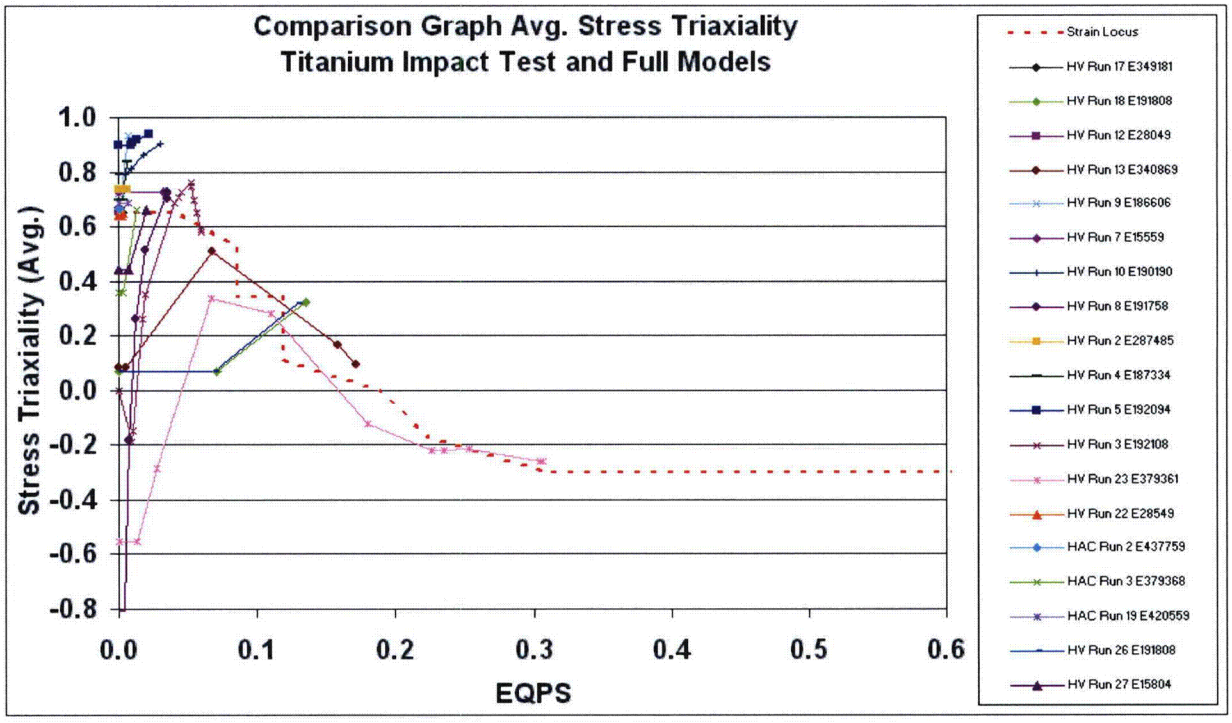

Figure 2-6. Summary of B-W Strain Locus Values for the Highest Tearing Parameter Elements.

As discussed in detail in Section 2.12.5.5.3, these curves all terminate below the critical Tearing Parameter of 1.012. Therefore, they do not to pose a threat to the integrity of the T-Ampoule body. From Figure 2-5 and Table 2-11 (which shows the peak Tearing Parameter value for all high speed impact analyses), the smallest margin of safety based on Tearing Parameter is 1.63 from the 831 g angled plutonium metal hollow cylinder high-speed CG-over-corner impact analysis case. Two important points must be noted when using this as a safety margin. First, this is not based on through-thickness failure of the T-Ampoule, but it is based on the stress-modified integrated strain limit for any element that might merely *initiate* a ductile tear. Second, there are many additional conservatisms inherent in the finite element analyses, which calculated the maximum plastic strains in the T-Ampoule wall. In addition to the plastic strains in the T-Ampoule wall, stresses in the TB-1 remain essentially elastic (except localized denting) and do not threaten the structural integrity of this vessel.

Table 2-11. High Velocity (Aircraft) Impact Analyses Peak Tearing Parameter Values

Run No.	Component	Model Orientation	Maximum Tearing Parameter (T-Ampoule)
1	831 g Plutonium Metal Hollow Cylinder, alpha Pu	Bottom position, top impact	0.0528
2	831 g Plutonium Metal Hollow Cylinder, alpha Pu	Bottom position (angled), top impact	0.2115
3	831 g Plutonium Metal Hollow Cylinder, alpha Pu	Bottom position (angled), CGOC impact	0.6177
4	831 g Plutonium Metal Hollow Cylinder, alpha Pu	Far side position, side impact	0.2896
5	831 g Plutonium Metal Hollow Cylinder, alpha Pu	Far side position (angled), side impact	0.2389
6	731 g Plutonium Metal Hollow Cylinder, alpha Pu	Bottom position, top impact	0.1507
7	731 g Plutonium Metal Hollow Cylinder, alpha Pu	Bottom position (angled), top impact	0.2831
8	731 g Plutonium Metal Hollow Cylinder, alpha Pu	Bottom position (angled), CGOC impact	0.3967
9	731 g Plutonium Metal Hollow Cylinder, alpha Pu	Far side position, side impact	0.4896
10	731 g Plutonium Metal Hollow Cylinder, alpha Pu	Far side position (angled), side impact	0.2842
11	SC-1 – Pu	Bottom position, support structure 0°, top impact	0.0319
12	SC-1 – Pu	Far side position, support structure 0°,side impact	0.2417
13	SC-1 – Pu	Far side position, support structure 45°, side impact	0.1958
14	SC-1 – Pu	Bottom position, support structure	0.0935

Run No.	Component	Model Orientation	Maximum Tearing Parameter (T-Ampoule)
		0°, CGOC impact	
15	SC-1 – Pu	Bottom position, support structure 45°, CGOC impact	0.3061
16	SC-2 – Pu	Bottom position, support structure 0°, top impact	0.0132
17	SC-2 – Pu	Far side position, support structure 0°,side impact	0.4788
18	SC-2 – Pu	Far side position, support structure 45°, side impact	0.5137
19	SC-2 – Pu	Bottom position, support structure 0°, CGOC impact	0.0953
20	SC-2 – Pu	Bottom position, support structure 45°, CGOC impact	0.0540
21	SC-1 – Be	Bottom position, angled Be, support structure 0°, top impact	0.0155
22	SC-1 – Be	Far side position, angled Be, support structure 0°, side impact	0.2075
23	SC-1 – Be	Far side position, angled Be, support structure 45°, side impact	0.4970
24	SC-1 – Be	Bottom position, angled Be, support structure 0°, CGOC impact	0.0597
25	SC-1 – Be	Bottom position, angled Be, support structure 45°, CGOC impact	0.1197
26	SC-2 – Pu	Far side position, support structure 45°, side impact, friction 0.4	0.4888
27	SC-2 – Pu	Far side position, support structure 45°, side impact, friction 0.2	0.4673

Numerous conservative assumptions were made in the modeling and assessment of the TB-1 and especially the T-Ampoule integrity. Other conservatisms include: neglecting the tantalum foil packing material which would perform some small load spreading and energy absorbing function, neglecting the rolled lid of the outer package skin in aircraft impacts, always assuming the content location and orientation most damaging to the T-Ampoule, e.g., "strongest" plutonium metal hollow cylinder dimensions to resist buckling; most dense, compact, and sharp shape for the delta Pu and Be composite cylinders; delta Pu contents have higher density of alpha Pu; sharpest orientation for the strong Be cylinders, etc. Also, the material properties for these contents are conservatively assumed to have infinite plasticity, when in fact the alpha Pu is very brittle and the Be has rather limited ductility. These conservative assumptions maximize the loading and damage potential to the T-Ampoule, yet it retains structural integrity as a eutectic barrier.

2.8.5 Bolt Analysis

Although the bolts in the PAT-1 package were already shown to remain elastic and the lid maintained containment during the original certification testing, a simplified analysis was performed on the bolts securing the TB-1 lid when subjected to the high-speed aircraft accident test condition (10 CFR 71.74). The bolts are not explicitly modeled in the TB-1, but the net balance of compression from the redwood in an end impact along with the bolt preload versus the internal impact loading from various impacting contents can be determined. The impulse loads, which are applied to the underside of the lid, are obtained from the high velocity impact analyses (see Section 2.12.5). The forces holding the lid in place are the bolt preload and the redwood contact force. These forces are plotted in Figure 2-506 and the analysis is described in Section 2.12.6, Bolt Analysis, in this addendum. As shown in the figure, the forces from the components are only a fraction of the bolt preload. The peak impulse load is a factor of 2.0 less than the bolt preload, and is a factor of 6 less than the total of the sum of the wood retaining force and the bolt preload. Therefore, the lid of the TB-1 will remain properly torqued during the aircraft impact accident.

Other factors, besides impact loads, can contribute to the loss of bolt preloads and proper seal compression.[16] Protecting the closure lid from direct impact, using a lid design that minimizes prying loads on bolts, recessing bolts within the lid, lubricating bolts to reduce necessary torque to achieve desired preload, using a large enough preload to minimize fatigue and loosening of bolts by vibration, and finally using similar thermal expansion coefficient materials for the bolt, lid, and cask body have all been done for the PAT-1. The TB-1 is a "protected lid and bolt head" closure design,[16] which is most resistant to potential shear and bending bolt loads. Bolt bending and prying forces are minimized by the design of the TB-1 closure, which has inner and outer bore surfaces (the inner with an O-ring bore seal) with a flange surface in between (with the primary copper metal gasket flange seal). The body of the TB-1 containment vessel is also significantly thickened in the bolted closure region to accommodate these multiple bore surfaces and resist bending loads in side and CGOC impacts. It is important to highlight that the TB-1's bolted closure met all containment requirements in SAR[1] aircraft accident condition testing with same-mass contents, and the effective bolt load calculations provided in Section 2.12.6 confirm that the solid metal contents do not adversely affect containment.

2.8.6 Summary

A series of analyses were performed on the PAT-1 package and its contents to determine the integrity of the TB-1 and T-Ampoule when subjected to the requirements of 10 CFR 71.71 (Normal conditions of transport), 10 CFR 71.73 (Hypothetical accident conditions) and 10 CFR 71.74 (Accident conditions for air transport of plutonium). Six sets of analyses were conducted, leading up to detailed impact analyses of the PAT-1 package, including its TB-1 containment vessel and the T-Ampoule eutectic barrier. Using a strain-based failure criterion, it was shown that the T-Ampoule would not rupture and would continue to function as a eutectic barrier between the stainless steel TB-1 vessel and the solid metal plutonium contents. In addition, an analysis of the bolts securing the TB-1 lid showed that the lid will remain intact and tight.

No fire simulations required for the air transport accident were conducted; however, a simple check of the potential for differential thermal expansion was performed, similar to the checks for the NCT and HAC conditions. Since the T-Ampoule is the only change being made from the

original package Hypothetical accident conditions, the only concern would be the expansion of the T-Ampoule resulting in contact with the TB-1.

The Military Handbook[6] reports a coefficient of thermal expansion (α) for Ti-6Al-4V used for the T-Ampoule of 5.1×10^{-6} in./in./°F in the range of temperatures of concern. A conservative estimate of the maximum expansion of the T-Ampoule can be calculated by assuming the T-Ampoule is a 7.418-in.-long cylinder (the actual T-Ampoule is capped) with a diameter of 4.22 in. The T-Ampoule is assumed to reach the maximum temperature of the TB-1 in the original fire test which was estimated at 1080°F (582°C). Assuming a temperature increase of 1010°F (1080°F – 70°F), the expansion produced equals $\alpha\Delta TL$, or 0.038 in. in the longitudinal direction, and 0.0683 in. in circumference (or 0.0217 in. in diameter). Since the gap between the T-Ampoule and the TB-1 is 0.015 in. around the entire perimeter, the expansion in the longitudinal direction is slightly more than the total gap (0.038 in. > 0.30 in.). However, the TB-1 would also expand outward, allowing for the expansion of the T-Ampoule. As shown in Section 2.12.4.9, the coefficient of thermal expansion of the Stainless PH13-8Mo used for the TB-1 is approximately 5.9E-6 in/in/°F. The same temperature change from 70°F to 1080°F produces a 1010° F temperature increase. Assuming that the TB-1 is a cylinder of length 8.68 in. with a 5.35 in. diameter (outer diameter of main TB-1 body) increases the length equal to $\alpha\Delta TL$, or 0.0517 in. in the longitudinal direction, and a increases the circumference by approximately 0.100 in. (0.0319 in. in diameter). The TB-1 expands outward more than the T-Ampoule, therefore, no stresses will be induced by differential thermal expansion for the air transport accident. In Section 4.3.1, the pressure generated within the TB-1, which included temperature, helium gas generation from alpha decay, and decomposition of O-rings, from the accident conditions for air transport of plutonium fire environment yielded a pressure of 964.2 psia which is less than that reported in the SAR[1] of 1110 psia.

2.9 Accident Conditions for Fissile Material Packages for Air Transport

For 10 CFR 71.55(f), the requirements for accident conditions for air transport of plutonium evaluated in this addendum cover this section.

2.10 Special Form

No change. This addendum covers transport of normal form material for PAT-1.

2.11 Fuel Rods

No change. This addendum does not consider transport of fuel rods for PAT-1.

2.12 Appendix

2.12.1 References

1. United States. Nuclear Regulatory Commission. NUREG-0361. "Safety Analysis Report for the Plutonium Air Transportable Package, Model PAT-1." Washington, D.C. 1978.

2. United States. Nuclear Regulatory Commission. Regulatory Guide 7.6. "Design Criteria for the Structural Analysis of Shipping Cask Containment Vessels," Revision 1. Washington, D.C.: March 1978.

3. United States. Nuclear Regulatory Commission. Regulatory Guide 7.8. "Load Combinations for the Structural Analysis of Shipping Casks for Radioactive Material," Revision 1. Washington, D.C.: March 1989.

4. United States. Nuclear Regulatory Commission. Code of Federal Regulations. 10 CFR 71.73. "Hypothetical Accident Conditions for the Packaging and Transport of Radioactive Materials."

5. American Society of Mechanical Engineers (ASME). "Boiler & Pressure Vessel Code." 2007.

6. Department of Defense. *Military Standardization Handbook: Metallic Materials and Elements for Aerospace Vehicle Structures.* MIL-HDBK-5E: May 1988.

7. Bao, Y., and T. Wierzbicki. "On the Cut-Off Value of Negative Triaxiality for Fracture." Engineering Fracture Mechanics, 72, pp. 1049-1069, 2005.

8. Steigerwald, E.A., "Plane Strain Fracture Toughness of High Strength Materials," *Engineering Fracture Mechanics*, Vol. 1 (1969): 473-494.

9. United States. Nuclear Regulatory Commission. Code of Federal Regulations. 10 CFR 71.74. "Accident Conditions for Air Transport of Plutonium."

10. Taylor, L.M. and D.P. Flanagan. "PRONTO3D: A Three-Dimensional Transient Solid Dynamics Program," SAND87-1912. Sandia National Laboratories. Albuquerque, NM. March 1989.

11. Davie, N., et al. "Test Report PAT-1/TB-1 Impact Test Series." Sandia National Laboratories. August 30, 2007.

12. Bao, Y. "Prediction of Ductile Crack Formation in Uncracked Bodies," Report 100, 2003. Impact & Crash Worthiness Laboratory. Massachusetts Institute of Technology. Cambridge, MS.

13. Wellman, G.W., Diegert, K.V., and Saizbrenner, R. "Two-Dimensional Quasistatic Modeling of Exclusion Region Barriers in Support of Design Guide Development." SAND93-0905. Sandia National Laboratories. Albuquerque, NM. 1993.

14. Dawson, D.B., Antoun, B.R., and Mosher, D.A. "MAVEN Progress Report for FY98 Second Half (Fracture of Weapons Materials)." Sandia National Laboratories Memo Report to Distribution, October 5, 1998.

15. Andersen, J.A., Duffey, T.A., Dupree, S.A., and Nilson, R.H., "PARC (Plutonium Accident Resistant Container) Program Research, Design, and Development, SAND76-0587, NUREG/CR-0030. Sandia National Laboratories. Albuquerque, NM. July 1978.

16. Mok, G.C., Fischer, L.E., and Hsu, S.T., "Stress Analysis of Closure Bolts for Shipping Casks," NUREG/CR-6007, UCRL-ID-110637, Prepared for the US NRC, April 1992.

17. Bessette, G.C., et al. "Methodology Assessment and Recommendations for the Mars Science Laboratory Launch Safety Analysis," SAND2006-4563. Sandia National Laboratories. Albuquerque, NM. September 2006.

18. Ammerman, D.J., and Hoffman, E.L., "Dynamic Pulse Buckling of Cylindrical Shells Under Axial Impact: A Comparison of 2D and 3D Finite Element Calculations With Experimental Data," SAND93-0350. Sandia National Laboratories. Albuquerque, NM. 1993.

19. United States. Nuclear Regulatory Commission. NUREG/CR-6672. Sprung, J.L., Ammerman, D.J., Breivik, N.L., Dukart, R.J., Kanipe, F.L., Koski, J.A., Mills, G.S., Neuhauser, K.S., Radloff, H.D., Weiner, R.F., and Yoshimura, H.R. "Re-examination of Spent Fuel Shipment Risk Estimates." SAND2000-0234. Sandia National Laboratories. Albuquerque, NM. March 2000.

20. United States. Nuclear Regulatory Commission. NUREG-1768. "Package Performance Study Test Protocols." February 2003.

21. VanGoethem, D. et al. "Test memo report for PAT-1/T-Ampoule drop table shock tests." Sandia National Laboratories. Albuquerque, NM. December 12, 2008.

22. Fischer, L. E., W. Lai, "Fabrication Criteria for Shipping Containers," NUREG/CR-3854, Lawrence Livermore National Laboratory, April 1984.

23. American Society of Mechanical Engineers(ASME). "Boiler and Pressure Vessel Code," Section VIII, Division 1, Rules for Construction of Pressure Vessels. July 1, 2009 Addenda.

24. Holmes-Siedle, A. and L. Adams. *Handbook of Radiation Effects, Section Edition.* pp. 568. UK: Oxford University Press, 2002.

25. Chao, A. W. C and M Tigner. *Handbook of Accelerator Physics and Engineering.* Singapore: World Scientific Publishing Co. Pte. Ltd., 2002.

26. American Society for Testing and Materials. Younger, C. L. and Haley, F. A. "Irradiation Effects at Cyrogenic Temperature on Tensile Properties of Titanium and Titanium-Base Alloys." *Irradiation Effects on Structural Alloys for Nuclear Reactor Applications*, STP 484, (1970), pp. 537-563.

2.12.2 Full Model Validation Analyses

2.12.2.1 Discussion

This section describes the side, end, and CG-over-corner high velocity impact analyses of the original PAT-1 package certification tests. There are two general overpack models, one to model the high-speed aircraft accident test condition (10 CFR 71.74[2]), and the other to model the NCT (10 CFR 71.71[2]) and HAC test conditions (10 CFR 71.73[2]). The original certification of the PAT-1 was performed through testing with only minimal instrumentation, so the overpack deformations were used for comparison to those analyzed in the validation model (with simplified PuO_2 contents and the certification test impact velocity of 445 ft/sec). Subsequently, similar overpack models with the detailed solid metal contents (and T-Ampoule) will be used to evaluate the position of the contents in NCT 4 ft impacts, and to determine the effect of the solid internal components on the integrity of the titanium T-Ampoule, which acts as a eutectic prevention barrier between the contents and the stainless-steel TB-1 vessel.

2.12.2.2 Model Description

The finite element model used in the high-velocity validation analyses is shown in Figure 2-7. This is a half-symmetry model, with the plane of symmetry running along the center axis. The principal components of the model are the redwood impact-limiting material, the load spreader assembly, the copper cylinder, the TB-1 containment vessel, and the plutonium oxide mass. The PAT-1 package is encased in a stainless drum approximately 41.5 in. in length. This includes an approximate 1–in. flange on each end for the outer drum lid and seal. To simplify the finite element model, the details of the outer drum lid are not included. This area consists mostly of thin sheet metal components, and the energy absorbed in their deformation is conservatively ignored. Therefore, the height of the finite element model is only 39.75 in., which is the length of the redwood impact-limiting material.

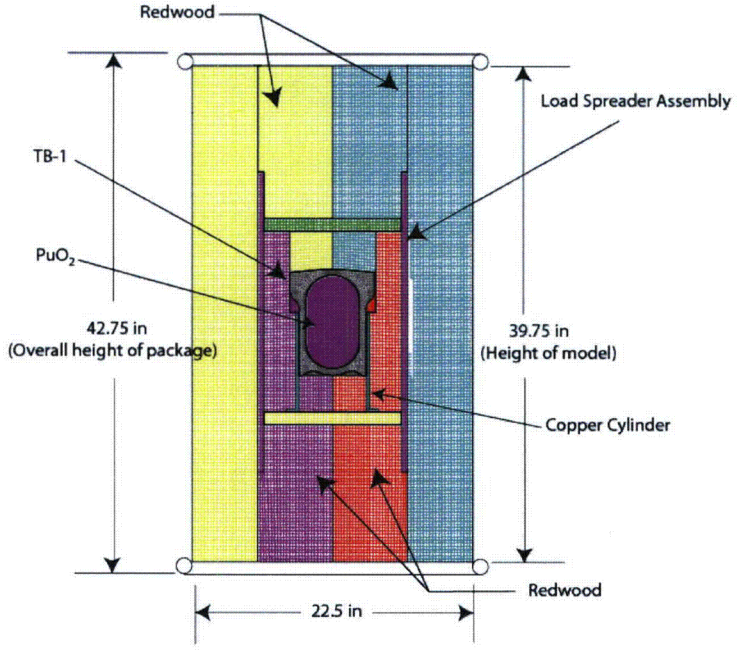

Figure 2-7. Finite Element Model of the Complete PAT-1 Package

In the full package validation model, the TB-1 is modeled as a solid, one-piece object. The bolted connection for the lid is not modeled; instead the net loading on the lid from contents impacts and overpack compression is shown to be significantly less than the bolt pre-load, and thus detailed modeling of the closure is not necessary. This bolted joint was also shown in the SAR[1] aircraft impact tests to meet containment requirements of < A_2/week release rate with same-mass contents. In addition, the plutonium oxide mass inside the TB-1 is modeled as a very soft elastic plastic material with the correct density. These simplifications are acceptable, since the primary purpose of the analysis is to validate the model's redwood overpack crush in the three certification high velocity impact tests.

The finite element validation model contains 378,439 elements: 366,258 hexahedral elements and 12,181 quadratic shell elements. All components with hexahedral elements have at least 3 elements through the thickness to accurately capture potential bending and shear responses, and aspect ratios of approximately 1.0, following common large-deformation explicit analysis practice for accurate FEA model response. As shown in Figure 2-8(a), the outside of the redwood material is wrapped in a 0.0625 in., stainless steel shell layer. The shells are attached to the hexahedral elements using coincident nodes to simulate the gluing of these components in the actual PAT-1 assembly. Their primary purpose is to provide confinement of the redwood material. Figure 2-8(b) shows the density of the mesh in the load spreader assembly region; three elements are used across the load spreader pipe to capture any potential bending.

The top removable plug, the removable disk, the TB-1, the PuO_2, and the lower removable plug are modeled as individual components; they are not attached to other components in the model. The remaining pieces are attached using coincident nodes in order to simulate the gluing together of these components in the actual assembly.

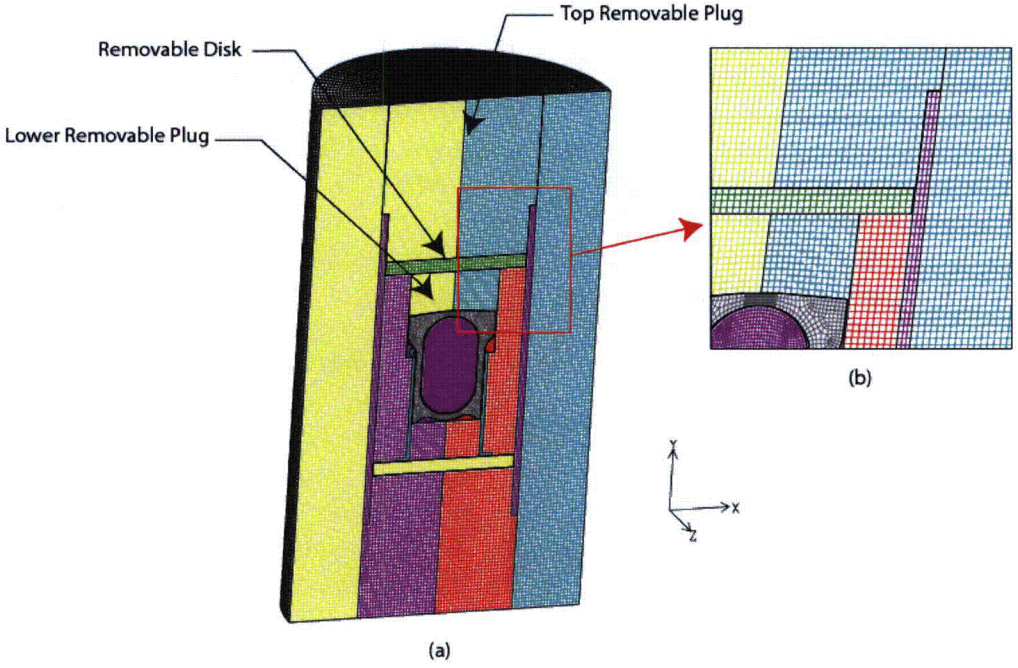

Figure 2-8. Details of the High-Velocity Finite Element Validation Model

The redwood material is modeled using the orthotropic crush model in PRONTO-3D.[3] The orthotropic crush model is an empirically based constitutive relation used to model materials like metallic honeycomb and wood. The force deflection curve used to simulate the compression of the redwood material is presented in Figure 2-9 along with data from Joseph and Hill.[4] These values, along with the other modeling parameters, are presented in Table 2-12; details of the material properties are presented in Section 2.12.4.

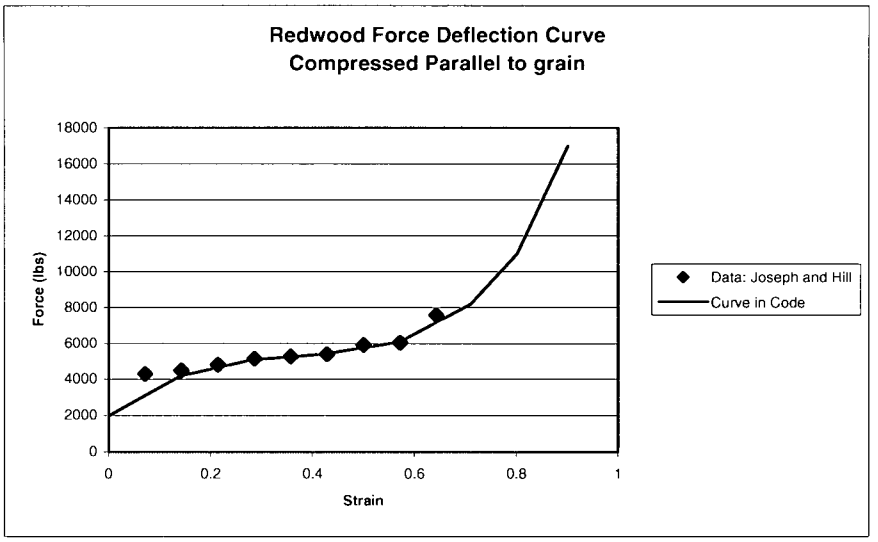

Figure 2-9. Redwood Force-Deflection Curve Used in Orthotropic Crush Model

The metal components were modeled using a power-law hardening constitutive model:

$$\sigma = \sigma_y + A(\varepsilon_p)^n \tag{2-1}$$

where σ_y is the yield stress, A is a hardening constant, and n is a hardening exponent. Values for the material parameters for each material are given in Table 2-13. The PuO_2 powder is also modeled as a very soft material using the power-law hardening model. This is deemed reasonable, since the mass of the material and its loading on the TB-1 and the redwood is the primary factor; modeling the detailed response of the oxide is not important.

The circumferential orientation of the pie-shaped redwood around the PAT-1 package ranges from 8 to 10 segments. This is an attempt to keep the grain of the wood parallel to the direction of the load. However, the orthotropic crush model in PRONTO-3D[3] is oriented relative to the three orthogonal global axes of the model; a local coordinate system is not available in this model. Therefore, modeling many small segments around the circumference is not possible. Instead, the model material blocks were constructed in 90° segments rotated 45° to the model's global axes; this is shown in Figure 2-10. This is an attempt to maximize the strength of the material in the radial direction during side impacts within the constraints imposed by the constitutive model.

Table 2-12. Redwood Orthotropic Crush Model Parameters

Parameter	Value	
Compacted YOUNGS MODULUS (psi)	1.5E6	
Compacted POISSONS RATIO	0.3	
Compacted YIELD STRESS (psi)	20000	
Full Compaction	0.9	
Modulus x (psi)	1.5E6	
Modulus y (psi)	0.3E6	
Modulus z (psi)	0.3E6	
Modulus xy (psi)	0.2E6	
Modulus yz (psi)	0.25E6	
Modulus zx (psi)	0.2E6	
Function 1 $ T-Direction	**Strain**	**Pressure (psi)**
	0.	2000
	0.14	4200
	0.28	5100
	0.42	5430
	0.57	6100
	0.71	10100
	0.80	15000
	0.90	20000
Function 2 $ L-Direction		
	0	400
	0.14	986
	0.28	1200
	0.42	1275
	0.57	1432
	0.71	2371
	0.80	3521
Function 4 $ sigxy or sigxz vs volume		
	0.0	1000
	0.6	1000
	0.7	10000
	0.9	10000
Function 5 $ sigyz vs volume		

Parameter	Value	
	0	1000
	0.6	1000
	0.7	10000
	0.9	10000

2.12.2.3 Original Certification Test Analyses with the Validation Model

The validation model was analyzed for the three basic impact directions, end-on, side-on, and center-of-gravity-over-corner (CGOC). The primary purpose of these analyses is to compare overpack deformations with the previous impact tests. Subsequent analyses with the same overpack model, but more detailed solid metal contents models (including the T-Ampoule) will be performed to verify structural integrity of the TB-1 and T-Ampoule in HAC dynamic crush, as well as high velocity impact conditions (see Section 2.12.5).

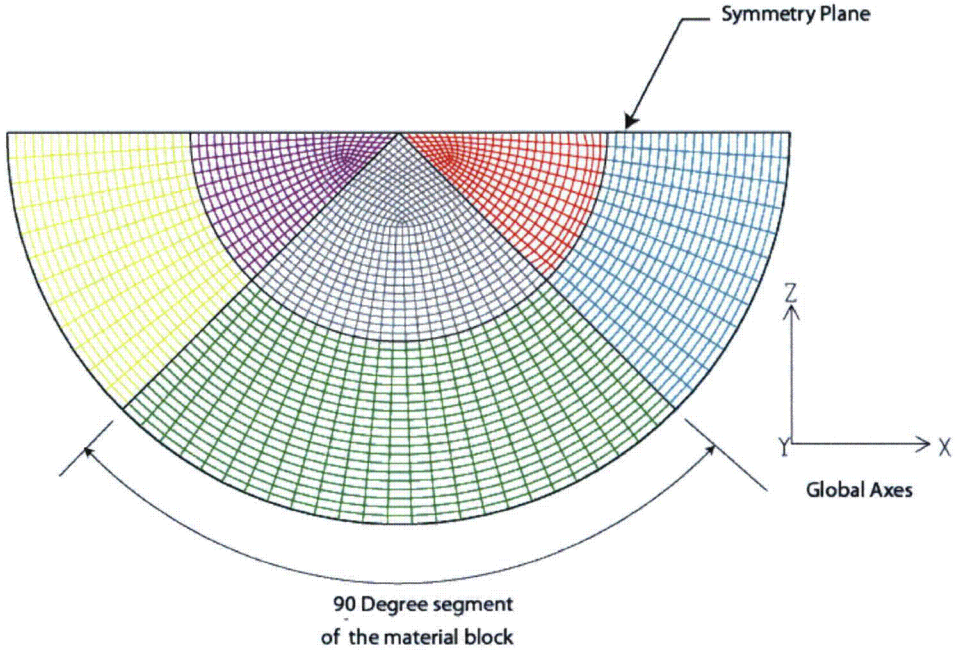

Figure 2-10. Model Slice Configuration for the Orthotropic Crush Material Model

Table 2-13. Power-Law Hardening Constitutive Model Parameters

Material	E (ksi)	ν	σ_y (ksi)	A (ksi)	n	Reference (from addendum)
Aluminum 6060-T6	9,900	0.3	45	37.8	0.55	2.12.4.3
Aluminum 7075-T6	10,400	0.33	73	37.8	0.55	2.12.4.5
Copper	17,200	0.33	45	38.0	0.55	2.12.4.7
Stainless Steel	28,000	0.27	40	192.7	0.748	2.12.4.12
Pu Oxide	1000	0.3	2	100	1.0	2.12.4.11
PH13-8MO	30,000	0.3	141.0[A]	30	1.0	2.12.4.9

[A] In the full model analyses to determine the deceleration of the whole package, a yield strength of 200 ksi was inadvertently used for the Ph138Mo TB-1 material. This represents the material in forged condition and does not reflect the subsequent heat treatment. However, since this model was used only to generate the rigid body deceleration of the package and not to determine the inelastic response of the TB-1 vessel, the change in the yield stress is immaterial. The table above reflects what is in the final model.

2.12.2.4 End Impact

The results from an end-on impact of the complete PAT-1 package for an initial velocity of 445 ft/sec are presented in Figure 2-11. This was the velocity used in the test, which is slightly higher than the 422 ft/sec specified in 10 CFR 71.74.[2] The overall length of the deformed model is 32.75 in., which is slightly longer that the 31.5 in. produced in the test as shown in Figure 2-12 (from Figure 2.18, Reference 1). This 4% difference in overpack crush is likely well within the variability of the redwood crush properties purely due to moisture content and age.[5] Note that the overpack skin buckling pattern observed in the test cannot be reproduced in the FEA model since the stainless steel skin is "tied" to the redwood (the nodes are equivalenced) and no slipping between the surfaces is allowed.

Since the crush distance of the finite element model is shorter than the crush distance observed in the same velocity end impact certification test, the TB-1 and contents loading applied using the shorter (and higher) finite element model acceleration will be more severe than the impulse applied in the certification test (i.e., the redwood properties are conservatively modeled as being slightly too stiff). The deceleration curve for the end impact analysis is shown in Figure 2-13.

2.12.2.5 Side Impact

The deformed shape of the full package model for side-on impact at a velocity of 445 ft/sec is shown in Figure 2-14. The resulting width of the package ranges from 15.5 in. to 16.5 in. This compares well to the deformed packages shown in Figure 2-15 (from Figure 2.24 of the SAR[5]), which gives deformed thicknesses of 15 to 15.5 in. The results of the finite element model are conservatively stiffer than the actual package. The deceleration curve for the side impact analysis is shown in Figure 2-16.

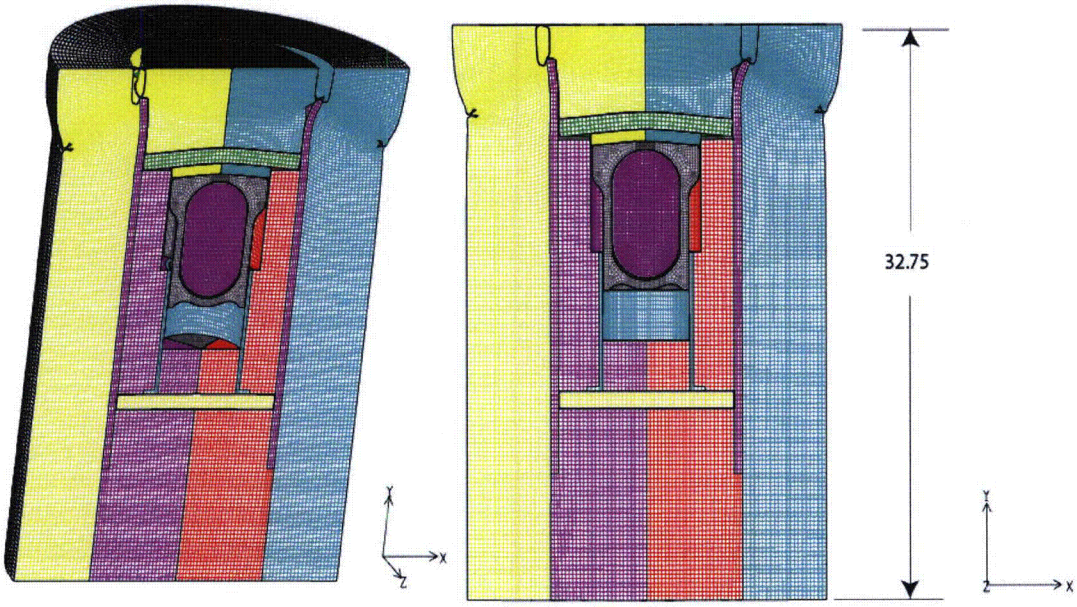

Figure 2-11. Deformation from an End-On Impact of 445 ft/sec

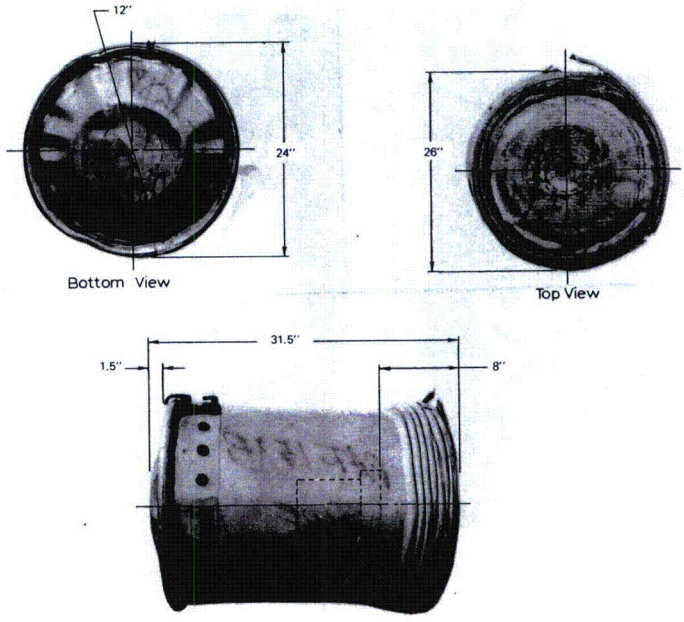

Figure 2-12. PAT-1 Dimensions Following 422-FPS Top End Impact (from SAR Figure 2.18[1])

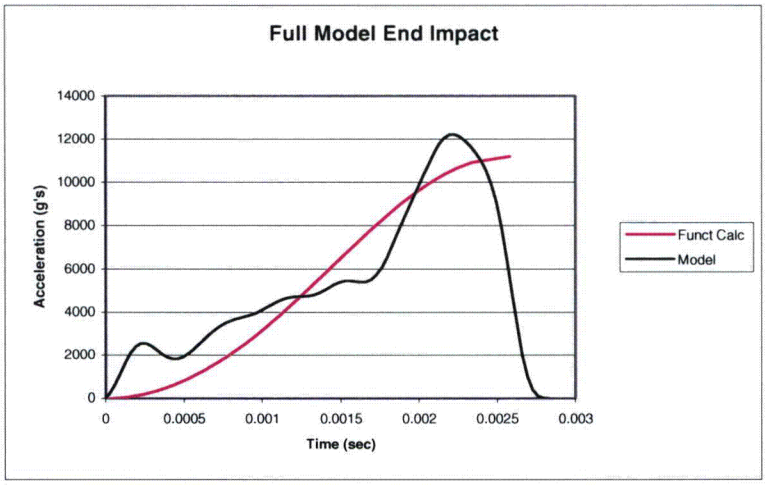

Figure 2-13. Full Model TB-1 Deceleration Curve for End-On Impact Analysis (10 CFR 71.74)

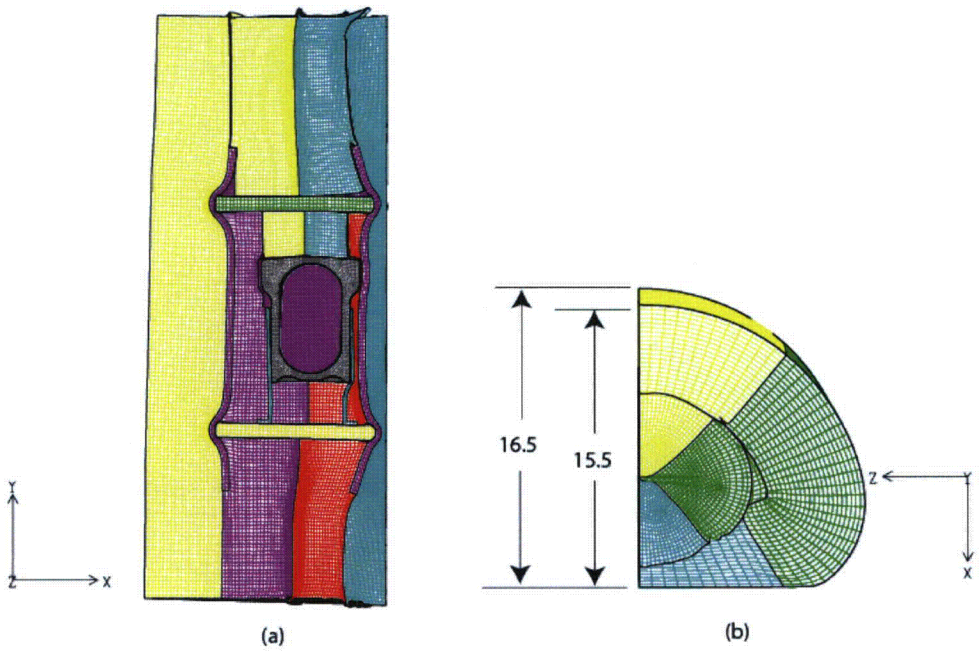

Figure 2-14. Deformation of the Full Package Model after a Side Impact of 445 ft/sec

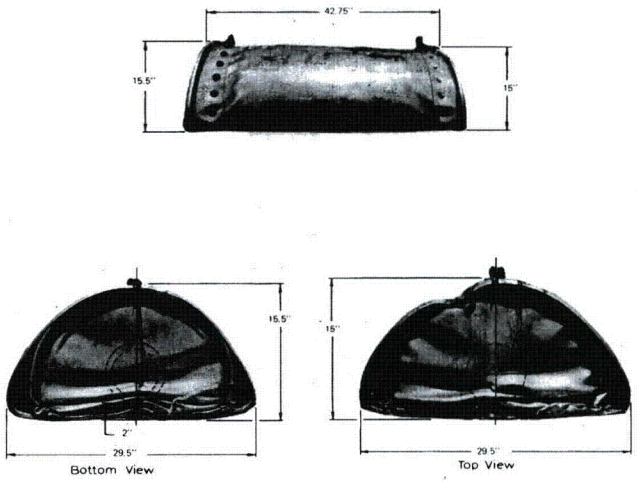

Figure 2-15. PAT-1 Dimensions Following 445 FPS Side Impact (from SAR Figure 2.24[2])

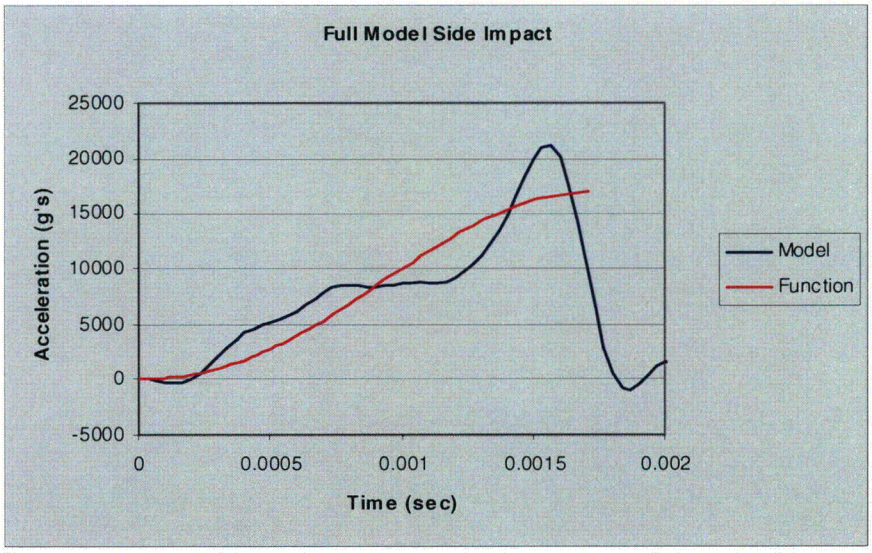

Figure 2-16. Full Model TB-1 Deceleration Curve for Side Impact Analysis (10 CFR 71.74)

2.12.2.6 CGOC Impact

The resulting deformation for the CGOC impact is shown in Figure 2-17. The finite element model has an unreformed side length of 23 in., which is longer than the 19 in. shown in Figure 2-18 (from Figure 2.27 of the SAR[1]). However, there is some rounding of the corner during the test, which is not seen in the model (probably due to the outer overpack skin shell elements being equivalenced to the redwood), and this makes measurement of the tested specimen less precise. This corner rounding would change this dimension without absorbing significant quantities of energy. The SAR figure also gives a nominal dimension of 25 in. to the edge of the TB-1 top. This agrees closely with the model results. Again, excepting the outer skin buckling pattern, the overpack deformation observed in the FEA validation model compares very well with the test results documented in the SAR.[1] The deceleration curve for the CGOC analysis is shown in Figure 2-19.

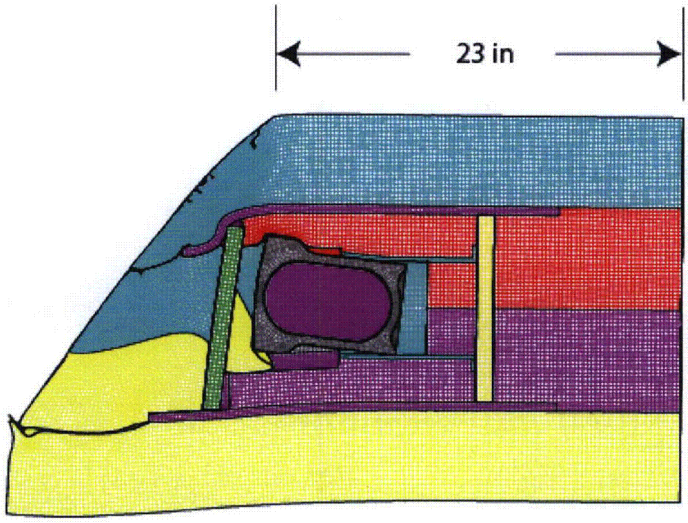

Figure 2-17. Deformation of the Full Package Model after a CGOC Impact of 445 ft/sec

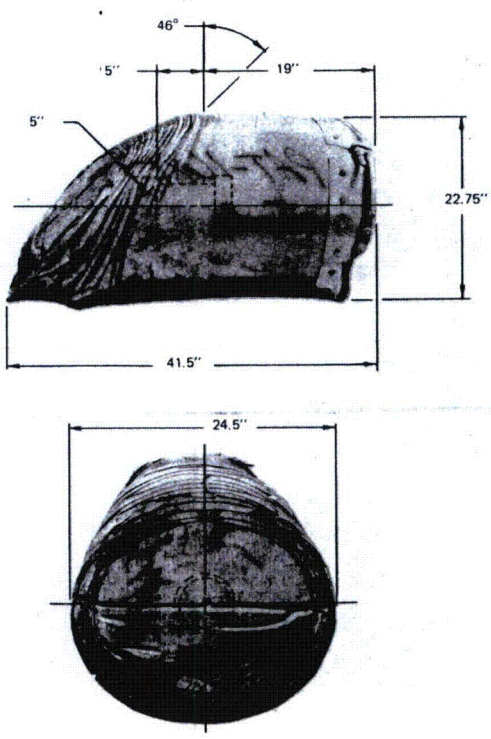

Figure 2-18. PAT-1 Dimensions Following 443-FPS Bottom Corner Impact (CGOC) (from SAR Figure 2.27 SAR[1])

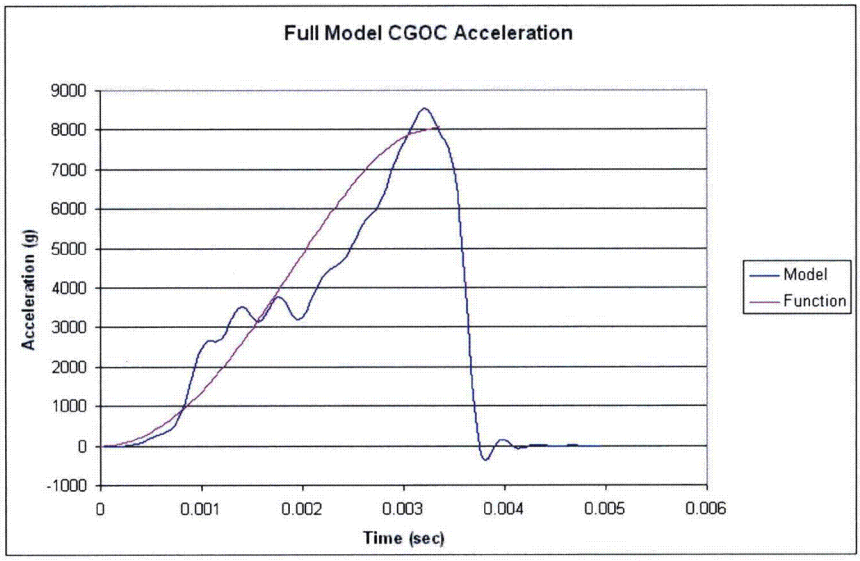

Figure 2-19. Full Model TB-1 Deceleration Curve for CGOC Impact Analysis (10 CFR 71.74)

2.12.2.7 Full Model NCT and HAC

The full package model (with detailed solid metal contents and T-Ampoule) will be analyzed for the NCT (10 CFR 71.71[2]) and HAC (10 CFR 71.73[2]) test conditions to verify contents positioning (NCT) for subsequent 10 CFR 71.74[2] analyses and to verify structural integrity of the TB-1 and T-Ampoule (HAC dynamic crush).

The orientation of the package for the full model NCT analyses will be of the side-on (0 and 45-degree-rotated) and lid end-on orientations, since these analyses generated the largest accelerations in the TB-1 containment vessel.

In addition, end, side, and CG-over-corner dynamic crush events were examined for the HAC to compare TB-1 through-thickness wall stresses with ASME allowables, and to verify T-Ampoule structural integrity. The same model used for the NCT positioning analyses was used for the HAC dynamic crush analysis. Some validation of this model is shown in Section 2.12.5.7.1, where the FEA side impact model overpack deformation matches the SAR[1] impact test results (see Figure 2-490 through Figure 2-495).

2.12.2.8 Model Description

As shown in Figure 2-20, the NCT full package model is very similar to the high-speed aircraft accident model. The only difference is the addition of the lid cover and ring clamp. While these components absorb very little of the kinetic energy during the high-speed impact, and were therefore ignored in that model, they are very important in the low-speed NCT accident condition. In the low-speed NCT condition, they are the primary energy absorber. Details of the lid area are presented in Figure 2-21. The lid and clamp ring consist of three separate pieces that are bolted to the package side and secured with a circumferential ring. The assembly is simplified and modeled in the finite element model as a group of shell elements joined by coincident nodes. The thickness of the shells is varied to account for the overlapping of the different components. To reduce the size of the end-on model, the flange elements were

removed from the non-impacting end in the NCT runs. Analysis results are detailed in Section 2.12.5.

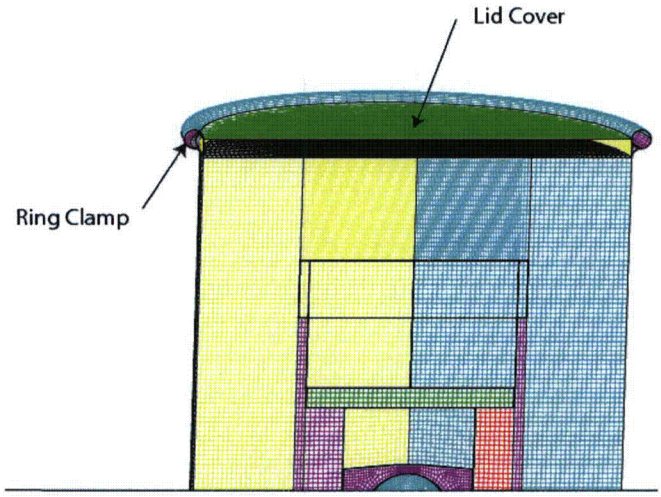

Figure 2-20. NCT and HAC Package Model with Lid Flange

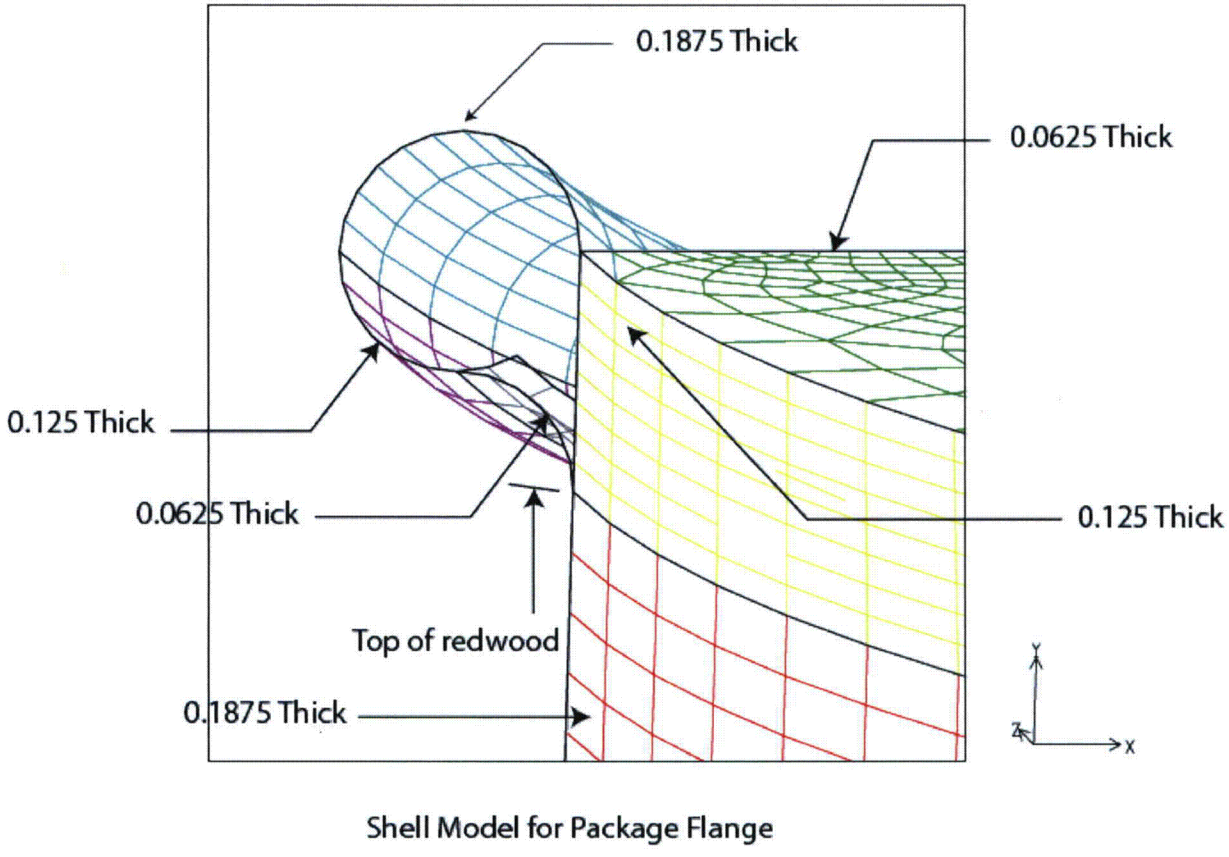

Figure 2-21. Flange Details of NCT Model (Dimensions in Inches)

2.12.2.9 References

1. United States. Nuclear Regulatory Commission. NUREG-0361. "Safety Analysis Report for the Plutonium Air Transportable Package, Model PAT-1." Washington, D.C. 1978

2. United States. Nuclear Regulatory Commission. Code of Federal Regulations, 10 CFR 71. "Packaging and Transportation of Radioactive Material." January 1, 2009.

3. Taylor, L.M. and D.P. Flanagan. "PRONTO3D: a Three-Dimensional Transient Solid Dynamics Program," SAND87-1912. Sandia National Laboratories. Albuquerque, NM. March 1989.

4. Joseph, Walter W. and Thomas K. Hill. "Energy-Absorbing Characteristics of California Redwood Subjected to High Strain." SAND76-0087. Sandia National Laboratories. Albuquerque, NM. 1976.

5. Cramer, S.M, Hermanson, J.C., and McMurtry, W.M. "Characterizing the Large Strain Crush Response of Redwood." SAND96-2966, Sandia National Laboratories. Albuquerque, NM. 1996.

2.12.3 Impact Test and Material Failure Criterion

2.12.3.1 Impact Test Description

In support of the PAT-1 SAR[1] analysis, a series of impact tests were conducted using the Sandia National Laboratories (SNL) 18" horizontal actuator and the DT-45 drop table. These tests had two main purposes: (1) to provide data for validating the finite element model, and (2) to provide data for estimating the margin in support of the strain-based failure criteria. Both test series were required to provide a sufficient range of data in stress space for the strain-based locus. A brief summary of the impact tests is given in this section (full details of the test can be found in "*Test Report PAT-1/TB-1 Impact Test Series*"[1] and "*Test Report PAT-1 T-Ampoule Drop Table Shock Machine Tests*"[2]). In addition, details of the finite element models used for code and model validation, along with the finite element models used to support the strain-based failure criterion, are also presented.

A schematic drawing of the impact test using the 18" horizontal actuator is presented in Figure 2-22. This is a reverse ballistic test in which the sled containing a cup, which represents the T-Ampoule and the TB-1 container, is propelled into a suspended impactor assembly containing a brass or titanium tip. The object of the test was to simulate the impact of the T-Ampoule contents on the T-Ampoule wall, and the T-Ampoule and its contents on the TB-1 inner surface, during a plutonium air transport accident. A brass tip was used to simulate a fine grain alpha-plutonium material impacting the T-Ampoule, and a titanium tip was used in an attempt to generate plastic strain in the T-Ampoule wall. Although the actuator assembly has a limited velocity of 200 ft/sec, which is less than the 422 ft/sec specified for the aircraft accident (10 CFR 71.74), this is not a problem, since the impact between the TB-1 wall and the contents will not be at the maximum velocity. The impact between the contents and the TB-1 occurs while the TB-1 is decelerating but is still moving. Therefore, the relative velocity between the TB-1 and the contents is only a fraction of the initial package velocity.

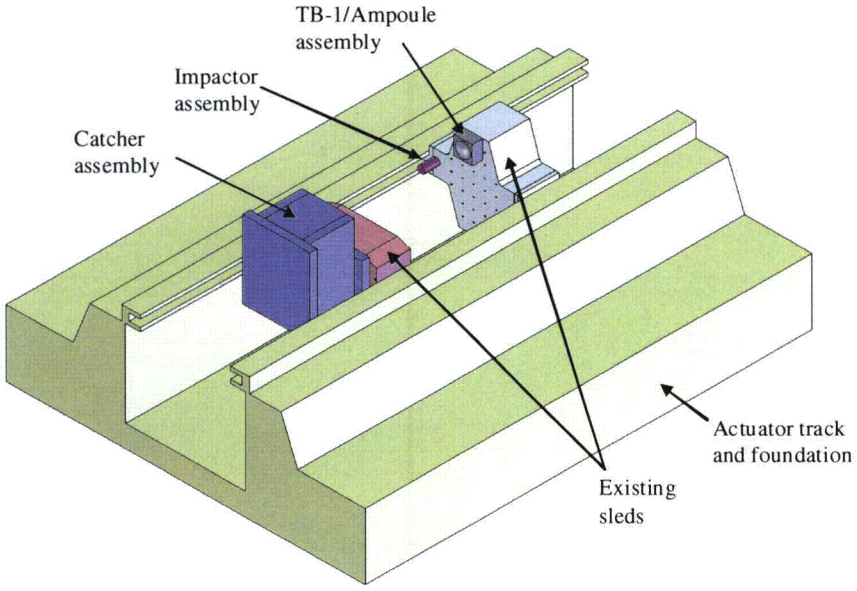

Figure 2-22. Experimental Concept[1]

Figure 2-23 is a schematic of the impactor and T-Ampoule assemblies for the 18" horizontal actuator test. A spherical titanium ampoule specimen is used to represent the top dome of the T-Ampoule in the TB-1. The TB-1 fixture is constructed with the same high-strength 13-8 Mo stainless steel, and an aluminum adaptor is used to secure the TB-1 fixture to the actuator sled. The body of the impactor is constructed from tungsten in order to provide sufficient mass and strength. An aluminum adapter is connected to the back end of the tungsten body to attach the accelerometers. The tip of the impactor, which has a spherical shape (not shown in the figure), is constructed from free cutting brass UNS C36000 (as drawn) or Titanium 6Al-4V (mill-annealed condition). The brass is a surrogate for a fine-grain alpha-plutonium material. The titanium tip is used to provide a material strong enough to produce plastic strain in the T-Ampoule specimen, and to provide additional data for the strain locus in the strain-based failure criteria.

Photos of the actual test setup are shown in Figures 2-24 and 2-25. Figure 2-24 shows the complete test assembly prior to the test. The impactor, suspended over the actuator track using Kevlar string has been meticulously aligned so that it impacts the center of the titanium cup. Figure 2-25(a) shows a close-up view of the titanium cup and TB-1 fixture bolted to the actuator sled, and Figure 2-25(b) shows a close-up view of the suspended impactor.

Additional impact tests were performed using the Drop Table Shock Machine, DT-45, located in Building 860 in Area I. A schematic view of the drop table is presented in Figure 2-26. The DT-45 is capable of a velocity change of 150 ft/s and a peak acceleration of 20,000 g. The pulse durations range from 0.2 to 150 ms. In this test, the test item is attached to the carriage assembly, which is raised above the reaction mass. Upon release, the carriage and the test item are accelerated by gravity and a series of bungee cords. The accelerated items strike a stack of programming material (typically wool felt) which is placed on top of the reaction mass to produce the desired shock pulse.

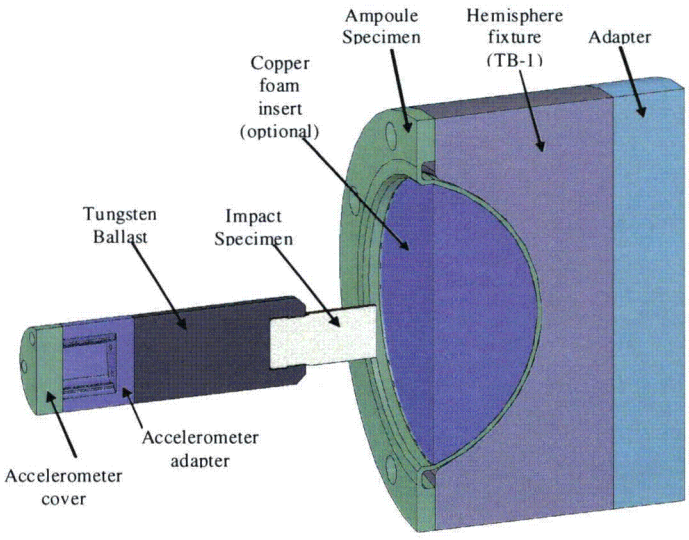

Figure 2-23. Cross-Section of Impactor Assembly and TB-1/Ampoule Assembly[1]

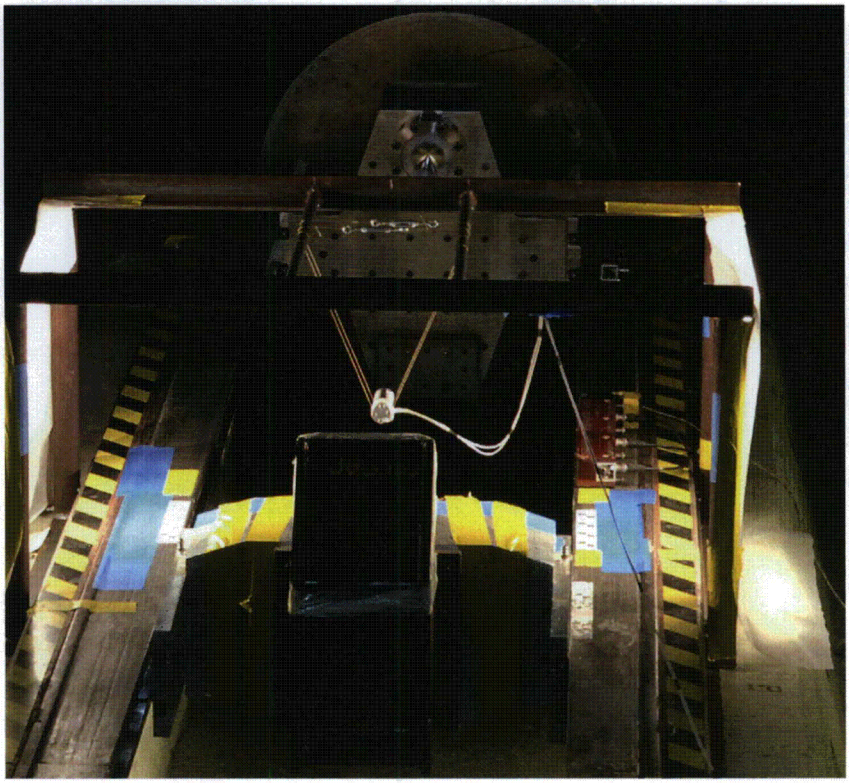

Figure 2-24. Complete Test Assembly Prior to the Test

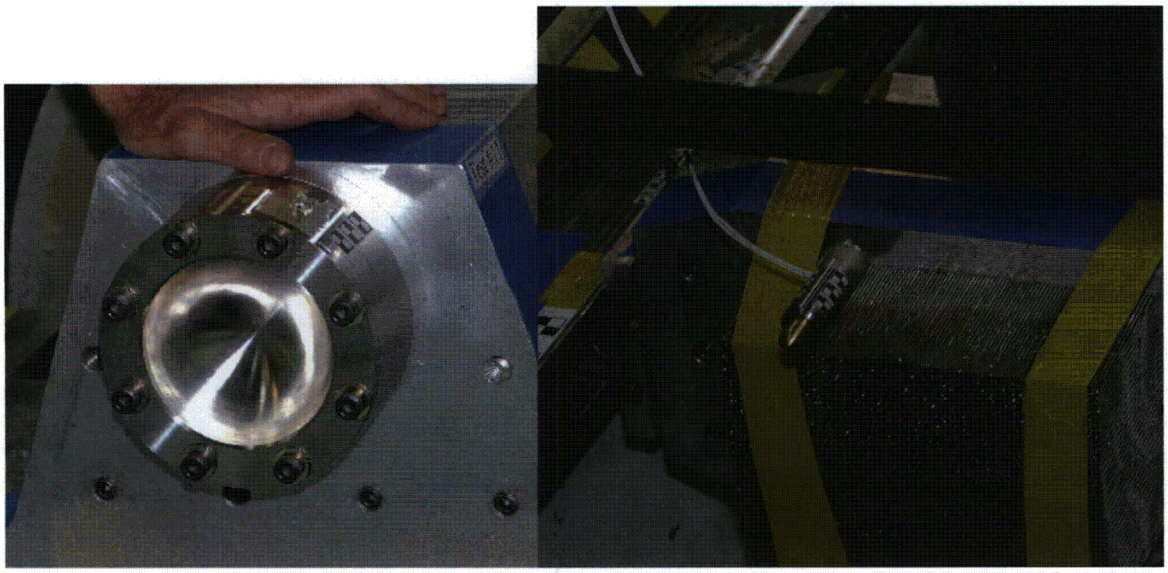

Figure 2-25. (a) Titanium Ampoule and TB-1 Fixture Attached to Actuator Sled; (b) View of Suspended Impactor

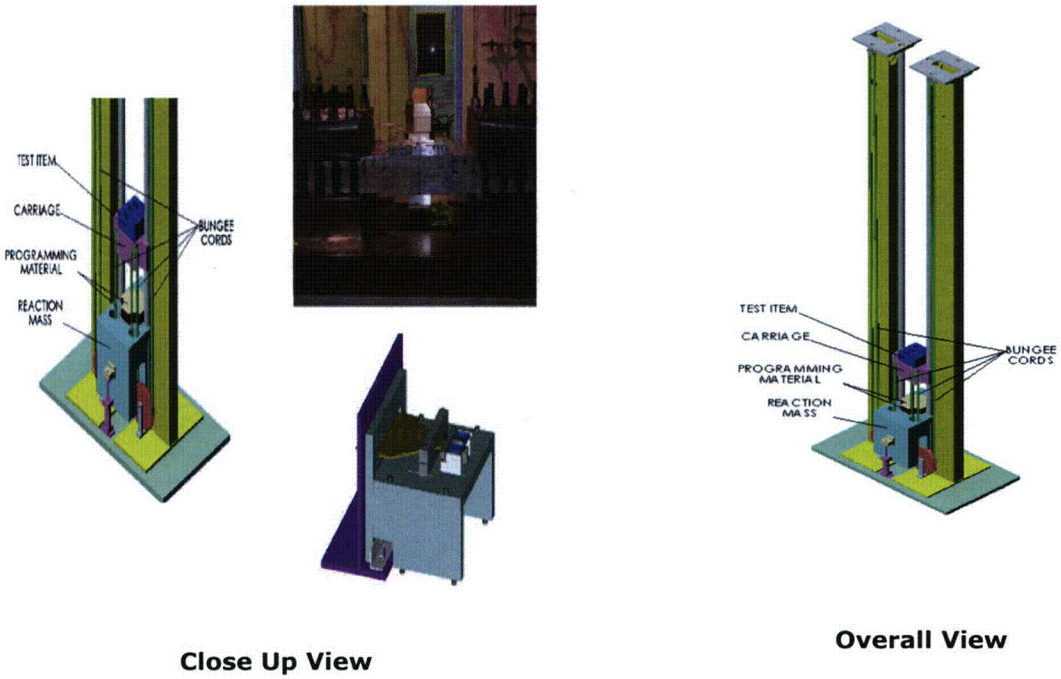

Figure 2-26. DT-45 Drop Table Shock Machine

A solid model of the ampoule test assembly for the drop table test is shown in Figure 2-27. The same type T-Ampoule specimen from the actuator tests is used in this test. The sample specimen is bolted to an adaptor plate, which is attached to the carriage. A 20 lb. crush plate is placed on top of the ampoule. During the deceleration of the carriage, the crush plate will compress and buckle the ampoule test specimen before it strikes the stop blocks. A photograph of the test assembly, prior to testing, is presented in Figure 2-28.

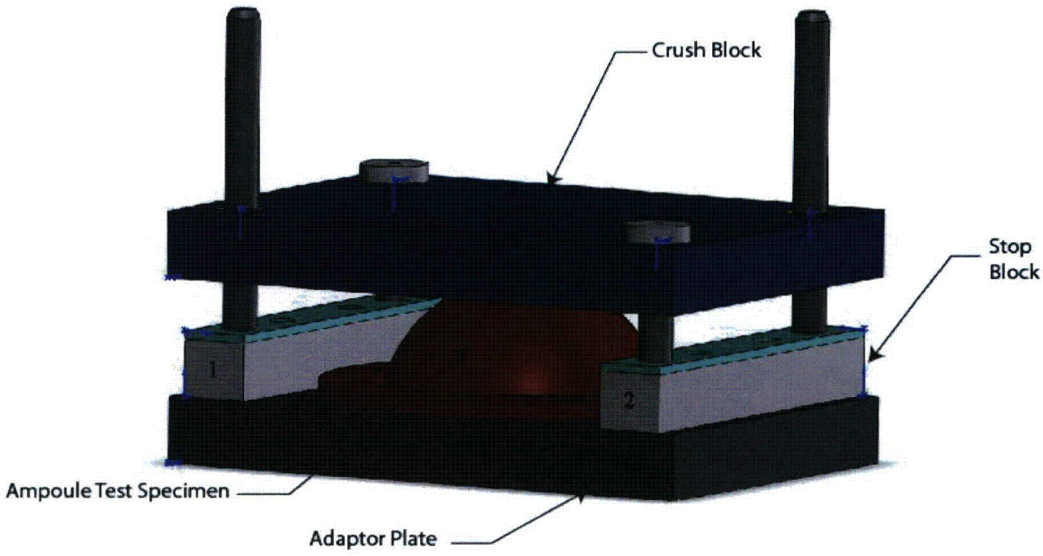

Figure 2-27. Solid model of the Ampoule Test Assemble for Drop Table Tests

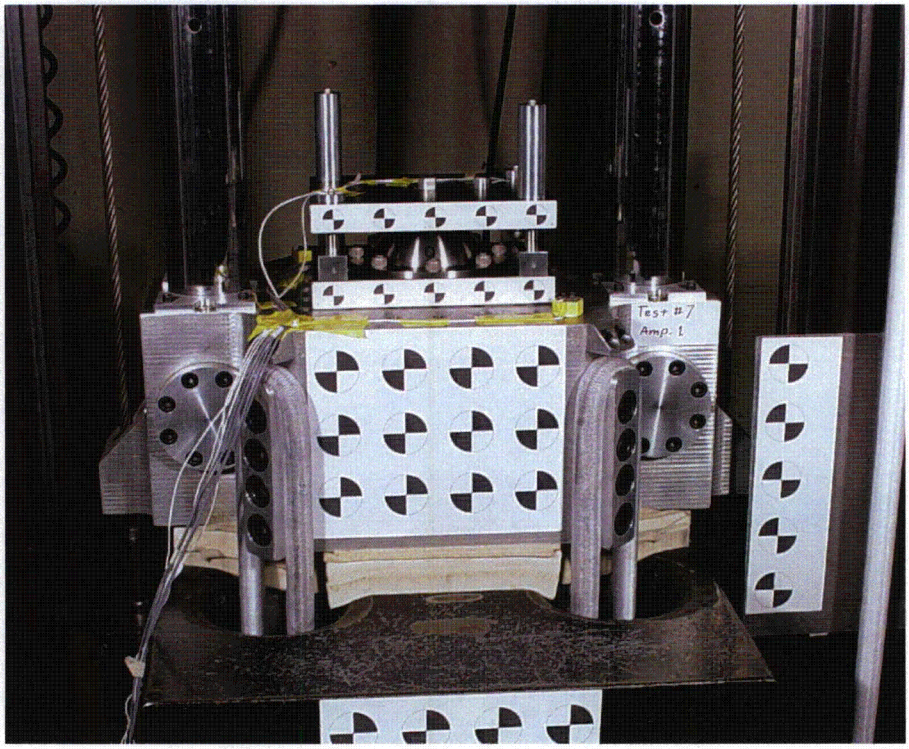

Figure 2-28. Photograph of Ampoule Test Assembly Prior to Testing

2.12.3.1.1 Brass Actuator Test Finite Element Model

The brass actuator test, finite element model provides additional validation of the PRONTO3D finite element code. The finite element model of the brass-tipped impactor and test fixture, shown in Figure 2-29(a) is a three-dimensional model composed of hexahedral elements. There is a plane of symmetry through the center of the model (Z=0), which contains 395,000 elements. The constitutive model of the brass material is given in Section 2.12.4.

The deformed mesh for an impact velocity of 175 ft/sec is shown in Figure 2-29(b). The maximum plastic strain in the ampoule is shown in Figure 2-30. A maximum value of 1% is calculated directly under the point of impact. The change in thickness of the ampoule at the point of impact is 0.00035 in. This is very close to the 0.0002-0.0005 in. measured in the impact tests.[1]

Figure 2-31(a) and (b) present a close-up view of the impactor mesh and the final deformed shape, along with the equivalent plastic strain in the impactor tip. As shown in the figure, very large strains of over 80% are produced in the center of the brass tip. Figure 2-32 shows the deformed tip overlaid on the deformed experimental specimen. The two deformed shapes match extremely well. Finally, a comparison of the acceleration measured in the experiment with the acceleration determined from the analysis is presented in Figure 2-33. The acceleration data from the analysis is determined by taking the nodal velocity of a node in the brass tip, differentiating it, and then filtering it, at the same frequency as the original acceleration data from the impact test. As shown in the figure, the two sets of data match very well.

(a)

(b)

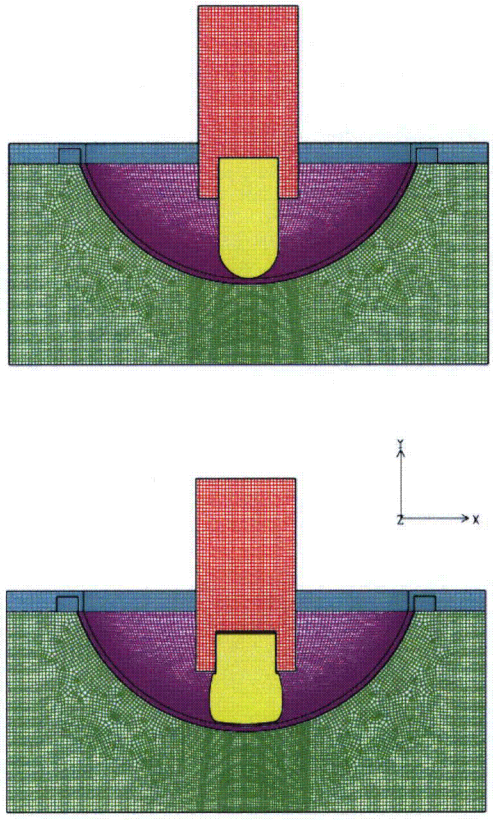

Figure 2-29. Finite Element Model for the Brass Impact Test

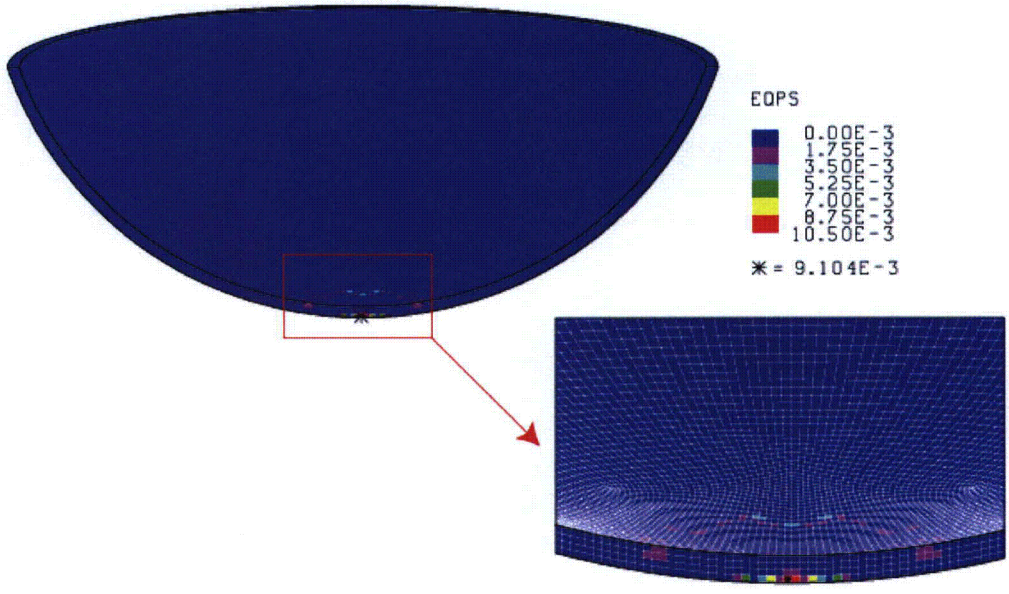

Figure 2-30. Equivalent Plastic Strain in the Ampoule Dish at an Impact Velocity of 175 ft/sec

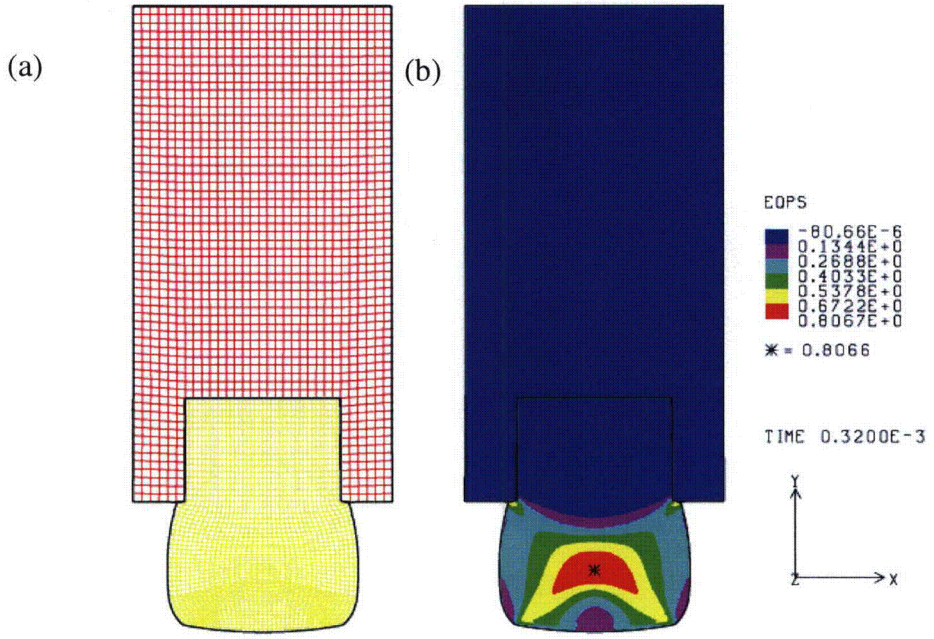

Figure 2-31. Deformed Shape of and Plastic Strain in the Brass-Tipped Impactor at an Impact Velocity of 175 ft/sec

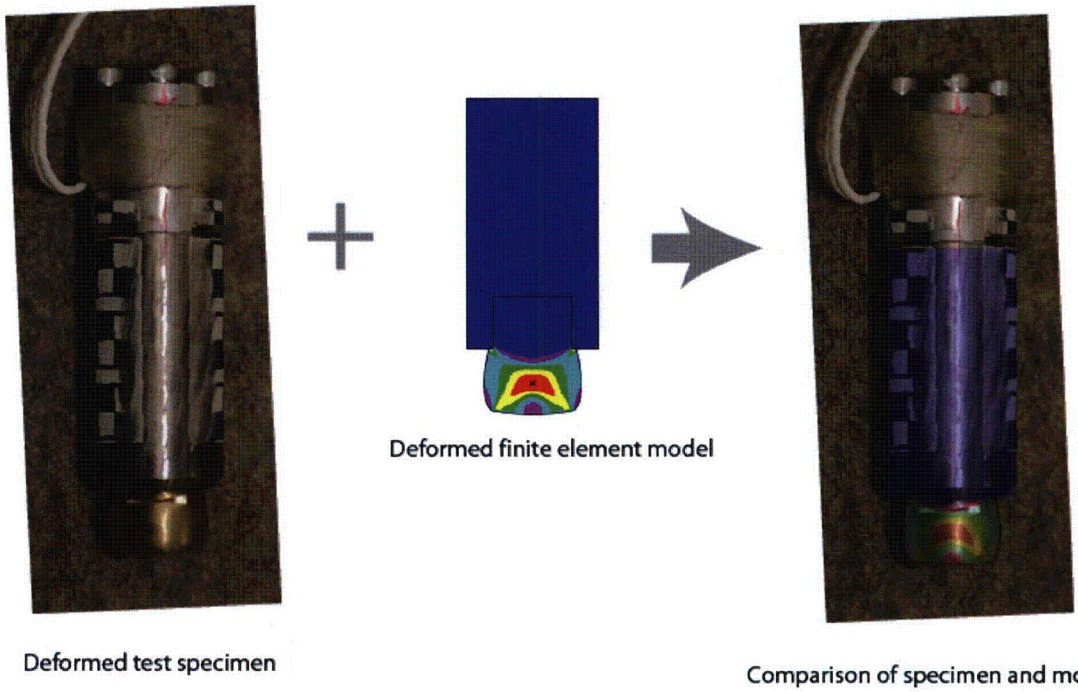

Figure 2-32. Deformed Shape of the Brass Impactor Overlaid on the Test Specimen

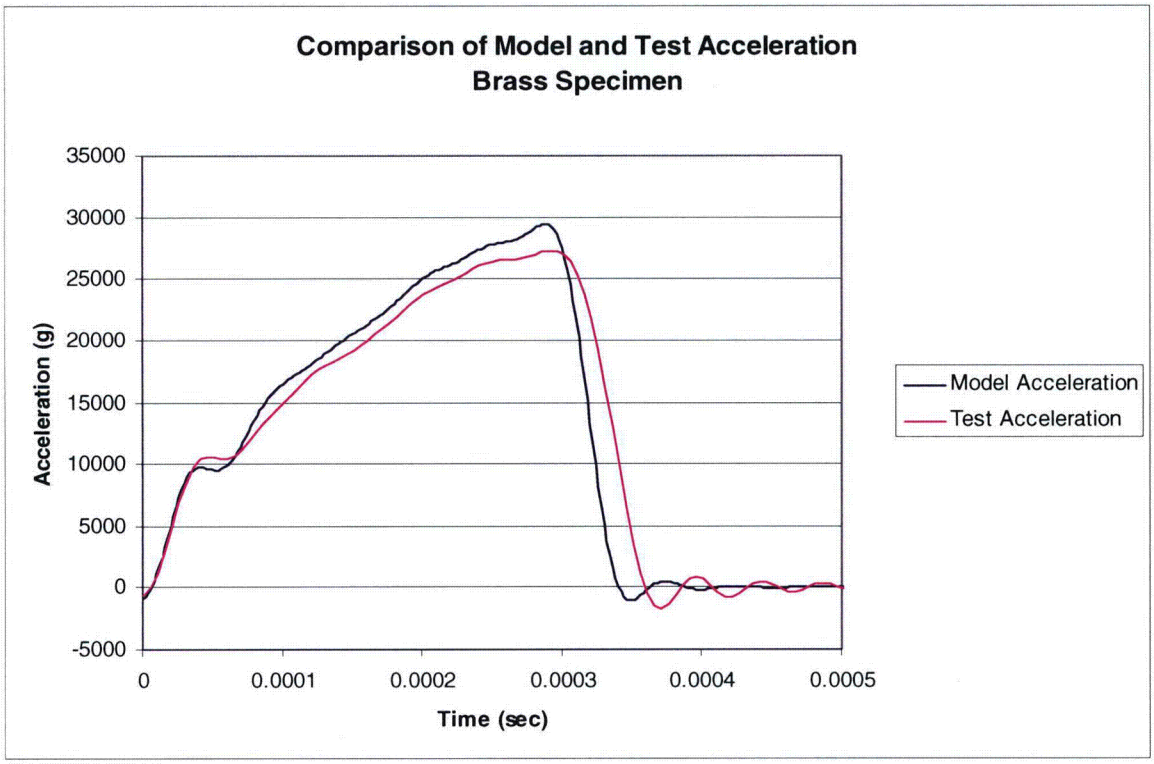

Figure 2-33. Comparison of the Brass-Tipped Impactor Acceleration from the Test and the Finite Element Model

2.12.3.1.2 Titanium Actuator Test Model

The purpose of the titanium-tipped impact model is to provide data for the strain locus used in the strain-based acceptability criterion. This data is obtained from both the T-Ampoule specimen and the tip of the impactor. The finite element model for the actuator titanium test is the same as those used in the brass, except for the constitutive model of the tip material. The constitutive model for the titanium tip is given in Section 2.12.4.

The deformed mesh of the titanium-tipped impactor for an impact velocity of 200 ft/sec is given in Figure 2-34. The maximum equivalent plastic strain and deformation in the ampoule specimen is presented in Figure 2-35. The maximum deformation of the ampoule under the tip of the impactor is 0.010 in., which is in good agreement with the 0.006 – 0.009 in. of deformation measured in the test specimens.[1] The maximum calculated plastic strain in the titanium cup is 17%. Figure 2-36 presents a close-up view of the deformed impactor along with the equivalent plastic strain in the impactor tip. As shown in the figure, very large strains of greater than 50% are produced in the center of the titanium tip. Figure 2-37 shows the deformed shape of the titanium impactor overlaid on the deformed experimental specimen. There is very good agreement between the experiment and the analysis.

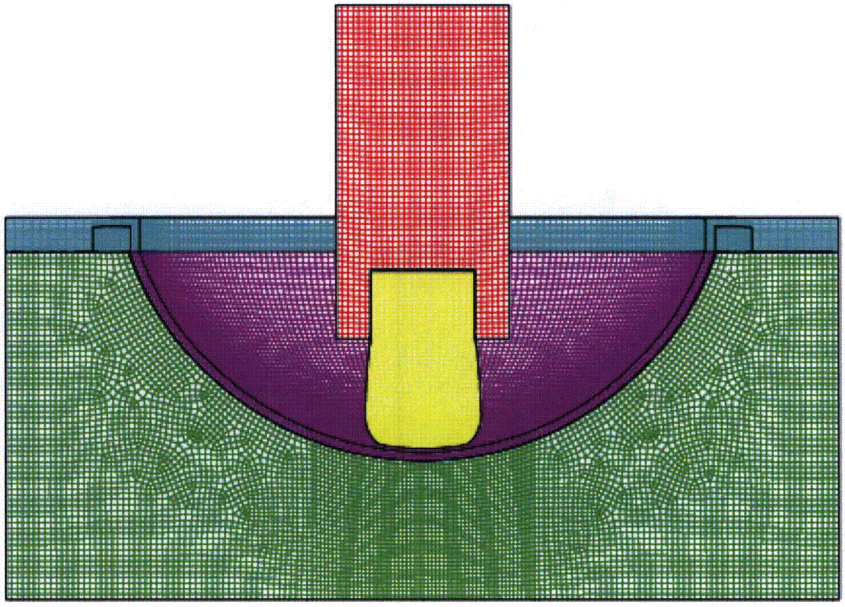

Figure 2-34. Deformed Mesh of the Titanium Tipped Impactor, at an Impact Velocity of 200 ft/sec

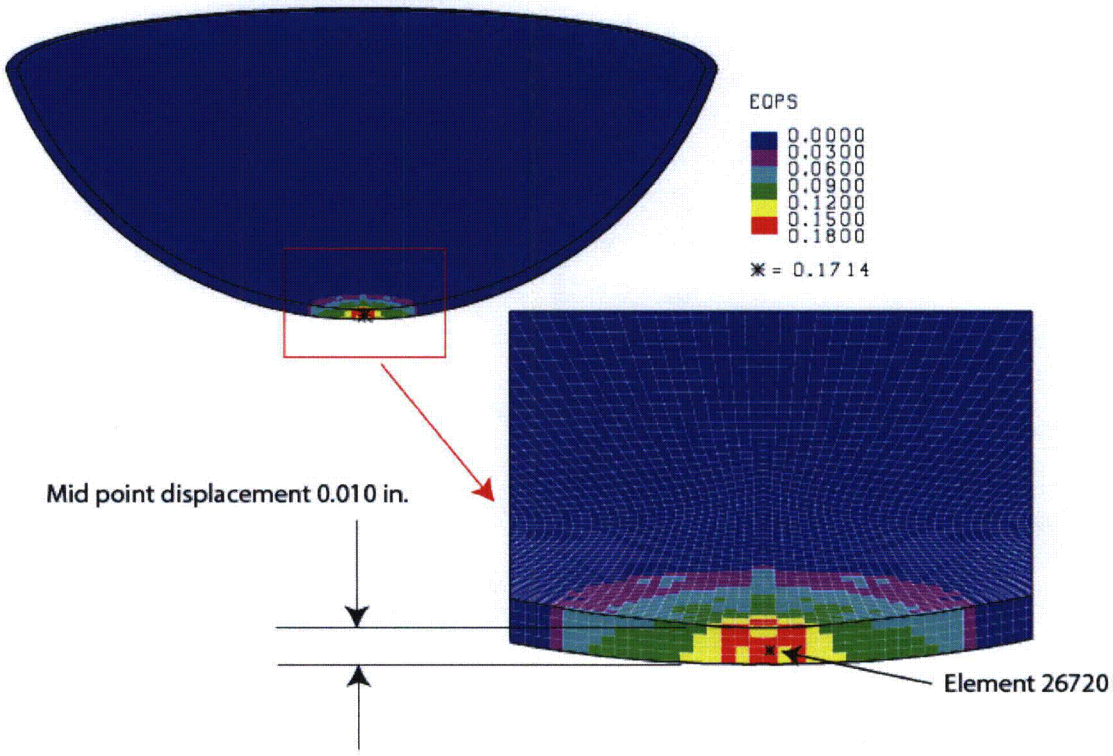

Figure 2-35. Equivalent Plastic Strain in the Ampoule Dish at an Impact Velocity of 200 ft/sec with a Titanium Tipped Impactor

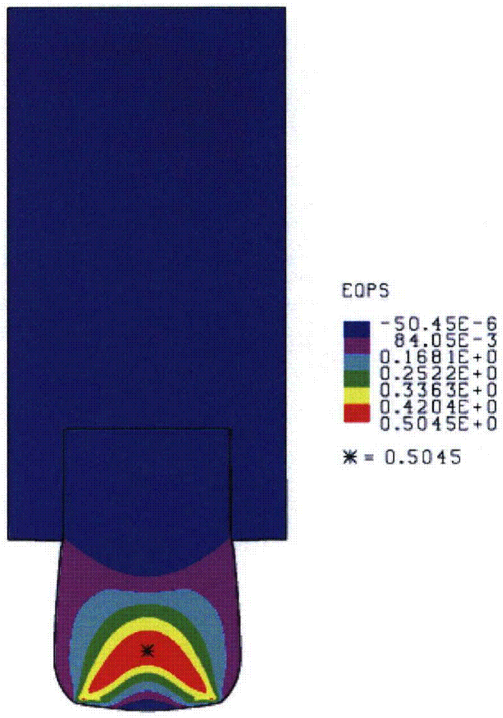

Figure 2-36. Deformed Finite Element Mesh of Titanium Impactor with Contours of Equivalent Plastic Strain

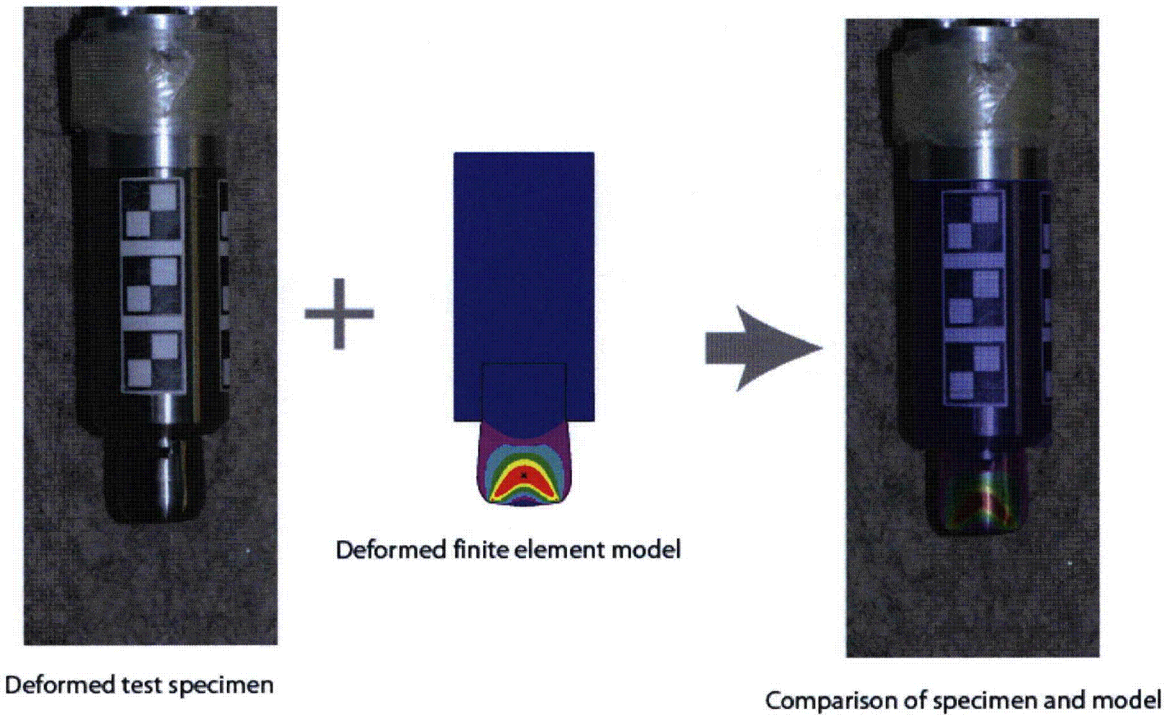

Figure 2-37. Deformed Shape of the Titanium Impactor Overlaid on the Test Specimen

2.12.3.1.3 Drop Table Test Finite Element Model

The purpose of the titanium ampoule drop table test is to provide additional data for the strain locus used in the strain-based failure criterion. This data is obtained as the result of the strain induced by buckling of the T-Ampoule specimen. The finite element model for the drop table test is shown in Figure 2-38. This is a three-dimensional model composed of hexahedral elements. There is a plane of symmetry through the center of the model (Z=0), and the model contains 297,000 elements. The constitutive model of the titanium material is given in Section 2.12.4. The crush plate and the adaptor plate are modeled as an elastic carbon steel material.

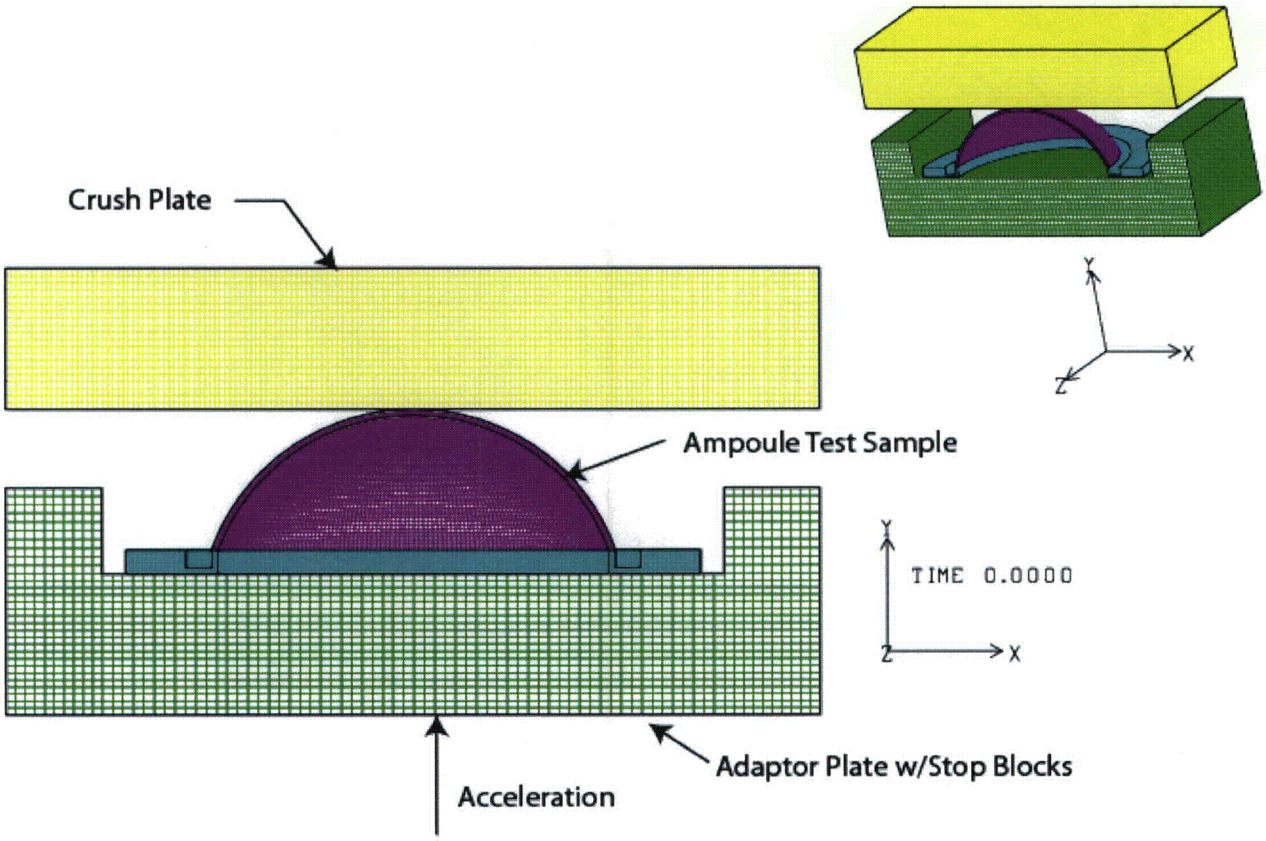

Figure 2-38. Finite Element Model of the Drop Table Ampoule Test

Figure 2-39 documents the drop table carriage acceleration recorded during the pretest calibration of the drop table. This acceleration was applied to the adaptor plate in the finite element model. The resulting deformation from the analysis is presented in Figure 2-40. The crush plate compresses the ampoule test specimen and contacts the stop blocks. There is a small quantity of elastic deflection of the crush plate, which increases the total crush of the ampoules. Post-test photographs of the ampoule test specimen are shown in Figure 2-41.

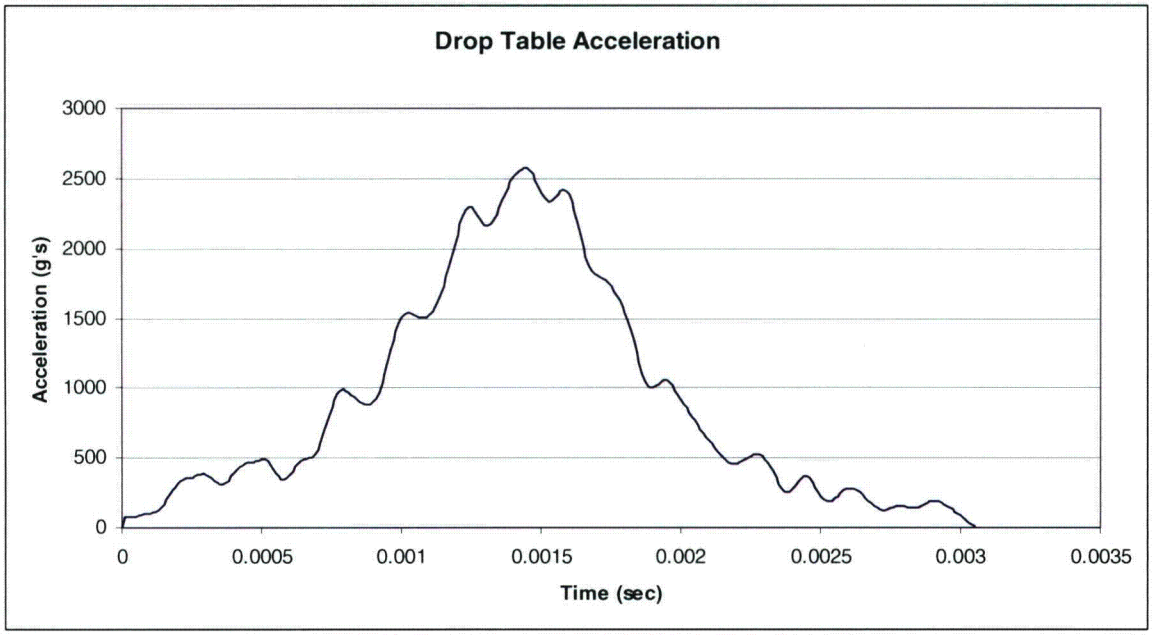

Figure 2-39. Drop Table Acceleration

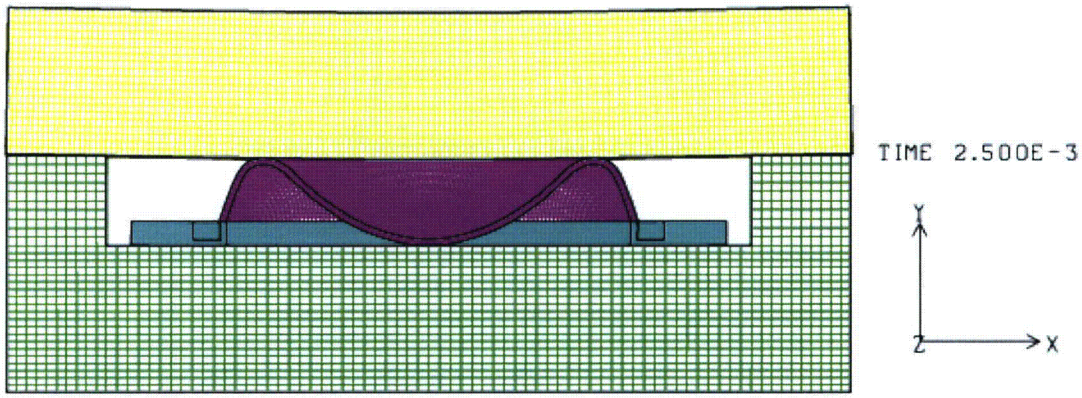

Figure 2-40. Finite Element Results Showing the Deformed Shape of the Ampoule Test Specimen

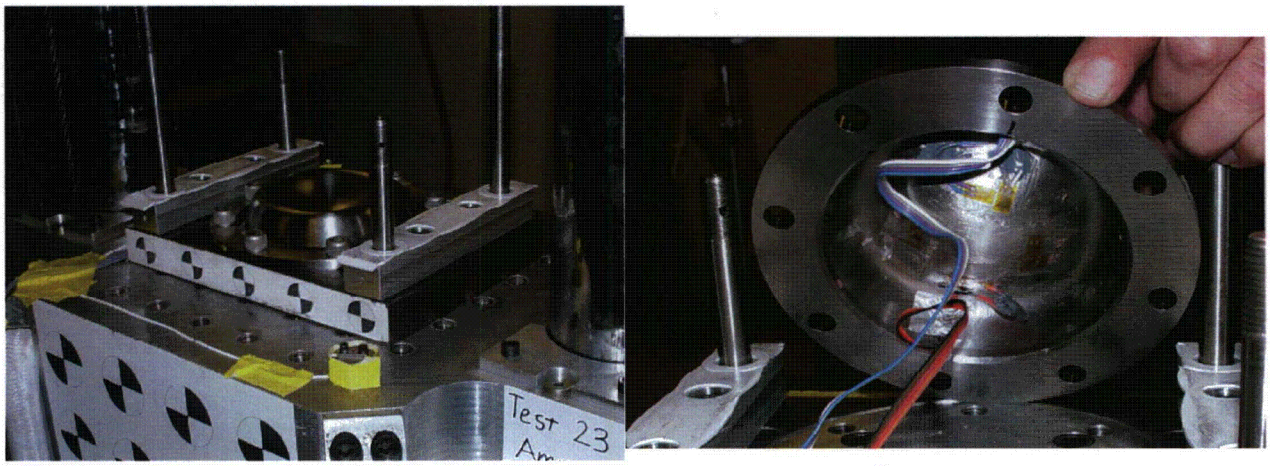

Figure 2-41. Photographs of the Deformed Ampoule Specimen (a) Top View (b) Inner Surface

The maximum calculated equivalent plastic strain is shown in Figure 2-42. A maximum value of 19.4% is found on the inside surface of the ampoule test specimen. Strain gauges were placed on the inside of the ampoule test specimen at a radius of 0.8 in. Figure 2-43 shows the nominal radial strain in an element at this location along with the data from the strain gauges. Due to the reversal in strain along the inside surface of the ampoule, the strain gauges detached halfway through the test. However, comparison of the nominal radial strain in the element to the strain measured by the gauges prior to failure shows good agreement.

Figure 2-42. Maximum Equivalent Plastic Strain in Sample Test Specimen

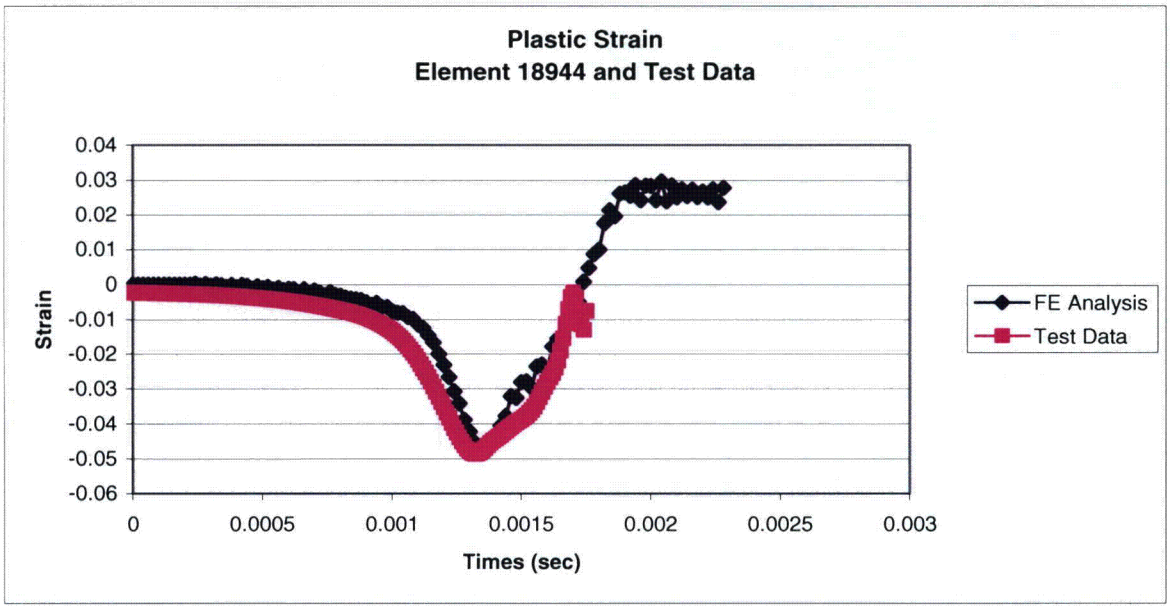

Figure 2-43. Nominal Element Radial Strain Compared to Strain Gage Data

Figure 2-44 shows the deceleration of the crush plate during the test and the deceleration calculated in the analysis. The impact of the crush plate with the stop blocks produced resonance in the accelerometers, which corrupted the data beyond this point. However, the two curves show good agreement during the crushing of the test ampoule specimen.

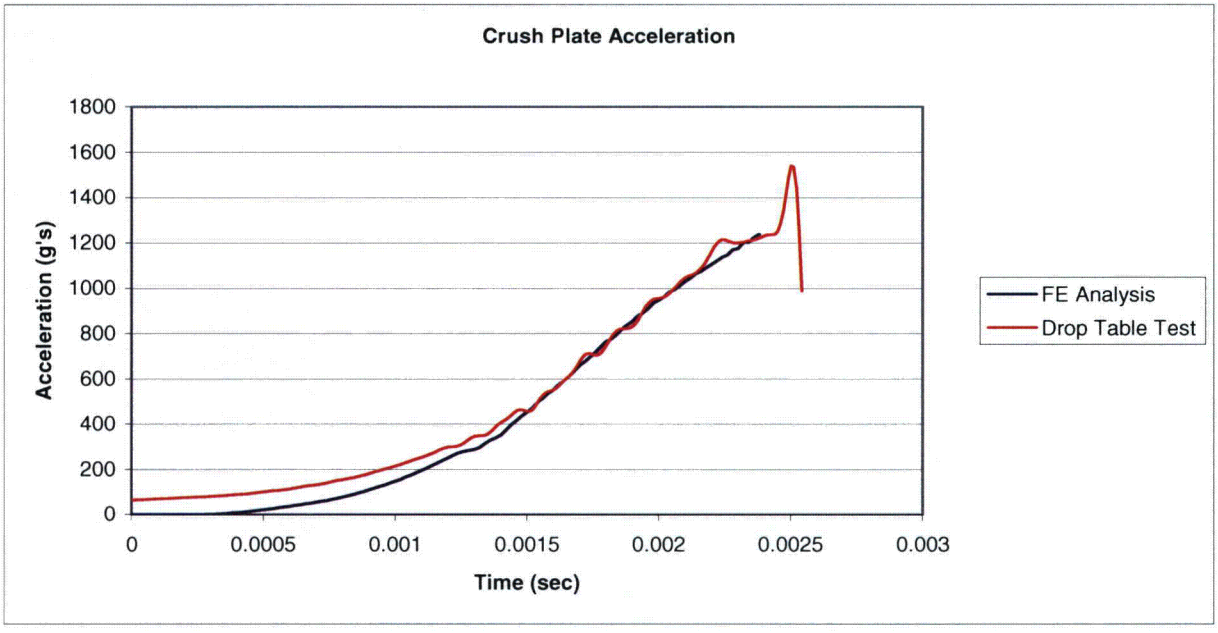

Figure 2-44. Crush Plate Acceleration

2.12.3.2 Strain-Based Failure

2.12.3.2.1 Discussion

Bridgman performed the seminal work on the effect of hydrostatic pressure on ductile rupture in the 1940s and 1950s.[4] He conducted over 350 tensile tests, on 20 different types of steel, of different heat treatments. These experiments showed that the strain to fracture is an increasing function of the superposed hydrostatic pressure. Brozzo, et al., simulated failure for the sheet metal forming industry and also noted that ductility diminishes with the hydrostatic stress.[3] Their experience with simulating testing to failure led to the following failure index:

$$I = \int_0^{\bar{\varepsilon}_{pf}} \frac{2\sigma_{\max}}{3(\sigma_{\max} - \sigma_m)} d\bar{\varepsilon}_p \qquad (2\text{-}6)$$

where σ_{max} is the maximum principal stress, σ_m is the average of the three principal or normal stresses, $\bar{\varepsilon}_p$ is the equivalent plastic strain, and $\bar{\varepsilon}_f$ is the equivalent plastic strain at failure.

This work was further developed by Johnson and Cook,[5] who developed fracture models for OFHC copper, Armco iron, and 4340 steel using notched tensile specimens. Their model contained three primary terms: one with a dimensionless strain rate; one for dimensionless temperature; and one with a dimensionless pressure-stress ratio $\sigma^* = \frac{\sigma_m}{\bar{\sigma}}$, where σ_m is the average of the three normal stresses and $\bar{\sigma}$ is the von Mises equivalent stress. The pressure-stress ratio is commonly referred to as the stress triaxiality. In their work, Johnson and Cook[5] noted:

> "It would appear that the pressure-stress ratio is of primary importance. As the hydrostatic tension is increased, the strain to fracture decreases rapidly. The strain rate and temperature effect appear to be less important."

Figure 2-45 shows a plot of the data developed by Johnson and Cook and the corresponding curves developed in their failure models.

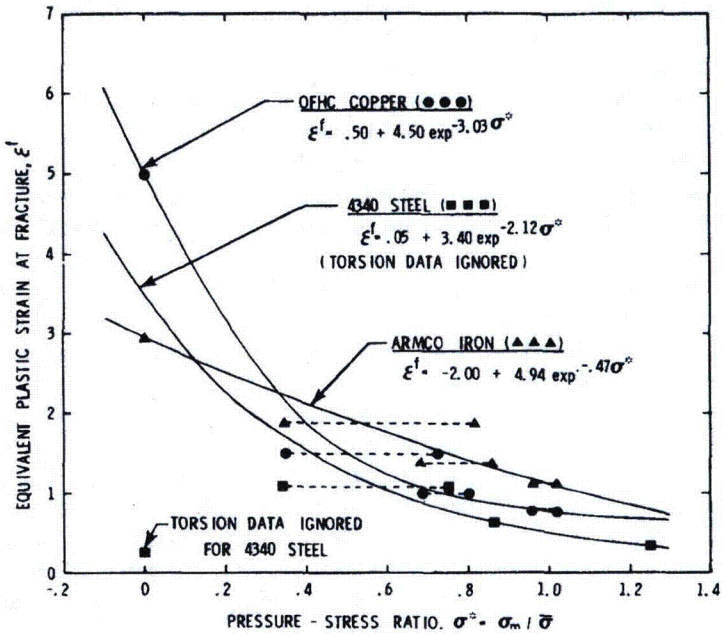

Figure 2-45. Plastic Strain versus Stress Triaxiality from Johnson and Cook[5]

More recently, Bao[7] developed a new criterion for ductile crack formation. This work is based on extensive testing of 2024-T351 aluminum. He developed the failure locus in stress triaxiality–equivalent plastic strain space shown in Figure 2-46, based on calculating the average stress triaxiality as:

$$\left(\frac{\sigma_m}{\bar{\sigma}}\right)_{av} = \frac{1}{\varepsilon_f}\int_0^{\bar{\varepsilon}_f} \frac{\sigma_m(\bar{\varepsilon})}{\bar{\sigma}(\bar{\varepsilon})} d\varepsilon \qquad (2\text{-}7)$$

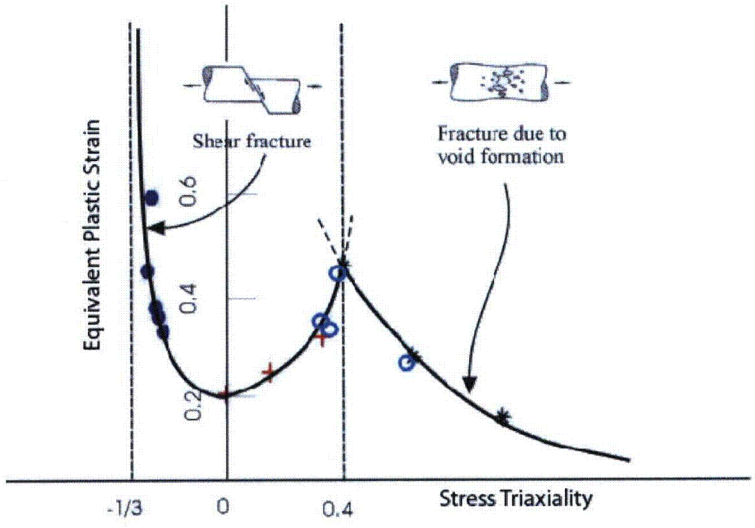

Figure 2-46. Stress Failure Locus of Al2024-T351 Developed from Bao[7]

In addition, using this formulation along with the data from Bridgman,[3] Bao and Wierzbicki[8] were able to show the existence of a limit in the negative average stress triaxiality space of -1/3, below which failure of the specimens never occurred. This limit is shown in Figure 2-46, as well as in Figure 2-47, which Bao and Wierzbicki showed to be generally true for numerous tested ductile metals. This figure also shows the different failure modes common to shear versus biaxial tension regions of stress triaxiality.

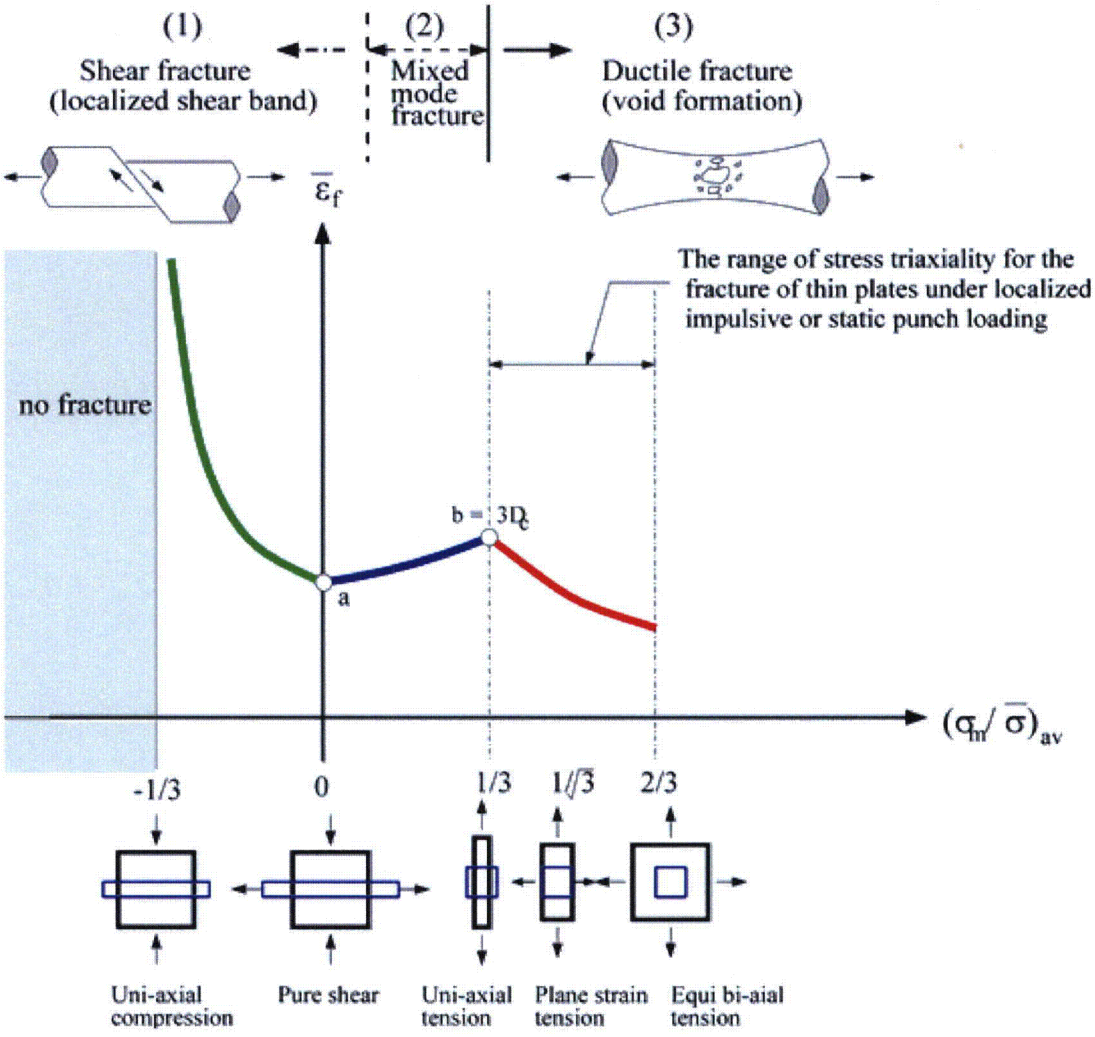

Figure 2-47. General Failure Locus of Ductile Metals Developed by Bao and Wierzbicki.[8]

2.12.3.3 Strain Locus for Titanium

Using Equation 2-7 and data from the titanium impact tests, a strain locus in stress triaxiality–equivalent strain space is developed for titanium. This strain locus is used along with the finite element analyses of the PAT-1 components (see Section 2.12.5) to determine a margin on fracture, based on equivalent plastic strain, for the T-Ampoule.

Figure 2-48 shows a close-up view of the equivalent plastic strain in the titanium tip from the actuator tests for an impact velocity of 200 ft/sec, and Figure 2-49 presents the equivalent plastic strain in the ampoule from the drop table test. The strains in the tip of the impactor reach a

maximum value of 50% at the center of the specimen, with smaller strains developing along the side. A maximum strain of over 19% is reached in the ampoule during the drop table test. Using the stress and equivalent plastic strain data from the finite element models along with Equation 2-7, the strain locus shown in Figure 2-50 was developed for the elements indicated in Figure 2-48 and Figure 2-49, as well as all the other elements in these models. The friction coefficients between the Ti-6Al-4V impactor and the Ti-6Al-4V simulated T-Ampoule were 0.30 for static friction and 0.36 for dynamic friction.[6] The figure also contains a curve from a finite element model of the tension test, as well as the limit line developed by Bao and Wierzbicki.[8] It should be noted that this is not a failure locus, since no cracks were formed in the tests. However, it does represent regions in strain space where failure does not occur; therefore, the part is safe. In this sense, the data from the PAT-1 package impact analyses (see Section 2.12.5) can be compared with the locus in Figure 2-50, and a safety margin based on the strain generated in the test can be calculated.

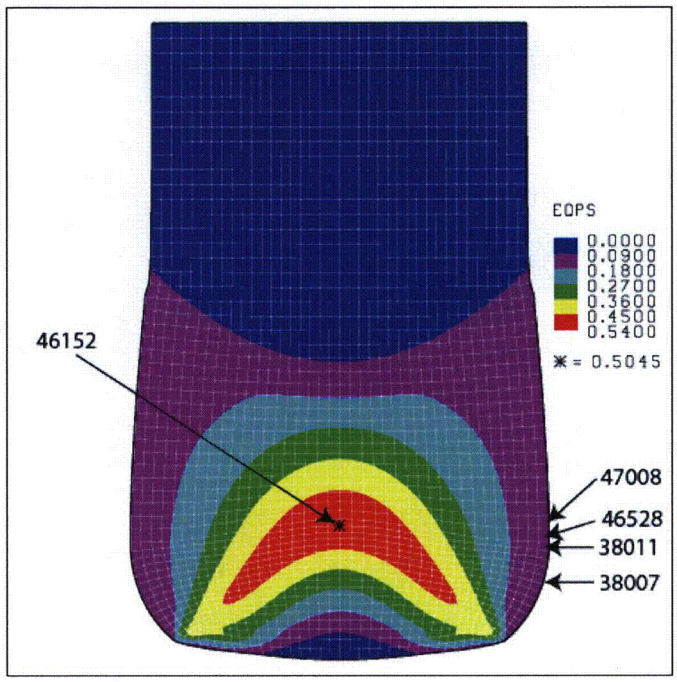

Figure 2-48. Equivalent Plastic Strain in the Titanium Tip for an Impact Velocity of 200 ft/sec

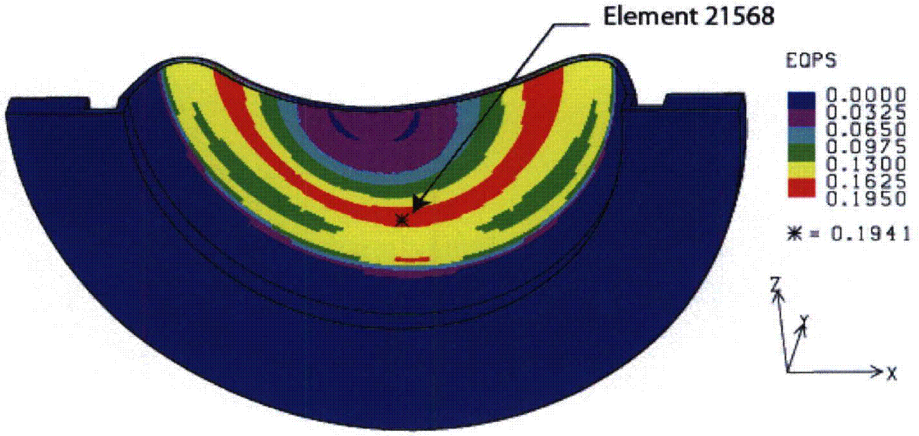

Figure 2-49. Equivalent Plastic Strain in the Titanium Ampoule in the Drop Table Test

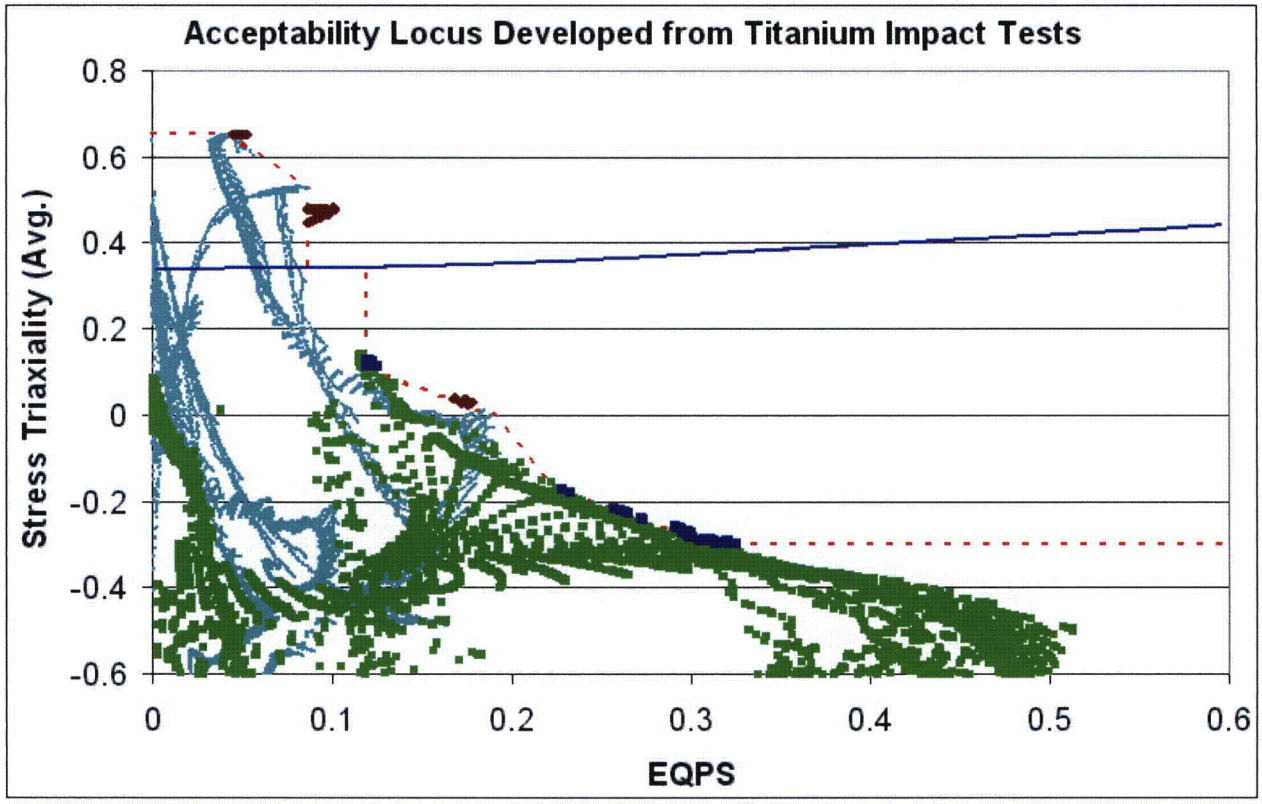

Figure 2-50. Locus in Equivalent Plastic Strain–Stress Triaxiality Space Developed from Titanium Impact Tests

2.12.3.4 Bounding Examples

To illustrate the construction of the locus in Figure 2-50, the development of the two bounding curves (maximum tension and maximum compression) will be presented in the following section. The maximum compression curve is derived using data for Element 46152 and data generated in the titanium impact test. The tension test curve is derived from a separate tension

test and a finite element model of the test, which was originally conducted to gather material data for the constitutive model.

2.12.3.5 Curves for Element 46152

The development of the average stress triaxiality function for the strain locus was done as a post-processing operation. First, the stress triaxiality, as defined in Equation 2-8, is calculated as a function of time using the element integration point stress

$$\frac{\sigma_m}{\overline{\sigma}} \tag{2-8}$$

Where σ_m is the average of the three normal stresses and $\overline{\sigma}$ is the von Mises equivalent stress. A plot of this function for Element 46152 is shown in Figure 2-51, along with the equivalent plastic strain. Next, the stress triaxiality is plotted as a function of equivalent plastic strain as shown in Figure 2-52. Then, using Equation 2-9, the average value of the stress triaxiality function over the interval of plastic strain is determined. The average stress triaxiality for Element 46152 as a function of plastic strain is also plotted in Figure 2-52.

$$\frac{1}{b-a}\int_a^b f(x)\,dx \quad \text{on the interval} \quad a \le x \le b \tag{2-9}$$

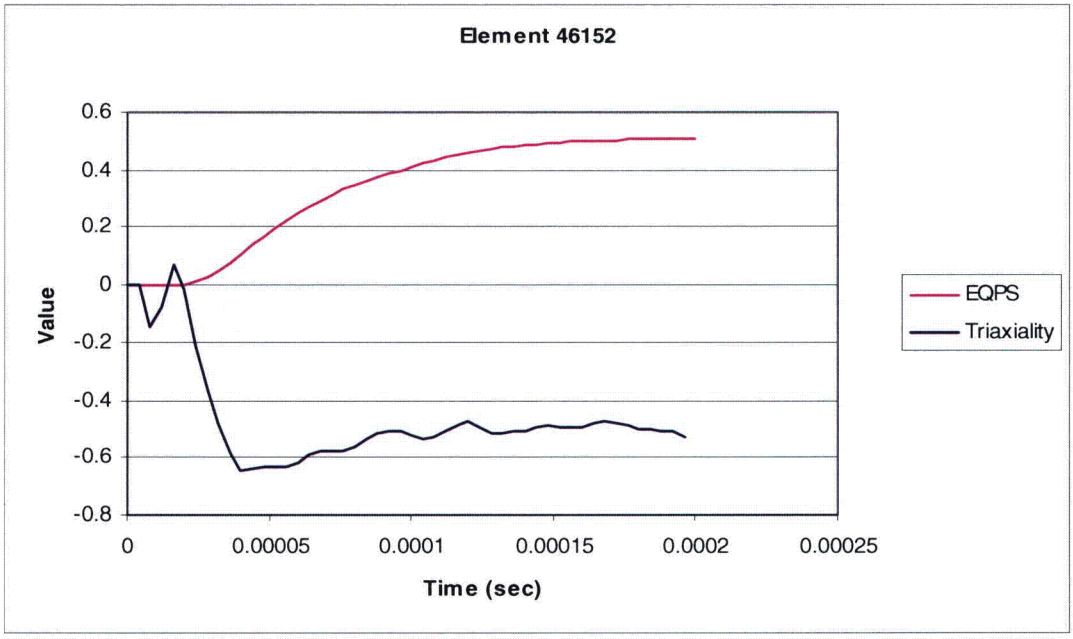

Figure 2-51. Stress Triaxiality and Equivalent Plastic Strain versus Time for Element 46152

2.12.3.6 Titanium Tension Test

A finite element analysis was conducted of the titanium test specimen. The analysis was performed using the SNL-developed finite element code JAS3D. JAS3D is a nonlinear quasi-static code that uses a conjugate gradient solver to solve the equation of equilibrium. The finite element model is shown in Figure 2-53(a). The model is an axi-symmetric, quarter-symmetry model with two planes of symmetry. The model is loaded by displacing the upper end at a constant rate. The mesh contains 1804 elements and is refined heavily along the center symmetry plane.

Figure 2-53(b) shows the deformed mesh at a point where the cross-sectional area at the centerline matched the reduction in area at failure during the tensile test. Figure 2-53(c) gives the distribution of plastic strain for this same configuration. The maximum plastic strain occurs in the center of the specimen and has a magnitude of 63%.

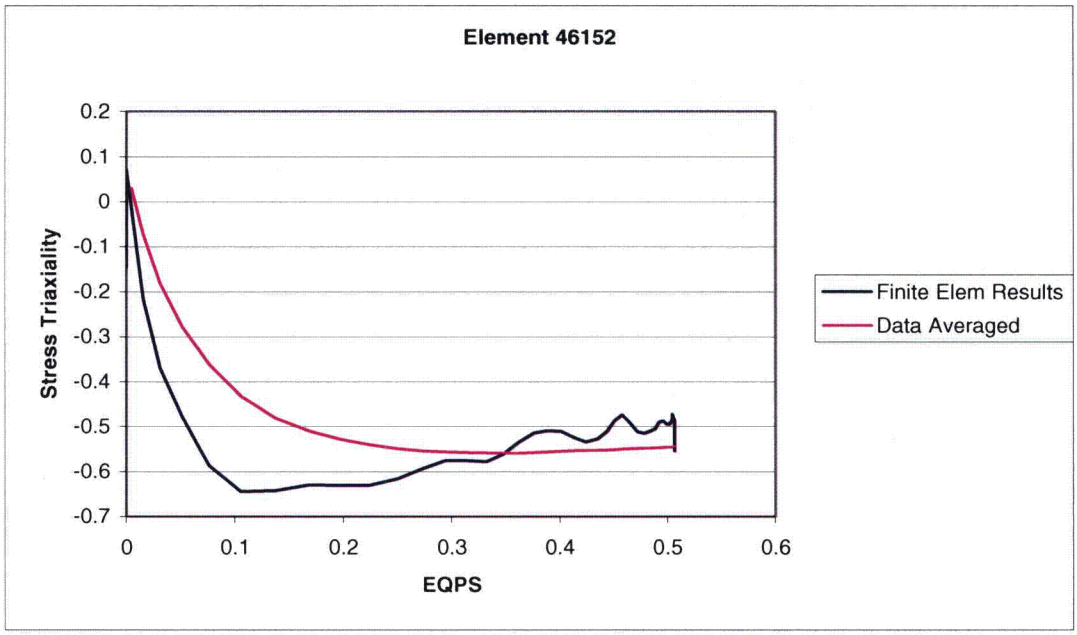

Figure 2-52. Stress Triaxiality and Average Stress Triaxiality as a Function of Equivalent Plastic Strain for Element 46152

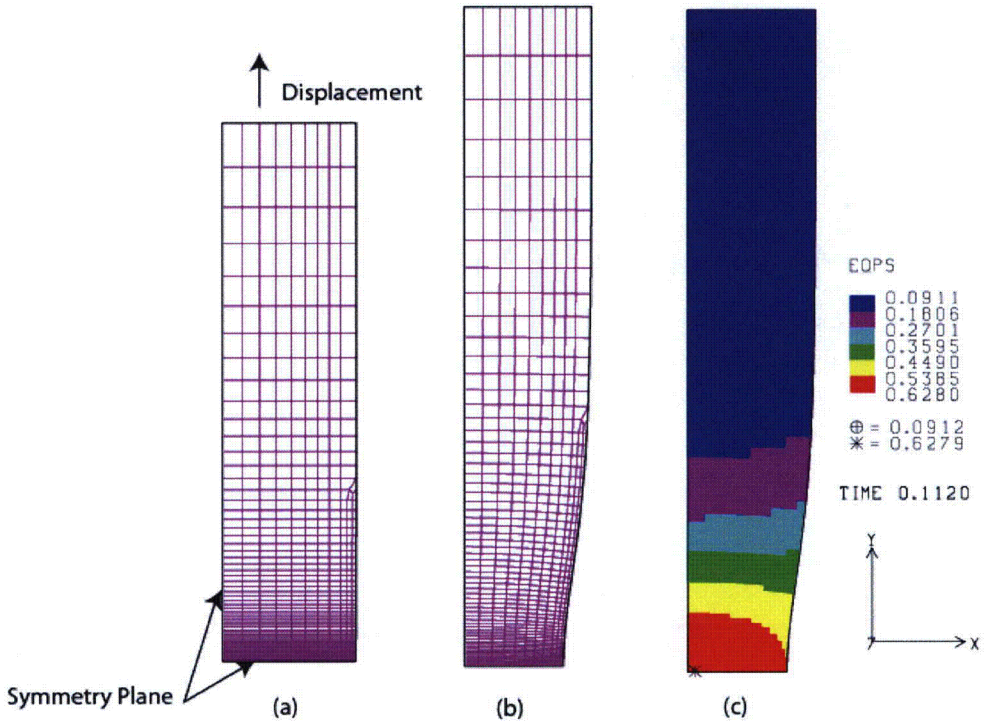

Figure 2-53. Finite Element Model of Titanium Tensile Test Specimen (a) Original Mesh (b) Deformed Mesh (c) Equivalent Plastic Strain

The plastic strain in the highest stressed element as a function of the specimen displacement is shown in Figure 2-54 along with the stress triaxiality. A plot of the stress triaxiality versus plastic strain for this element is presented in Figure 2-55, along with the averaged stress triaxiality.

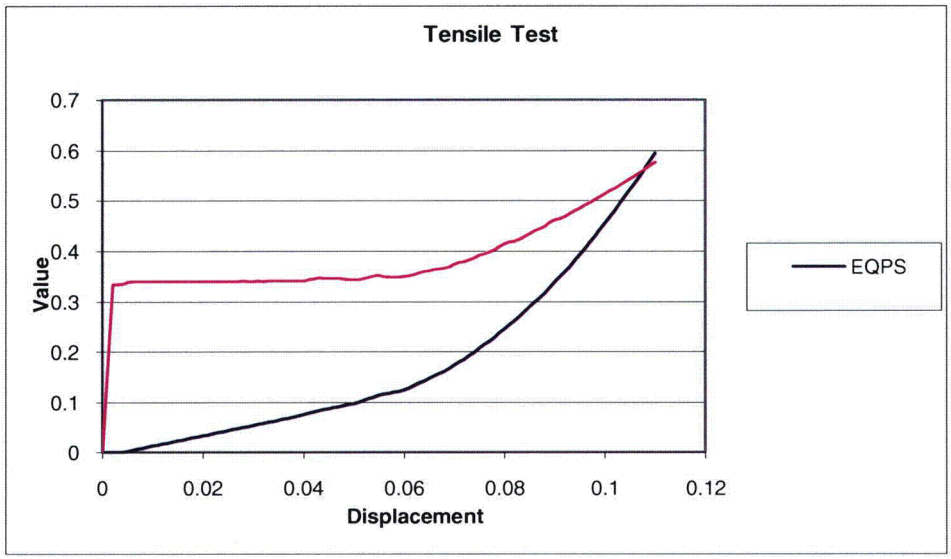

Figure 2-54. Stress Triaxiality and Equivalent Plastic Strain versus Displacement for Center Element

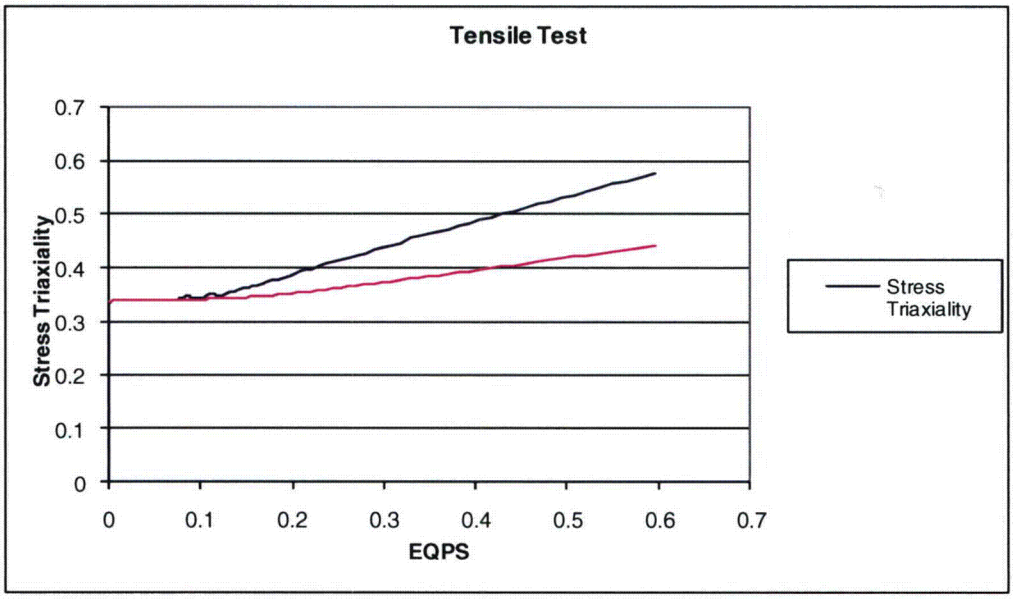

Figure 2-55. Stress Triaxiality and Average Stress Triaxiality as a Function of Plastic Strain for the Highest Stressed Element

2.12.3.7 Alternate Failure Criteria Used to Model Failure in Sample Containers and T-Ampoule

Prior to the work of Bao and Wierzbicki, Wellman et al.[10] and Dawson et al.[11] developed a failure criterion, which also uses an evolution equation based on the plastic strain. This model has been implemented in the PRONTO3D finite code under the material model Ductile Tearing. This is a power-law-hardening model with a ductile failure criterion. The ductile failure criterion is based on an evolution equation in which the plastic strain increment, scaled by the stress ratio, is accumulated until a critical value is reached, at which point the initiation of the ductile tearing is predicted. The evolution equation calculates the Tearing Parameter (TP) as follows:

$$TP = \int_0^{\bar{\varepsilon}_p} \left(\frac{\langle \sigma_{\max} \rangle}{(\sigma_{\max} - \sigma_m)} \right)^4 \qquad (2\text{-}10)$$

where $\bar{\varepsilon}_p$ is the plastic strain at failure in a tensile test, $\sigma_{\max}$ is the maximum principal stress, and σ_m is the mean (hydrostatic) stress. Note that Tearing Parameter is identical to the failure indicator Brozzo, et al. developed in the 1970's, with the exception of the 4th power. This was added in the late 1990's at Sandia National Laboratories to not only fit uniaxial tensile test data, but also notched tensile specimens with higher stress triaxiality.[11]

The integral accumulates plastic strain only when the maximum principal stress is positive, as indicated by the Heavyside function brackets, $\langle\ \rangle$. Thus, plastic strain with a negative maximum principal stress causes no change in the values of TP. Due to restriction of the Heavyside function, regions of positive stress triaxiality cause the integral to accumulate value quickly (the denominator becomes small), which fits well with experimental data showing low plastic strains

to failure in bi- and tri-axial tension for ductile materials. In addition, it is easy to implement, since the critical value of TP for a particular material is established by performing an analysis of a tensile test specimen. The TP for the specimen is then calculated using the computed stress state from the finite element model and substituting the plastic strain-to-failure, $\bar{\varepsilon}_f$, as the upper integration limit. This provides a critical value of TP, which can be used to predict failure in other analyses. The strain-to-failure is computed from the reduction in area of the tensile specimen in the actual tensile test. This ductile Tearing Parameter has been used successfully at Sandia National Laboratories for many years to simulate ductile failure.[11,12,13,14,15,16,17,18]

In the component analyses presented in Section 2.12.5, large plastic strains are developed in the outer shell of the sample containers. To prevent the sample containers from absorbing unrealistic quantities of energy through unrealistic quantities of plastic deformation, a failure criterion was needed to allow the shell to rupture during theses analyses. Since the Ductile Tearing model has already been incorporated in PRONTO3D, and since it performs well in the high stress triaxiality region, it was used in the element death criteria of the sample container models to allow the shells of the sample containers to fracture.

To determine the required failure parameter needed for the Ductile Tearing model, the same tensile test finite element model discussed above was used. The output data was post-processed using Equation 2-10 (and the constitutive model in Figure 2-59, Section 2.12.4.14), and the results of this analysis are presented in Figure 2-56. A value of 1.012 was used in the material model to initiate failure of the sample container shells and this same value is used for comparison with calculated Tearing Parameter values in the eutectic barrier T-Ampoule.

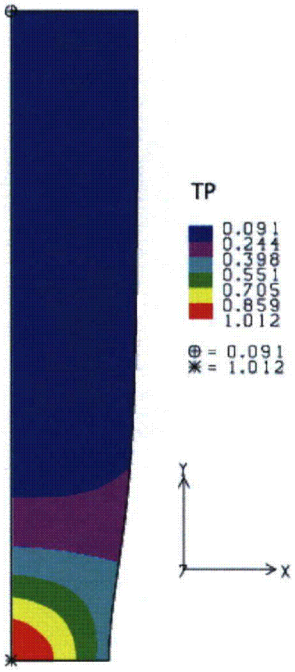

Figure 2-56. Tensile Test Results Showing Peak Value of Failure Parameter TP

2.12.3.8 References

1. Sandia National Laboratories. "Test Report PAT-1/TB-1 Impact Test Series." Albuquerque, NM. August 30, 2007.

2. VanGoethem, D. "PAT-1 Ampoule Drop Table Shock," MECH-678, Sandia National Laboratories. Albuquerque, NM. November 25, 2008.

3. Bridgman, P.W. "Studies in Large Plastic Flow and Fracture" Harvard University Press. Cambridge, MS. 1964.

4. Brozzo, P., Deluca, B., Redina, R.A. "A New Method for the Prediction of the Formability Limits of Metal Sheets," Proceedings of the 7th Biennial Conference of the International Deep Drawing Research Group. 1972.

5. Johnson, G.R., and Cook, W.H., "Fracture Characteristics of Three Metals Subjected to Various Strains, Strain Rates, Temperature and Pressures." *Engineering Fracture Mechanics* 21 (1985):31-48.

6. Sliding and Static Friction Coefficients for Various Materials: http://www.roymech.co.uk/Useful_Tables/Tribology/co_of_frict.htm

7. Bao, Y. "Prediction of Ductile Crack Formation in Uncracked Bodies," Report 100. Impact & Crash Worthiness Laboratory. Massachusetts Institute of Technology, Cambridge, MA. 2003.

8. Bao, Y., and Wierzbicki, T. "On the Cut-Off Value of Negative Triaxiality for Fracture." *Engineering Fracture Mechanics*, 72 (2005): 1049-1069.

9. Wierzbicki, T., Bao, Y., and Teng, X. "High Velocity Impact Fracture." Seminar Presented to Sandia National Laboratories. January 2004.

10. Wellman, G.W., Diegert, K.V., and Salzbrenner, R. "Two-Dimensional Quasistatic Modeling of Exclusion Region Barriers in Support of Design Guide Development." SAND93-0905. Sandia National Laboratories. Albuquerque, NM. 1993.

11. Dawson, D.B., Antoun, B.R., and Mosher, D.A. "MAVEN Progress Report for FY98 Second Half (Fracture of Weapons Materials)." Sandia National Laboratories Memo Report to Distribution. October 5, 1998.

12. Wellman, G.W, and Boyce, B.L. "Exclusion Region Barrier Crush Specimens Made from 304L Stainless Steel." Sandia National Laboratories Memo Report to R.D. Pedersen. August 26, 2004.

13. Wellman, G.W, and Boyce, B.L. "Materials Properties and Modeling Techniques used in the Analysis of Exclusion Region Barrier Test Specimens." Sandia National Laboratories Memo Report to R.D. Pedersen. December 13, 2005.

14. Wellman, G.W. 4th MIT Workshop on Fracture. November 1, 2007.

15. Metzinger, K. E. "Structural Analysis of a Frangible Nut Used on the NASA Space Shuttle." SAND93-1720. Sandia National Laboratories. Albuquerque, NM. 1993.

16. Gwinn, K.W. and Metzinger, K.E. "Analyses of Foam Impact Onto the Columbia Shuttle Wing Leading Edge Panels Using PRONTO3D/SPH." SAND2003-3853C. Sandia National Laboratories. Albuquerque, NM. 2003.

17. Hinnerichs, T. "Constitutive Model Report for the B61 Radar Nose Assembly Crush Model." Sandia National Laboratories Memo Report to Distribution. August 2, 2000.

18. Duong, H., Hinnerichs, T., Pott, J., Gwinn, K., Lo, D. "Independent Technical Review of Intermediate Angle Impact Analysis for B61 Common Radar Nose." September 11, 2001.

2.12.4 Material Data

This section discusses the material data used in the finite element analyses. Material test data and references are provided along with the appropriate power-law hardening curves. Table 2-14 lists the model component, the material of the component, and the section in Section 2.12.4 containing the material data and constitutive model.

Table 2-14. Listing of Material for Each Components in the Finite Element Models

Model	Component	Material	Section
Full PAT-1Models			
	Redwood Impact Material	Redwood	2.12.4.1
	Load Spreader Cylinder	Aluminum 6061	2.12.4.3
	Load Spreader Top Plate	Aluminum 7075	2.12.4.5
	Load Spreader Lower Plate	Aluminum 7075	2.12.4.5
	Copper Cylinder	Copper	2.12.4.7
	TB-1 Container	Stainless PH13-8-Mo	2.12.4.9
	TB-1 Contents	Elastic Plastic Soft	2.12.4.11
	Can Shell and Flange	Stainless 304	2.12.4.12
	T-Ampoule	Titanium 6Al-4V	2.12.4.14
	Sample Container	Titanium 6Al-4V	2.12.4.14
	Sample Container Cylinder	Plutonium (delta)	2.12.4.18
	ER Cylinders	Plutonium (alpha)	2.12.4.16
	Be Composite Cylinder	Beryllium	2.12.4.24
Impact Test Model			
	Tungsten Ballast	Tungsten	2.12.4.20
	Impact Specimen Brass	Brass UNS 36000	2.12.4.22
	Impact Specimen Titanium	Titanium 6Al-4V	2.12.4.14
	Ampoule Specimen	Titanium 6Al-4V	2.12.4.14
	Hemisphere Fixture	Stainless PH13-8-Mo	2.12.4.9

2.12.4.1 Redwood

The redwood material is modeled using the Orthotropic Crush model in PRONTO-3D. The Orthotropic Crush model is an empirically based constitutive relation used to model material like metallic honeycomb and wood. The force deflection curve used to simulate the compression of the redwood material is presented in Figure 2-57 along with data from Joseph and Hill. These values along with the other modeling parameters for the Orthotropic Crush model are presented in Table 2-15.

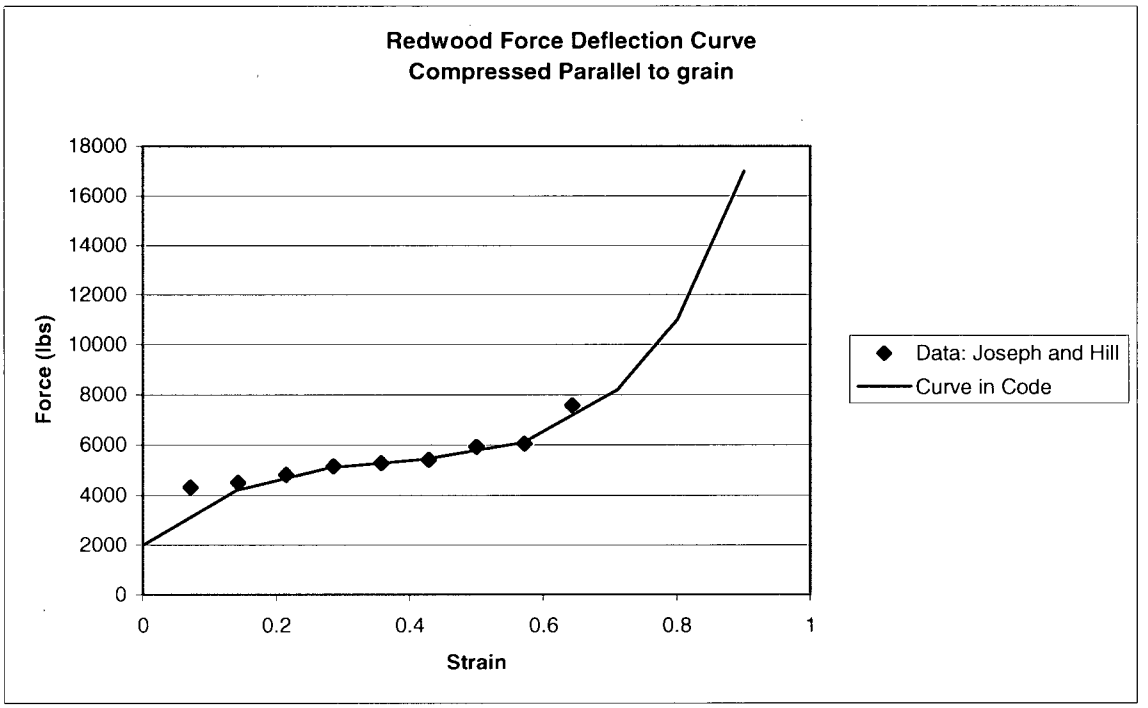

Figure 2-57. Redwood Force Deflection Curve Compared to Test Data from Joseph and Hill

Table 2-15. Redwood Orthotropic Crush Model Parameters

Parameter	Value
Compacted YOUNGS MODULUS (psi)	1.5E6
Compacted POISSONS RATIO	0.3
Compacted YIELD STRESS (psi)	20000
Full Compaction	0.9
Modulus x (psi)	1.5E6
Modulus y (psi)	0.3E6
Modulus z (psi)	0.3E6
Modulus xy (psi)	0.2E6
Modulus yz (psi)	0.25E6
Modulus zx (psi)	0.2E6

Table 2-15. Redwood Orthotropic Crush Model Parameters (Continued)

Parameter	Value	
	Strain	Pressure (psi)
Function 1 $ T-Direction	0	2000
	0.14	4200
	0.28	5100
	0.42	5430
	0.57	6100
	0.71	10100
	0.80	15000
	0.90	20000
Function 2 $ L-Direction		
	0	400
	0.14	986
	0.28	1200
	0.42	1275
	0.57	1432
	0.71	2371
	0.80	3521
Function 4 $ sigxy or sigxz vs volume		
	0.0	1000
	0.6	1000
	0.7	10000
	0.9	10000
Function 5 $ sigyz vs volume		
	0	1000
	0.6	1000
	0.7	10000
	0.9	10000

2.12.4.2 Reference

1. Joseph, Walter W., Thomas K. Hill. "Energy-Absorbing Characteristics of California Redwood Subjected to High Strain." SAND76-0087. Sandia National Laboratories. Albuquerque, NM. 1976.

2.12.4.3 Aluminum 6061

Property		Reference
Density	0.098 lb/in^3	
Young's Modulus	9.9E06 psi	1, 2
Poisson's Ratio	0.3	1, 2
Yield Stress	45000 psi	1
Hardening Constant	37852 psi	
Hardening Exponent	0.55	
Reduction in Area	0.503-0.520	1

The aluminum 6061 components were modeled using a power-law hardening constitutive model:

$$\sigma = \sigma_y + A(\varepsilon_p)^n$$

where σ_y is the yield stress, A is a hardening constant, and n is a hardening exponent.

2.12.4.4 Reference

1. Wellman, J. "Sandia National Laboratories, Personal communication regarding Organization 1800 Laboratory Tests on Aluminum. (April 19, 1991)." 2007.

2. Rice, R. C., Jackson, J. L., Bakuckas, J., and Thompson, S. "Metallic Materials Properties Development and Standardization (MMPDS) DOT/FAA/AR-MMPDS-01." January 2003.

2.12.4.5 Aluminum 7075

Property		Reference
Density	0.098 lb/in^3	1
Young's Modulus	10.4E6 psi	1
Poisson's Ratio	0.3	
Yield Stress	73.0E3 psi	1
Hardening constant,	37852 psi	
Hardening exponent	0.55	

The aluminum 7075 components were modeled using a power-law hardening constitutive model:

$$\sigma = \sigma_y + A(\varepsilon_p)^n$$

where σ_y is the yield stress, A is a hardening constant, and n is a hardening exponent.

2.12.4.6 Reference

1. Department of Defense. *Military Standardization Handbook: Metallic Materials and Elements for Aerospace Vehicle Structures.* MIL-HDBK-5E pp. 3-337, Figure 3.7.4.1.6(n): May 1986.

2.12.4.7 Copper Cylinder

Property		Reference
Density	0.322 lb/in^3	1
Young's Modulus,	17.2E06 psi	1
Poisson's Ratio,	0.33	1
Yield Stress,	45.0E03 psi	1
Hardening Constant,	38000 psi	
Hardening exponent	0.55	

The copper cylinder was modeled using a power-law hardening constitutive model:

$$\sigma = \sigma_y + A(\varepsilon_p)^n$$

where σ_y is the yield stress, A is a hardening constant, and n is a hardening exponent.

2.12.4.8 Reference

1. ASTM B152/B152M. "Standard Specification for Copper Sheet, Strip, Plate and Rolled Bar." ASTM International. West Conshochocken, PA.

2.12.4.9 Stainless PH13-8-Mo

Property		Reference
Density	0.286 lb/in^3	1, 2, 3
Young's Modulus	30.E06 psi	2, 3
Poisson's Ratio	0.30	2, 3
Yield Stress,	141.0E03 psi	4
Hardening Constant	30.0E4 psi	
Hardening exponent	1.0	
Thermal Expansion Coefficient (from 70°F to 203°F and from 70°F to 401°F, respectively)	5.9E-6 to 6.0E-6 in./in./°F	5 (Figure 2.6.5.1.1)

The TB-1 was modeled using a power-law hardening constitutive model:

$$\sigma = \sigma_y + A(\varepsilon_p)^n$$

where σ_y is the yield stress, A is a hardening constant, and n is a hardening exponent.

2.12.4.10 Reference

1. Shigley, J.E. *Mechanical Engineering Design.* McGraw-Hill: 1977.

2. Harvey, P.D., ed. *Engineering Properties of Steels.* American Society for Metals: Metals. Park, OH: 1982.

3. Boyer, H.E., and Gall, T.L. ed. *Metals Handbook.* American Society for Metals: Materials. Park, OH: 1985.

4. American Society of Mechanical Engineers (ASME), "Boiler and Pressure Vessel Code," Section II, Part A, Table 3: Mechanical Test Requirements After Age Hardening Heat Treatment. pp. 1287. 2007.

5. Department of Defense. *Military Standardization Handbook: Metallic Materials and Elements for Aerospace Vehicle Structures."* (Effect of temperature on tensile ultimate and yield strength, Figure 2.6.5.1.1, pp. 2-148). MIL-HNDBK-5E: June 1, 1987.

2.12.4.11 TB-1 Contents

Property		Reference
Density	0.051 lb/in^3	See below
Young's Modulus	1.0E06 psi	See below
Poisson's Ratio	0.30	See below
Yield Stress	2000 psi	See below
Hardening Constant	100000 psi	
Hardening Exponent	1.0	

The material was modeled as Elastic-Plastic with a density to match the oxide powder. The material properties were based on approximating the behavior of oxide power. The material is used inside the TB-1 in the full model analyses. Those analyses are used only to determine rigid body motion of the TB-1, and the yield stress and hardness behavior will not affect the rigid body motion of the TB-1.

2.12.4.12 Stainless 304

Property		Reference
Density	0.286 lb/in^3	1
Young's Modulus	28.0E06 psi	1
Poisson's Ratio	0.33	1
Yield Stress	40000 psi	1
Hardening Constant	192746 psi	
Hardening Exponent	0.74819	

The stainless steel components were modeled using a power-law hardening constitutive model:

$$\sigma = \sigma_y + A(\varepsilon_p)^n$$

where σ_y is the yield stress, A is a hardening constant, and n is a hardening exponent.

2.12.4.13 Reference

1. United States. Nuclear Regulatory Commission. NUREG-1768. "Package Performance Study Test Protocols." 2003.

2.12.4.14 Titanium 6Al-4V

Property		Reference
Density	0.160 lb/in^3	2
Young's Modulus	15.5E06 psi	2
Poisson's Ratio	0.3	2
Yield Stress	141700 psi	1, 3
Hardening Constant	12.6E4 psi	
Hardening Exponent	0.6554	
Failure Value (TP)	1.012	
Thermal Expansion Coefficient 4.9E-6 to 5.1E-6 in./in./°F (from 70°F to 100°F and from 70°F to 312°F, respectively)		2 (Figure 5.4.1.0

The titanium components were modeled using a power-law hardening constitutive model:

$$\sigma = \sigma_y + A(\varepsilon_p)^n$$

where σ_y is the yield stress, A is a hardening constant, and n is a hardening exponent.

The Ductile Tearing model was used for the sample containers to allow the material to fracture under tensile strains. Figure 2-58 shows the power-law curve fit and data taken from a tensile test. Figure 2-59 and Figure 2-60 show the relative temperature insensitivity of Ti-6-4 alloy, justify the use of nominal (ambient) material properties in the analyses, and negate any brittle fracture concern at NCT cold temperatures.

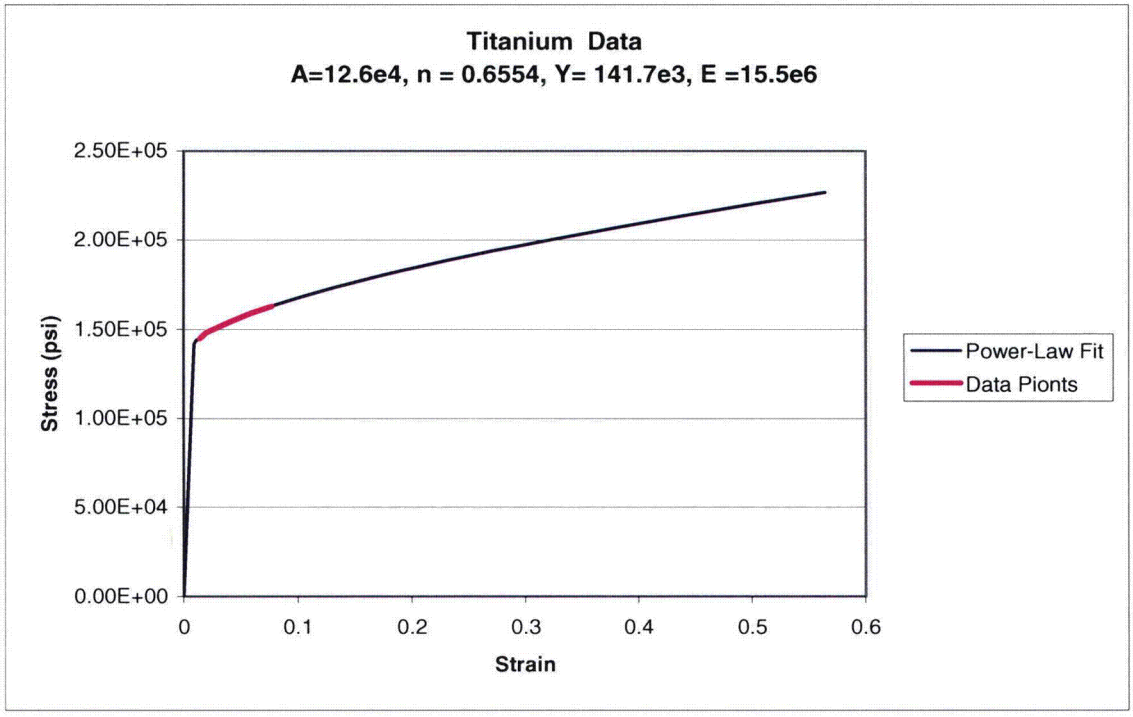

Figure 2-58. Comparison of Power-Law Curve Fit with Data from Tensile Test

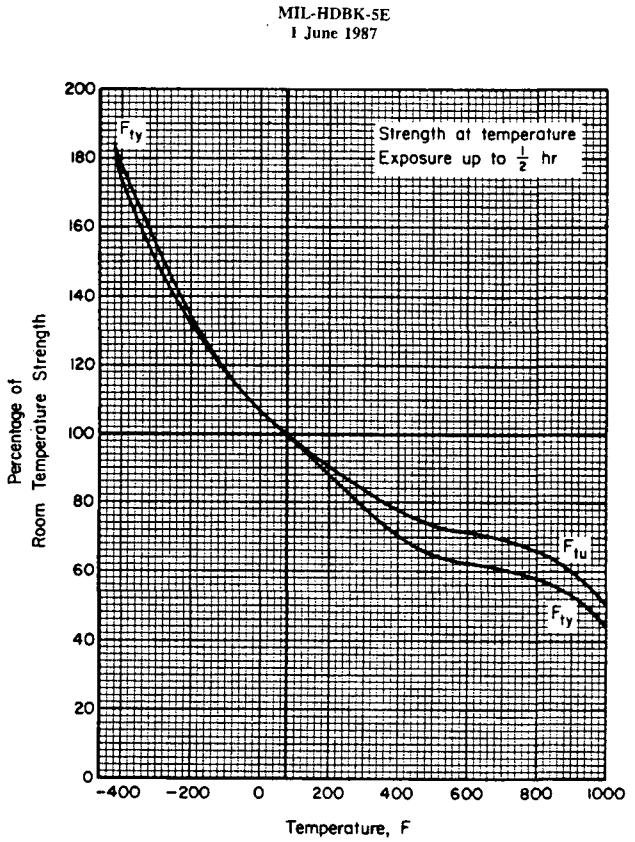

Figure 2-59. Effect of Temperature on the Tensile Ultimate Strength and Tensile Yield Strength of Annealed Ti-6-Al-4V Alloy (Ref. 2, Taken from MIL-HDBK-5E, Figure 5.4.1.1.1)

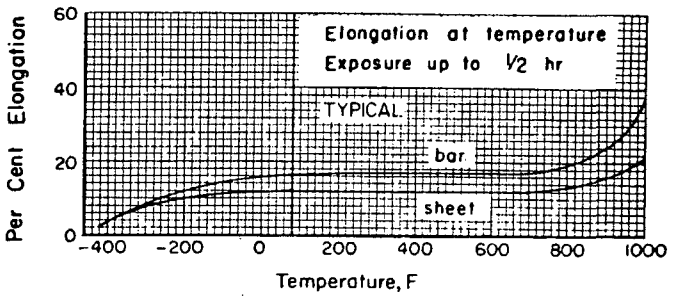

Figure 2-60. Effect of Temperature on the Elongation of Annealed Ti-6-Al-4V Alloy (Ref. 2, Taken from MIL-HDBK-5E, Figure 5.4.1.1.5)

2.12.4.15 Reference

1. Westmoreland Mechanical Testing and Research Inc. "WMT&R Report No. 7-38060." Youngstown, PA. 2007.

2. Department of Defense. *Military Standardization Handbook: Metallic Materials and Elements for Aerospace Vehicle Structures.* MIL-HDBK-5E: May 1988.

3. PAT-1040, Titanium and O-Ring Materials and Component Fabrication Specification, August 3, 2009. (Provided in Section 1.3.3.1 of this addendum.)

2.12.4.16 Plutonium (alpha phase)

Property		Reference
Density	0.716 lb/in^3	1
Young's Modulus	14.1E06 psi	1
Poisson's Ratio	0.3	1
Yield Stress	36000 psi	
Hardening Constant	85000 psi	
Hardening Exponent	0.4	

The alpha-plutonium components were modeled using a power-law hardening constitutive model:

$$\sigma = \sigma_y + A(\varepsilon_p)^n$$

where σ_y is the yield stress, A is a hardening constant, and n is a hardening exponent. As shown in Figures 2-61 and 2-62, alpha-plutonium is a brittle material. The alpha-plutonium material in Figure 2-62 has a finer grain structure than the alpha-plutonium material in Figure 2-61 and it is therefore more ductile. The material parameters were fit to the curve in Figure 2-62. To conservatively maximize the load induced by the impacting Pu material, it was modeled as a continuously hardening material that does not fracture (and is thus, "infinitely ductile," with hardening), matching the finer grain structure stress-strain curve of Figure 2-62.

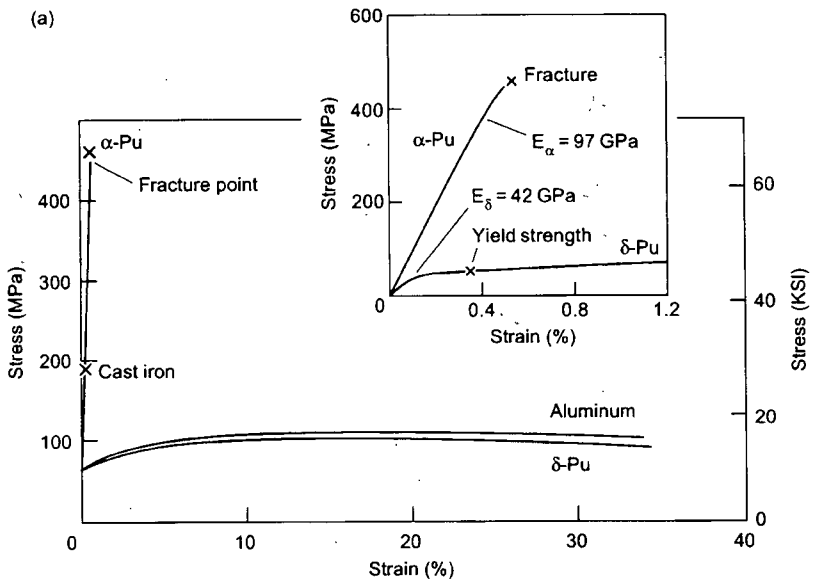

Figure 2-61. Pu Stress-Strain Curves Taken from Hecker and Stevens [Figure 2(a)]

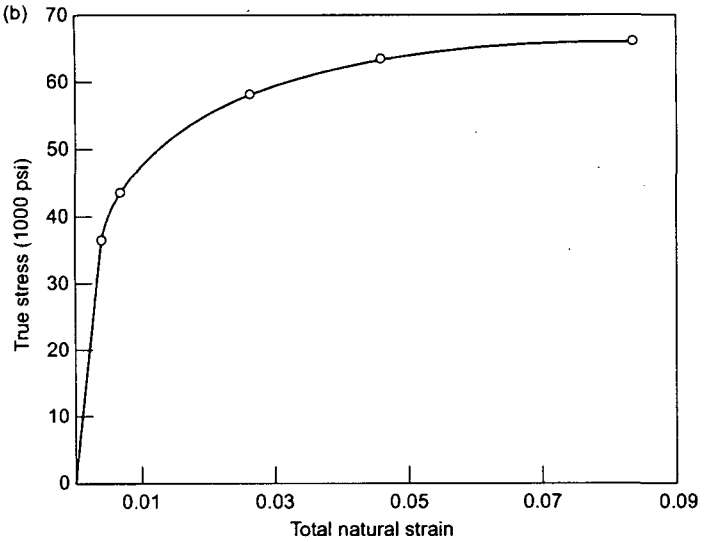

Figure 2-62. Pu Stress-Strain Curves Taken from Hecker and Stevens (Figure 10[b]).

2.12.4.17 Reference

1. Hecker, Siegfried S. and Michael F. Stevens. "Mechanical Behavior of Plutonium and Its Alloys." *Los Alamos Science* Number 26 (2000).

2.12.4.18 Plutonium (delta phase)

Property		Reference
Density	0.716 lb/in^3	1
Young's Modulus	6.1E06 psi	1
Poisson's Ratio	0.3	1
Yield Stress	9200 psi	
Hardening Constant	9000 psi	
Hardening Exponent	0.4	

The delta-plutonium components were modeled using a power-law hardening constitutive model. As shown in Figure 2-61 this is a fairly soft and ductile material. The material parameters were fit to the delta-phase curve in Figure 2-61. To maximize the load induced by the impacting Pu material, it was modeled as a continuously hardening material that does not fracture. The density of alpha phase plutonium was conservatively used as the density for the delta phase plutonium in the modeling.

2.12.4.19 Reference

1. Hecker, Siegfried S. and Michael F. Stevens. "Mechanical Behavior of Plutonium and Its Alloys." *Los Alamos Science* Number 26 (2000).

2.12.4.20 Tungsten

Property		Reference
Density	0.680 lb/in^3	1
Young's Modulus	58.3E06 psi	1
Poisson's Ratio	0.3	1
Yield Stress	80000 psi	
Hardening Constant	78000 psi	
Hardening Exponent	0.4	

The tungsten holder was modeled using a power-law hardening constitutive model with nominal hardening values. The actual component remained elastic.

2.12.4.21 Reference

1. Lassner, Erik and Wolf-Dieter, Schubert. "Tungsten: Properties, Chemistry, Technology of the Element, Alloys, and Chemical Compounds." Academic/Plenum Publishers (1999).

2.12.4.22 Brass (UNS C36000)

Property		Reference
Density	0.309 lb/in^3	2
Young's Modulus	13.1E06 psi	2
Poisson's Ratio	0.3	2
Yield Stress	43300 psi	1
Hardening Constant	79400 psi	
Hardening Exponent	0.6248	

The brass components were modeled using a power-law hardening constitutive model:

$$\sigma = \sigma_y + A(\varepsilon_p)^n$$

where σ_y is the yield stress, A is a hardening constant, and n is a hardening exponent. Figure 2-63 shows the power-law curve fit and data taken from the tensile test.

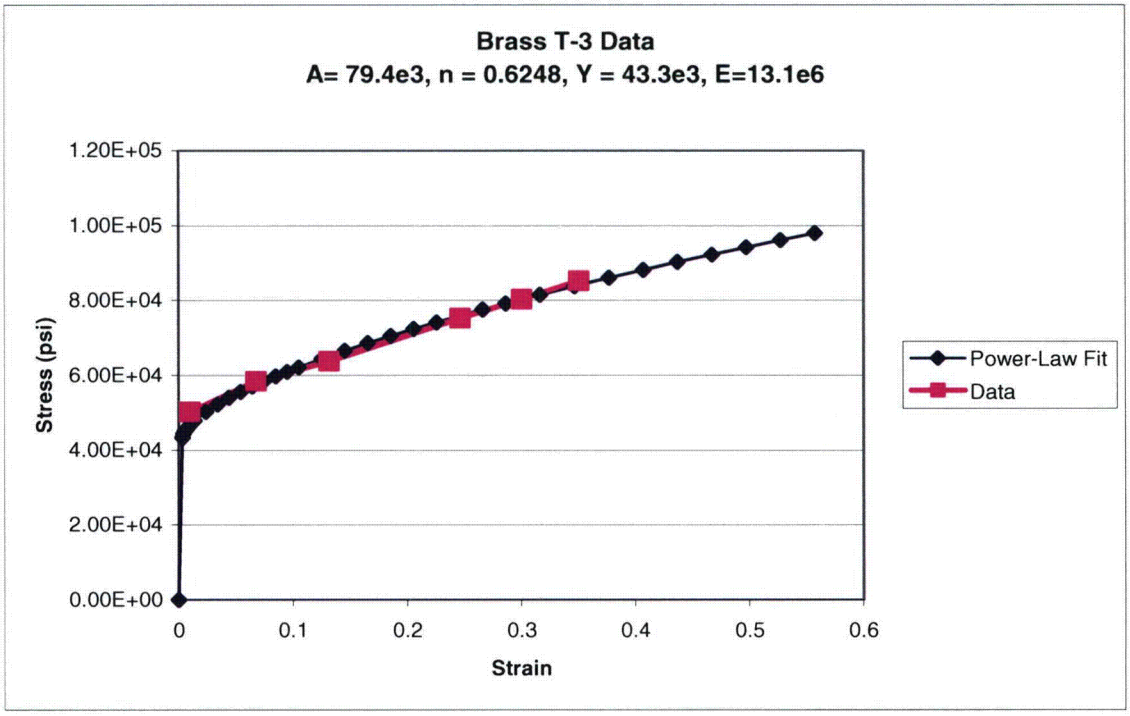

Figure 2-63. Comparison of Power-Law Curve Fit with Data from Tensile Test

2.12.4.23 Reference

1. Westmoreland Mechanical Testing and Research Inc. "WMT&R Report No. 7-38060." Youngstown, PA. 2007.

2. ASTM B16 CDA 360, Free Cutting Brass, Copper Alloy No C36000.

2.12.4.24 Beryllium

Property		Reference
Density	0.5745 lb/in^3 (conservatively assumed density of delta Pu)	
Young's Modulus	1.7092E7 psi	1
Poisson's Ratio	0.3	1
Yield Stress	23929 psi	1
Hardening Constant	38350 psi	
Hardening Exponent	0.461407	

The Be composite cylinder was modeled using a power-law hardening constitutive model:

$$\sigma = \sigma_y + A(\varepsilon_p)^n$$

where σ_y is the yield stress, A is a hardening constant, and n is a hardening exponent. Figure 2-64 shows the power-law curve fit and data taken from the tensile test.

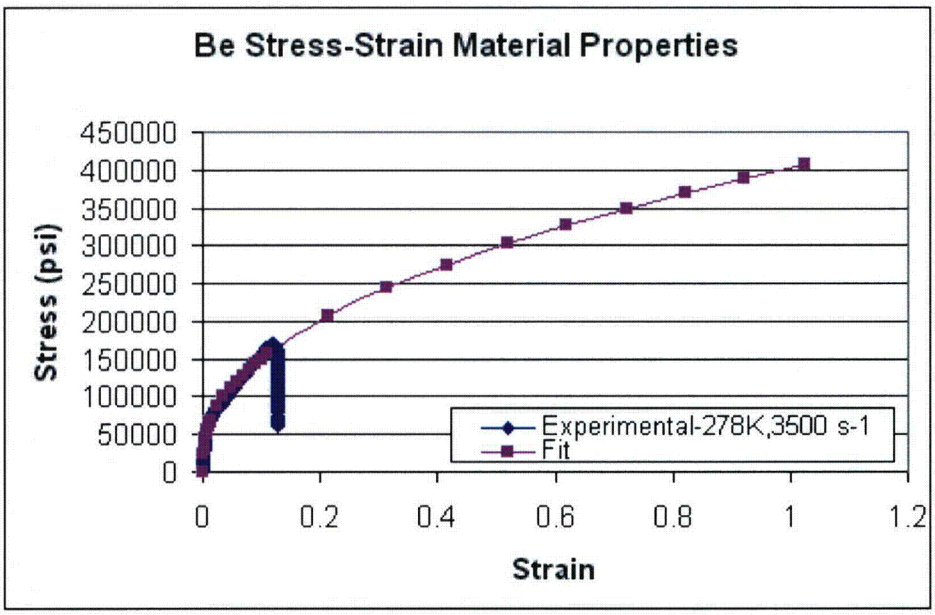

Figure 2-64. Comparison of Power-Law Curve Fit with Data from Tensile Test

2.12.4.25 References

1. Wick, O.J., ed. *Plutonium Handbook: A Guide to the Technology, Volume 1*. American Nuclear Society, 1980.

2. Lindholm, U.S., and Yeakley, L.M. "Effect of Strain rate, Temperature, and Multiaxial Stress on the Strength and Ductility of S200E Beryllium and 6Al-4V Titanium." Air Force Materials Laboratory Report. AFML-TR-71-37. Wright-Patterson Air Force Base. OH. 1971.

2.12.5 Component Analyses Using Complete Model

The following section describes the full model analyses of the TB-1 containment vessel and its detailed components. As discussed in Section 1, the components within the titanium T-Ampoule consist of either cast plutonium (Pu) cylinders with a mass of 831 g or 731 g, small sample containers (SC-1), or medium sample containers (SC-2) containing Pu material or a Be composite material. Each component will be analyzed for three orientations, the end-on impact, the side-on impact, and the CGOC impact for the high-speed aircraft impact. For the hypothetical accident conditions (HAC) dynamic crush analyses, the same sets of analyses were performed. In the NCT 4-ft-drop scenario, only the side and end impact for the SC-1 and SC-2 cases were analyzed to assure the positioning of the sample containers did not require adjustment for the HAC and high-speed aircraft impact analyses.

2.12.5.1 Finite Element Model

2.12.5.1.1 Common Model Components

The common components of the models are presented in Figures 2-65 and 2-66. The T-Ampoule is designed to fit snugly inside the TB-1 and to be loaded primarily in compression during impact. The finite element models of the T-Ampoule and TB-1 have a plane of symmetry along the center axis of the TB-1 (Z=0). Figure 2-65 shows the T-Ampoule and the TB-1 model for the top impact orientation. A hexagonal mesh with .015-in. elements is used to model the top of the T-Ampoule. This results in four elements through the thickness of the T-Ampoule shell. Since the primary strains are compressive, this allows for a time step which keeps the problem tractable, while providing adequate resolution of the T-Ampoule strain field. The mesh of the TB-1 is refined in the upper region with a hexagonal element size of 0.040 in. to adequately model the contact between the T-Ampoule top and the TB-1. The titanium Ring Filler, which fills the small void between the T-Ampoule and the TB-1 near the bottom of the TB-1 lid, is installed during preparations for shipment to provide uniform support to the ellipsoid T-Ampoule. As shown in Figure 2-66, the Ring Filler is not modeled explicitly, but is modeled as an integral part of the TB-1 body, with PH13-8-Mo material properties. Although the elastic moduli do differ, the yield strengths of the 13-8 (141 ksi) vs. Ti-6-4 (141.7 ksi) materials do not differ significantly, and this small gap-filling component was simplified to be continuous with the TB-1 since it provides no additional strength and only provides a smoothed inner surface for contact with the T-Ampoule and its contents. The stresses in this region are monitored to ensure that they do not threaten the integrity of the Ring Filler. For end impacts, the lower region of the TB-1 is modeled with a coarser mesh; for side impacts, the non-impact side has the coarser mesh. The TB-1 halves are tied together using the tied contact algorithm.

In the TB-1 finite element model, the lid and the body are modeled as one unit. The bolted connection is not modeled. There is a separate analytical bolt analysis in Section 2.12.6. This analysis uses the peak impulse force from the component finite element models to determine the bolt loading.

The model developed for the side-on impact analyses is presented in Figure 2-66. The model is similar to the top impact model except that the mesh for the TB-1 is refined on the sides of the component. The mesh discretization of the T-Ampoule top and T-Ampoule bottom is the same

0.015-in. hexagonal element size as that used in the end-on impact analysis. The thread region, where the top and bottom of the T-Ampoule are joined, is modeled using coincident nodes.

The SC-1 and SC-2 are fit inside a support structure within the T-Ampoule. This structure, shown in Figures 2-67 and 2-68, is constructed from Titanium 6Al-4V (see Section 2.12.4.14). The support structure consists of two dishes placed on each end of the T-Ampoule for vertical positioning (with a thickness that varies from 0.055 in. at the edge to 0.025 in. at the center), 4 upper and lower legs which centrally position the containers within the T-Ampoule (with a thickness of 0.063 in.), two rings which hold the legs in place (0.094 in. diameter), and either one or two spacers for the SC-1 and SC-2, respectively to separate the containers (with a thickness of 0.043 in. and a height of 0.749 in. and 1.008 in., respectively). The legs and rings were meshed to have 4 elements through the thickness, while the dishes have 5 elements through the thickness (see Figure 2-69 for mesh refinement). Figure 2-67 shows the support structure as used for the 0° rotated models while Figure 2-68 shows the structure used for the 45° rotated models. These two orientations were used to ensure worst cases analyses were performed in terms of loads on the support structure and loads on the T-Ampoule.

As detailed in Section 2.12.4.9, the high-strength PH13-8Mo stainless steel TB-1 is modeled using an elastic-plastic, power-law constitutive model to assure accurate capture of denting internally within the TB-1. The Ti-6Al-4V T-Ampoule and support structure are modeled using an elastic-plastic, power-law constitutive model.

The PRONTO3D code used in this analysis uses the Flanagan-Belytschko hexahedral element with one center integration point. The results are presented with contour plots showing element integration point values; they are not smoothed contours of extrapolated nodal values. Although the plots will look rough, the integration point strains are the primary variable of concern, since these values will be used in the strain locus plots. Therefore, integration point contours will be used throughout the analysis.

Included in the high speed aircraft analysis results and the HAC results are plots of kinetic energy versus time. These were included to demonstrate that the peak loads were captured in the analyses. The models were all run without built-in units, thus the kinetic energy plots presented for the high speed aircraft analyses and HAC analyses do not have labels. The x-axis of these plots, time, is in units of seconds. The y-axis of these plots, kinetic energy, is in units of pounds inches.

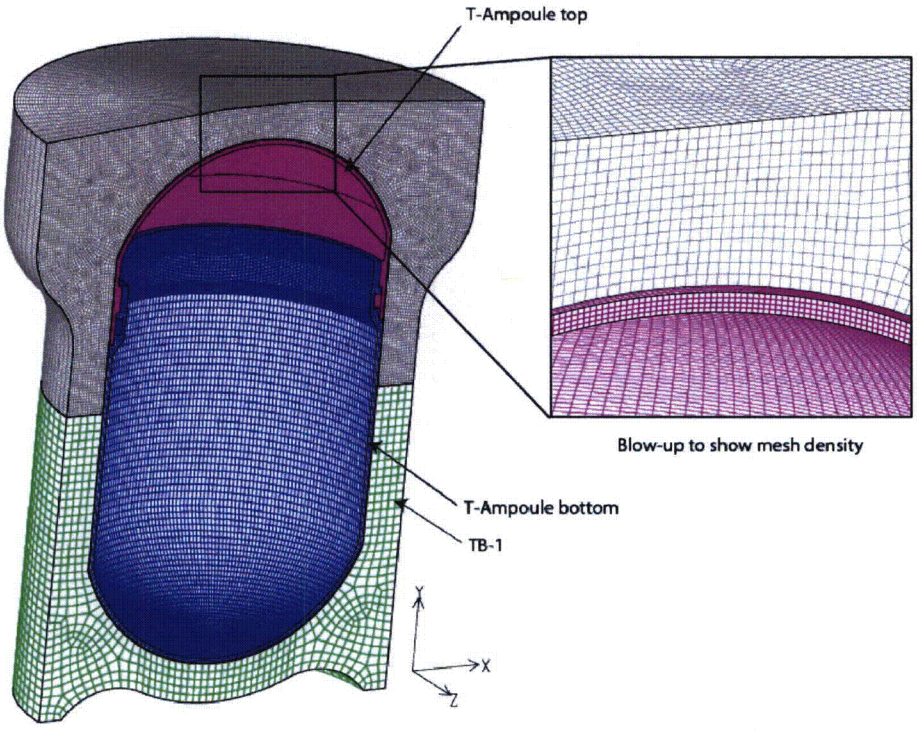

Figure 2-65. Common Components of the Model for Top and CGOC Impact Orientation

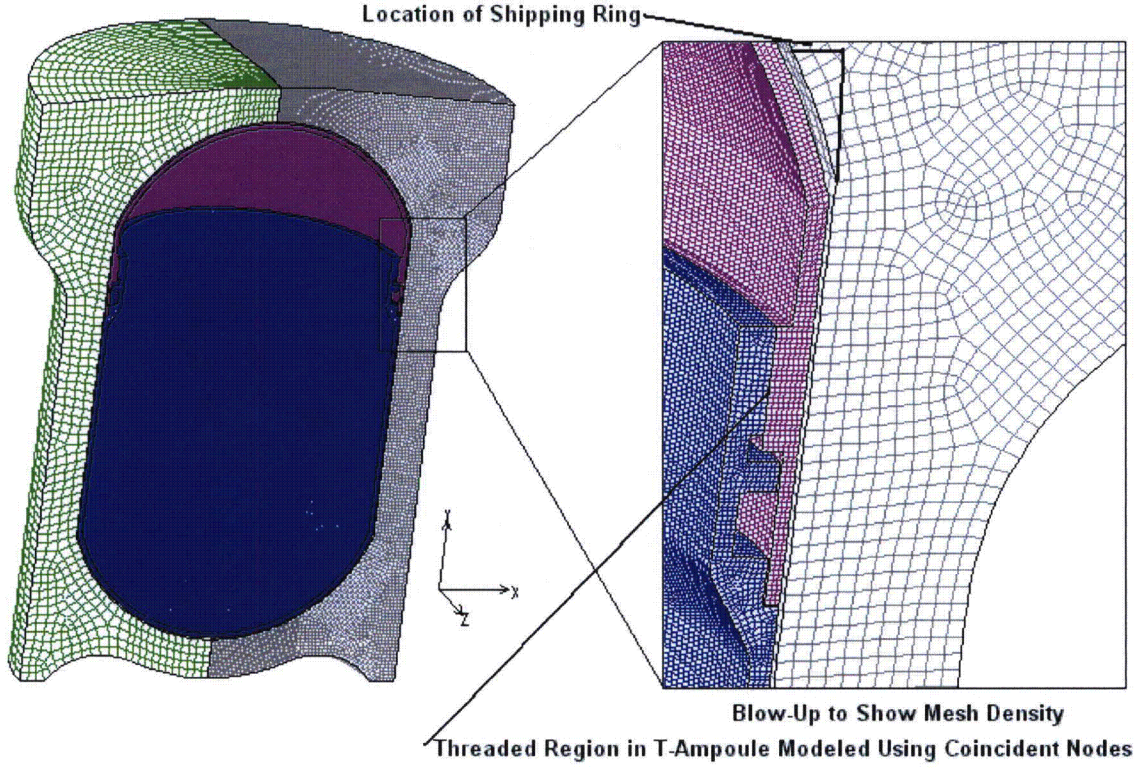

Figure 2-66. Common Components of the Model for a Side Impact Orientation

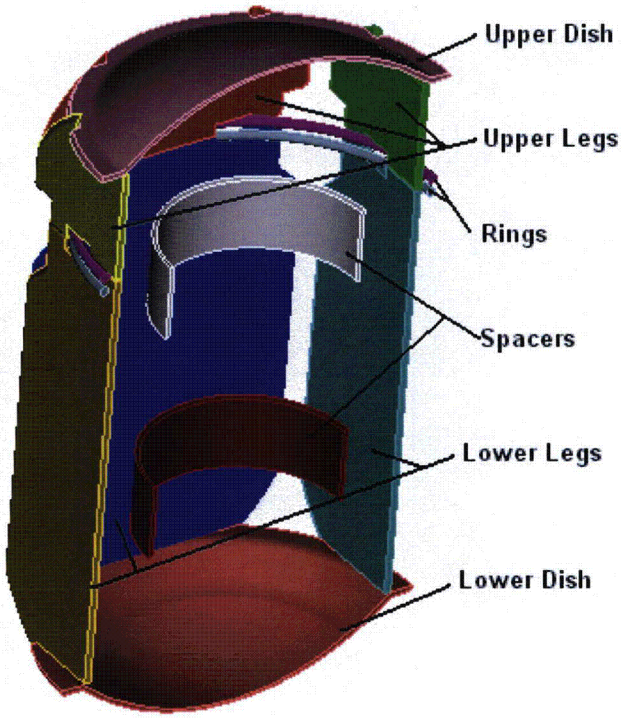

Figure 2-67. Support Structure with 0° Rotation and Spacers for SC-1

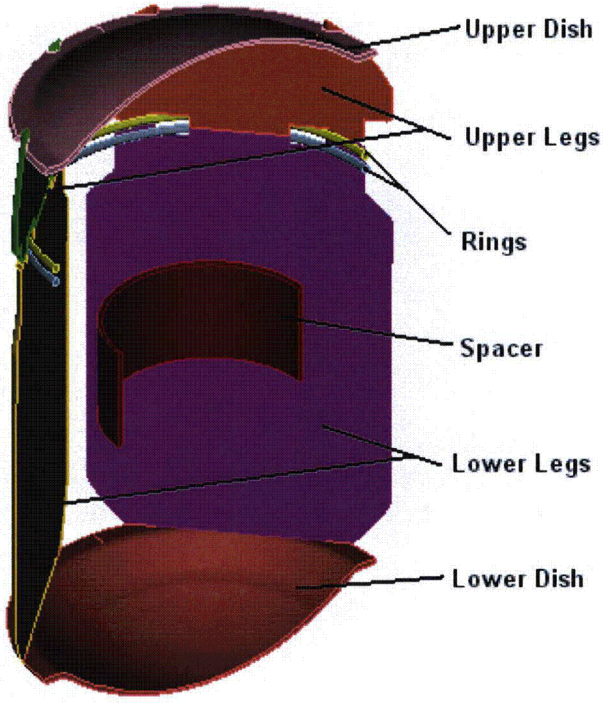

Figure 2-68. Support Structure with 45° Rotation and Spacer for SC-2

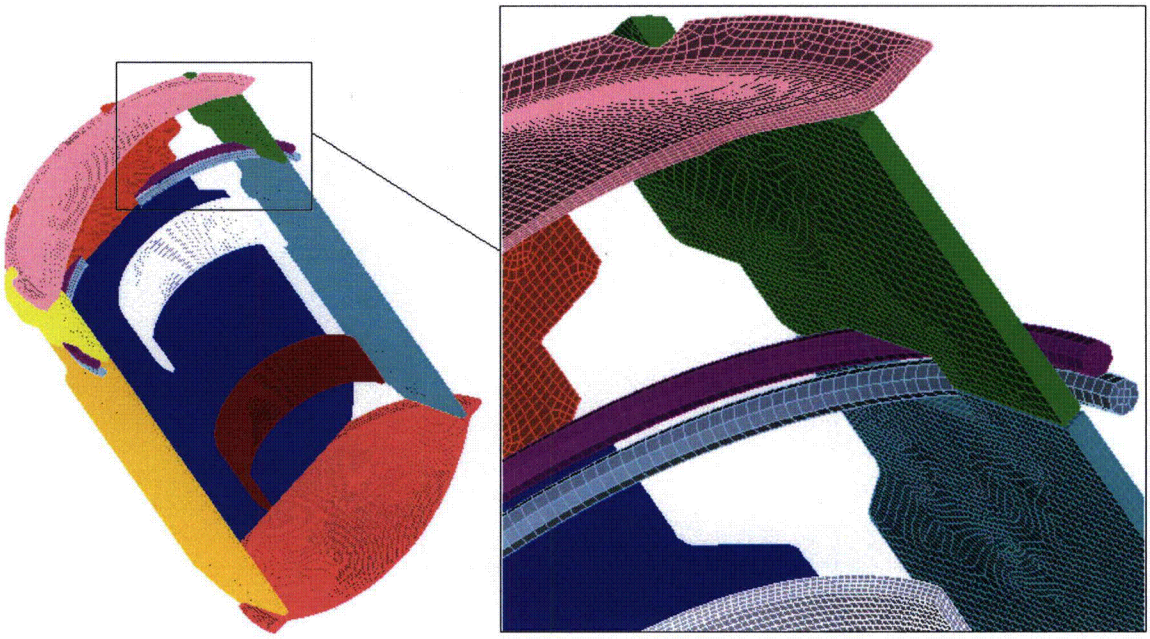

Figure 2-69. Mesh Refinement in Support Structure with 0° Rotation and Spacer for SC-1

2.12.5.2 Component Models

Models of the content components consist of an 831-g plutonium metal hollow cylinder, a 731-g plutonium metal hollow cylinder, a small sample container (SC-1) and a medium sample container (SC-2). The sample containers will be used to transport Pu and a Pu/Be composite. These components are presented in Figures 2-70 through 2-73. The 831-g plutonium metal hollow cylinder shown in Figure 2-70 has a 2.51-in. diameter and a 2.903-in. length. The wall thickness is 0.118 in. It is modeled using 0.018 in. hexahedral elements, which results in 6 elements through the thickness. The material of the cylinder is modeled as alpha-plutonium as described in Section 2.12.4.16. The 731-g plutonium metal hollow cylinder model is very similar to the 831-g model, except that the length is reduced to account for the reduced material weight. It is also modeled as an alpha-plutonium material.

The finite element models for the sample containers are also similar to each other. The SC-1 model shown in Figure 2-72 is 3 in. in diameter and 2 in. high. The shell thickness is 0.065 in. The container is meshed with 0.020-in. hexagonal elements, which results in 3 elements through the shell thickness. The model is shown with the 0.88-in. diameter X 0.88-in. long right circular cylinder, which is modeled as delta-plutonium and has a mass of 174 g. Note that the Pu cylinder is located in the bottom of the sample container, which is farthest away from the T-Ampoule for a top-end impact (producing the highest net velocity difference between the two upon impact, and thus the highest load to the T-Ampoule). For a right side impact case, the Pu cylinder would be located on the far left side of the sample container, for the same reason. The contents of the sample containers are packed in the T-Ampoule with the support structure shown in Figures 2-67 and 2-68. The SC-2, shown in Figure 2-73, has the same basic geometry and mesh as the SC-1. The length of the sidewall has been lengthened by 1 in., and the mass of the

contents has been increased. The contents of the SC-2 are modeled using a 1.1 in. diameter X 1.1-in. long right circular cylinder, which has a mass of 338 g.

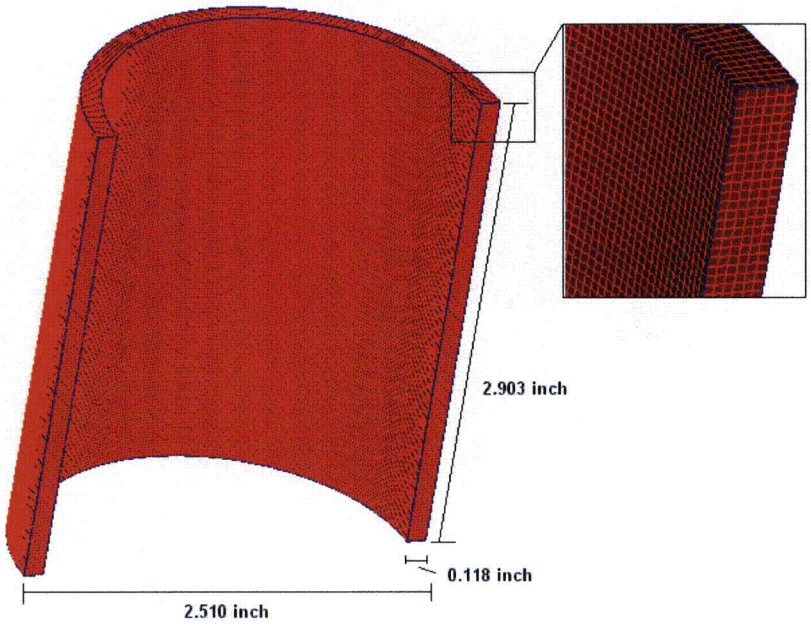

Figure 2-70. 831-g Cylinder Finite Element Model

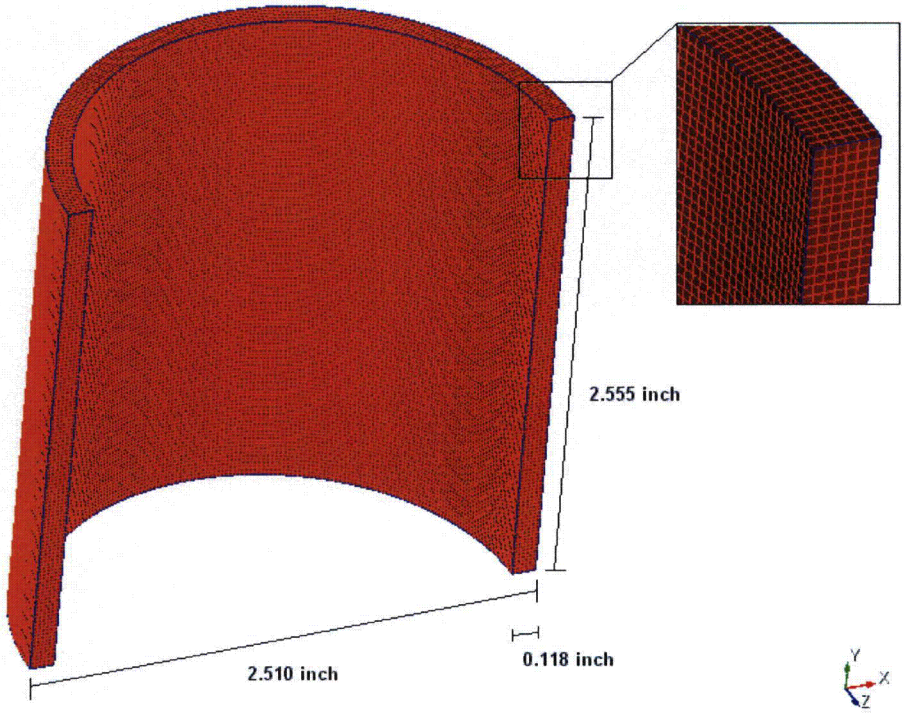

Figure 2-71. 731-g Cylinder Finite Element Model

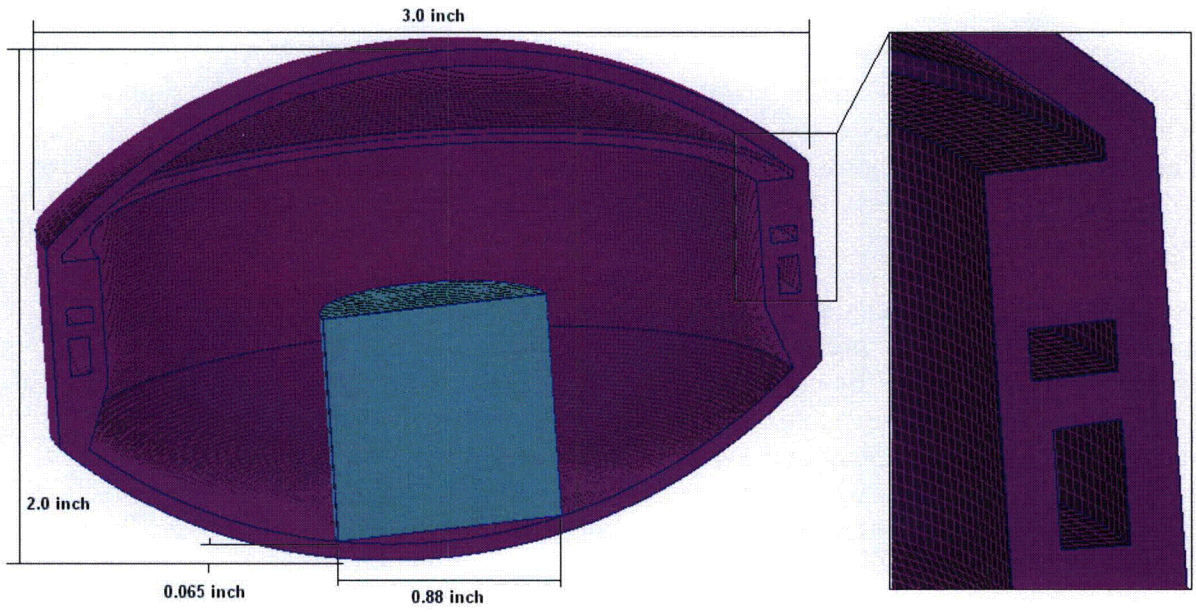

Figure 2-72. Finite Element Model of SC-1 with Pu Cylinder Contents

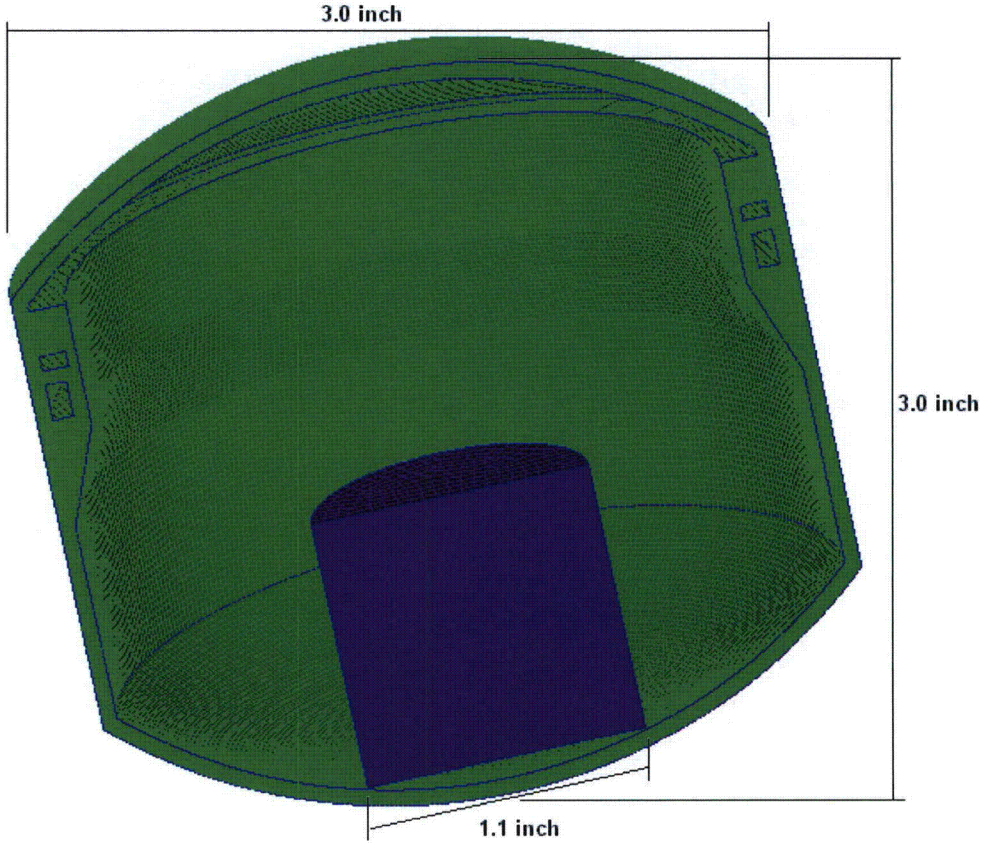

Figure 2-73. Finite Element Model of SC-2 with Pu Cylinder Contents

2.12.5.3 Normal Conditions of Transport Displacement Analyses

The plutonium contents in the sample containers will be packaged in the T-Ampoule using the support structure shown in Figures 2-67 and 2-68. Under the NCT free drop, the support structure integrity must be assessed to assure the positioning of the sample containers for HAC and high-speed crash need not be adjusted. Therefore, the SC-1 and SC-2 were evaluated for 4-ft-drop end and side impacts. Under side impact, the model was oriented with the support structure at 0 and 45 degrees.

These analyses were completed for only the sample container components. The design of the support structure is meant to prevent the sample containers from shifting during normal operating conditions. If the Pu and Pu/Be-composite cylinders did shift to the outer edge of the T-Ampoule, and subsequently traveled across its entire width during an HAC or high speed impact, this would increase loads on the T-Ampoule and TB-1 vessel. Due to the thin walls and open shape of the hollow cylinder components which are extremely soft, the positioning of the plutonium metal hollow cylinders did not need restriction, and no support structure was designed to cradle the cylinders. The Ta foil packing material for the plutonium metal hollow cylinders and the sample container contents was conservatively neglected to allow for bounding higher net impact velocities between contents and T-Ampoule wall, and to conservatively omit any energy absorbing or load spreading from the packing material. In the high-speed impact analyses, the cylinders were positioned to allow for the maximum displacement (most conservative with the largest velocity difference between the cylinder and T-Ampoule at time of contact). The NCT analyses were performed to assure the positioning of the sample containers does not change after the 4-ft-drop. This was done by confirming the support structure does not undergo large plastic deformation throughout its thickness.

Three examples of the models created to determine the behavior of the support structure and sample containers when subjected to the NCT (10 CFR 71.71) performance tests are shown in Figures 2-74 through 2-76. Not shown are the SC-1 side impact at 45 degrees, the SC-2 side impact at 0 degrees, and the SC-2 end impact at 0 degrees, due to their similarity to the models shown. The support structure, sample containers, and plutonium are given an initial velocity of 192 in/sec, corresponding to the NCT regulatory condition. The models are half symmetry models, with the plane of symmetry passing through the center of the TB-1.

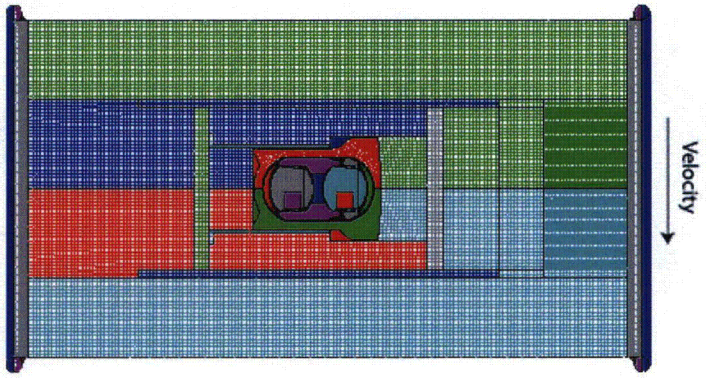

Figure 2-74. NCT SC-2 Side Impact with Support Structure Rotated 45°

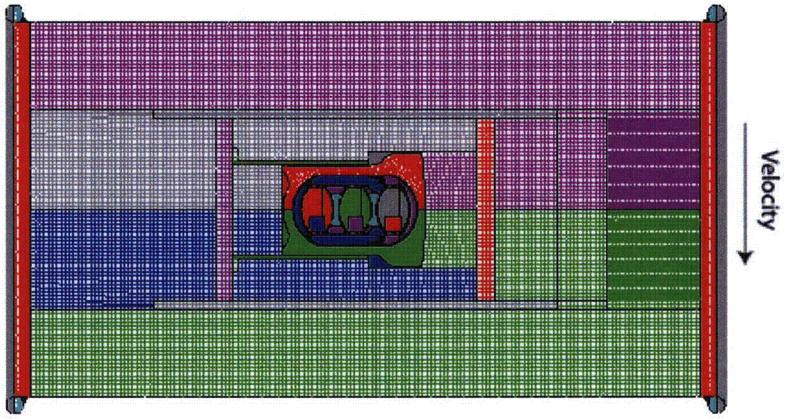

Figure 2-75. NCT SC-1 Side Impact with Support Structure Rotated 0°

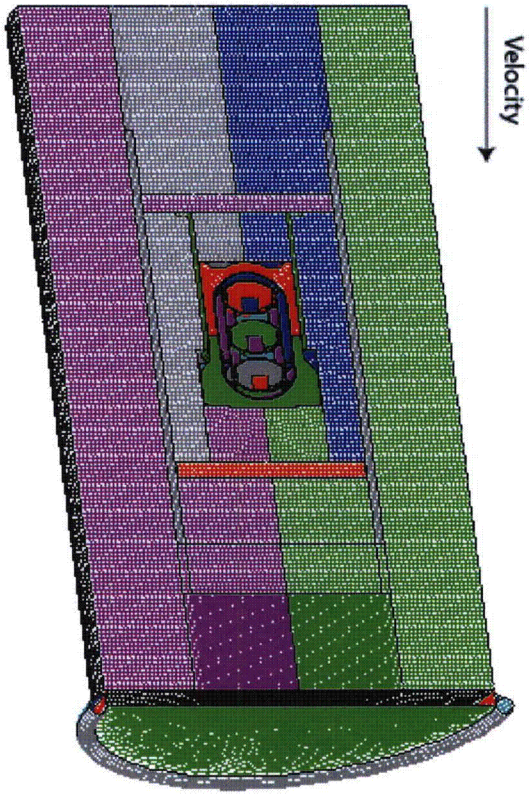

Figure 2-76. NCT SC-1 End Impact with Support Structure Rotated 0°

2.12.5.3.1 NCT End Drop Analysis

The models created for the 4-ft-drop end impact for the SC-1 and SC-2 at time 0 are shown in Figures 2-76 and 2-77, respectively. The post-4-ft-drop models are shown in Figures 2-78 and 2-79, although almost no discernable difference can be seen since the package overpack lid ring is only slightly dented. The kinetic energy histories for these two impacts are shown in Figures 2-80 and 2-81, indicating that sufficient analysis time transpired to capture the entire impact event, and the PAT-1 package actually bounced after impact. As shown in Figures 2-82 through 2-85 and Table 2-16, the minimal plasticity (less than 4%, and only in small localized areas of internal or external corners) observed in the titanium support structure, or cradle, verifies that the overall structure remained essentially elastic and the original position of the sample containers would remain unchanged.

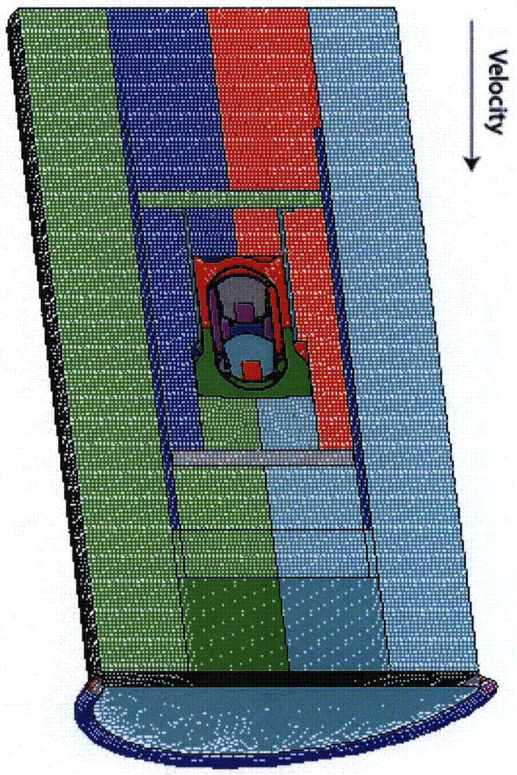

Figure 2-77. NCT SC-2 End Impact with Support Structure Rotated 0°

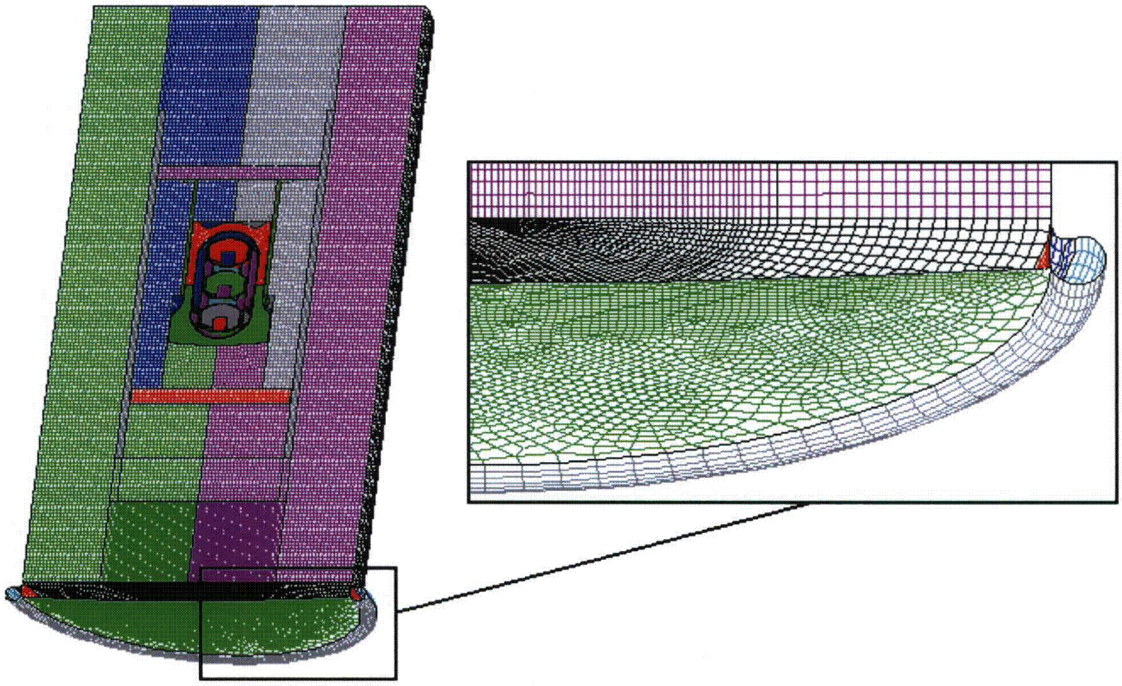

Figure 2-78. NCT SC-1 End Impact with Support Structure Rotated 0° – Final Displacement

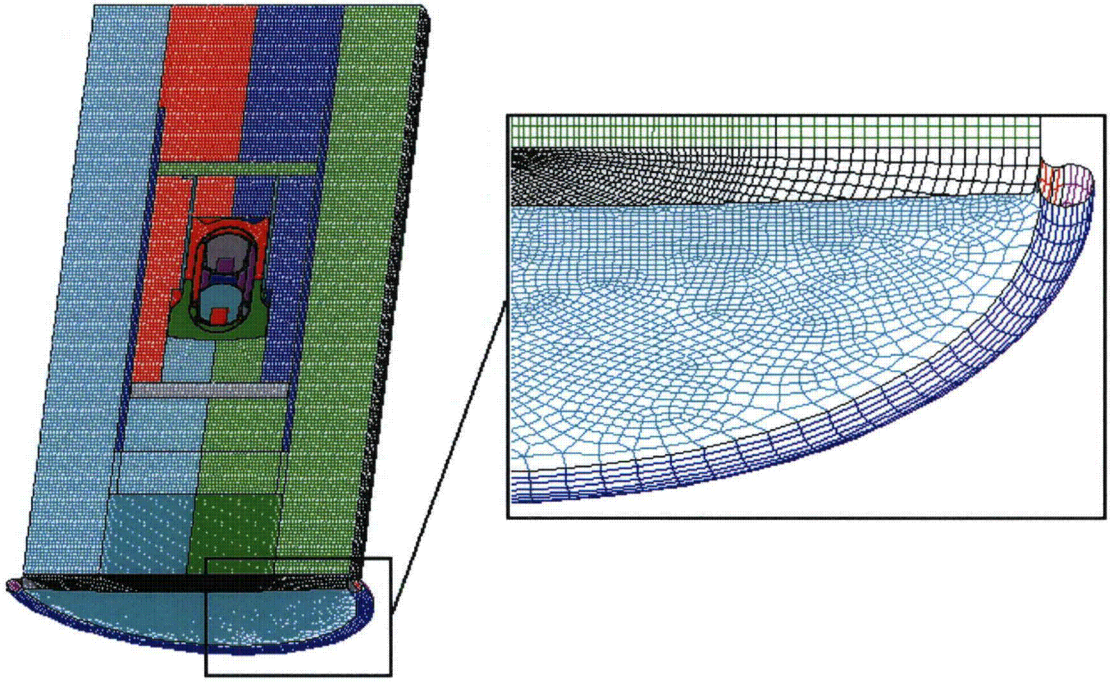

Figure 2-79. NCT SC-2 End Impact with Support Structure Rotated 0° – Final Displacement

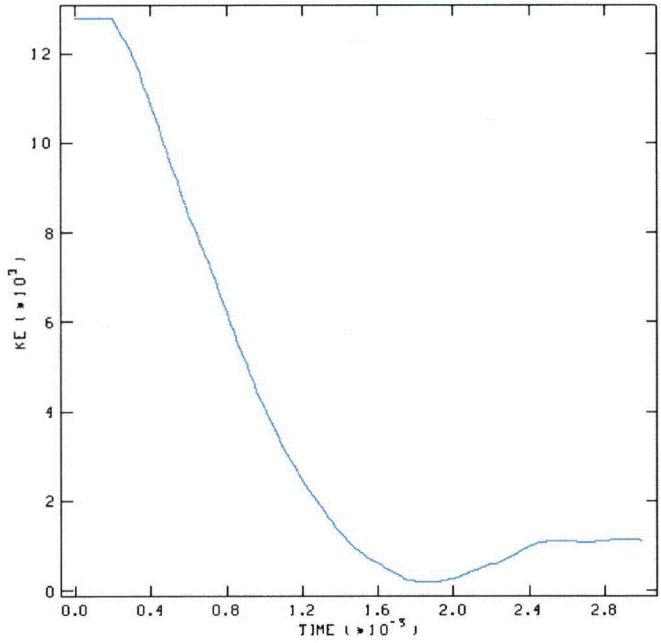

Figure 2-80. NCT SC-1 End Impact with Support Structure Rotated 0° - Kinetic Energy Time History

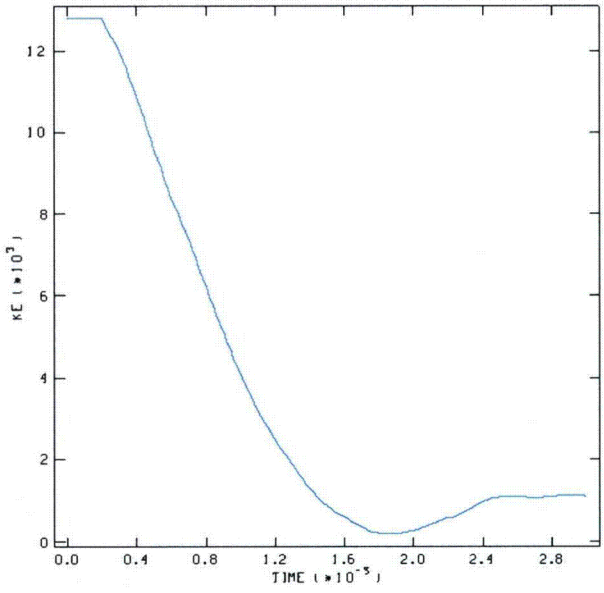

Figure 2-81. NCT SC-2 End Impact with Support Structure Rotated 0° - Kinetic Energy Time History

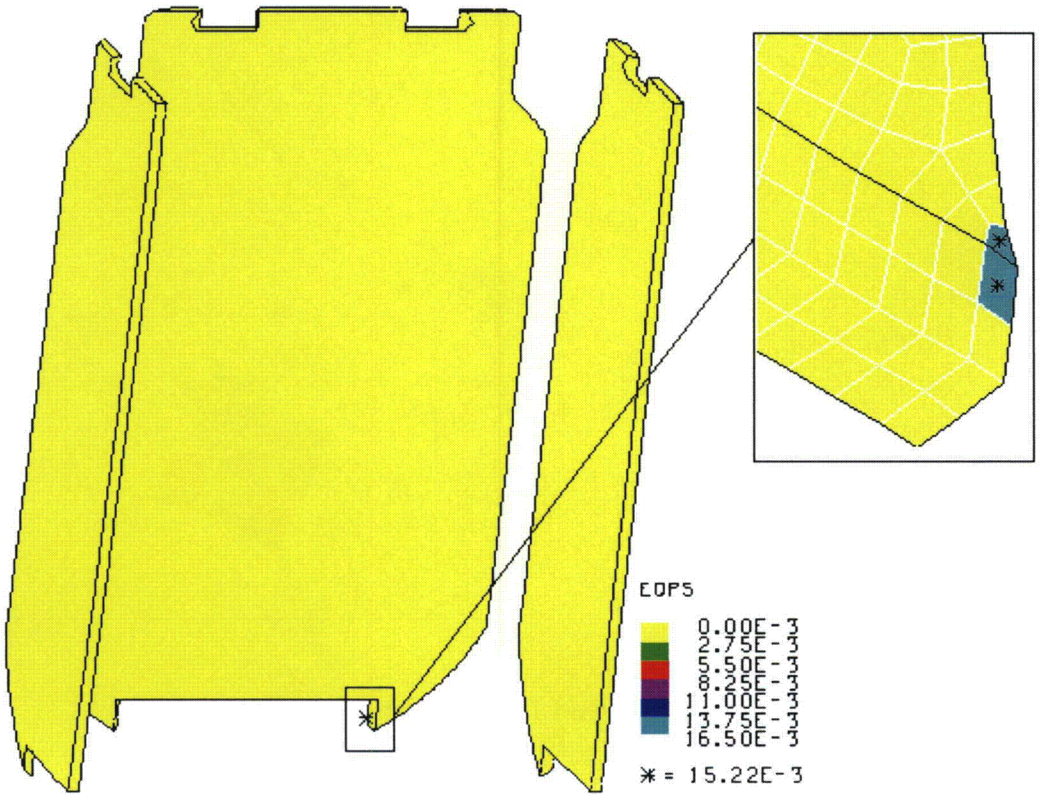

Figure 2-82. NCT SC-1 End Impact with Support Structure Rotated 0° - EQPS in Bottom Legs

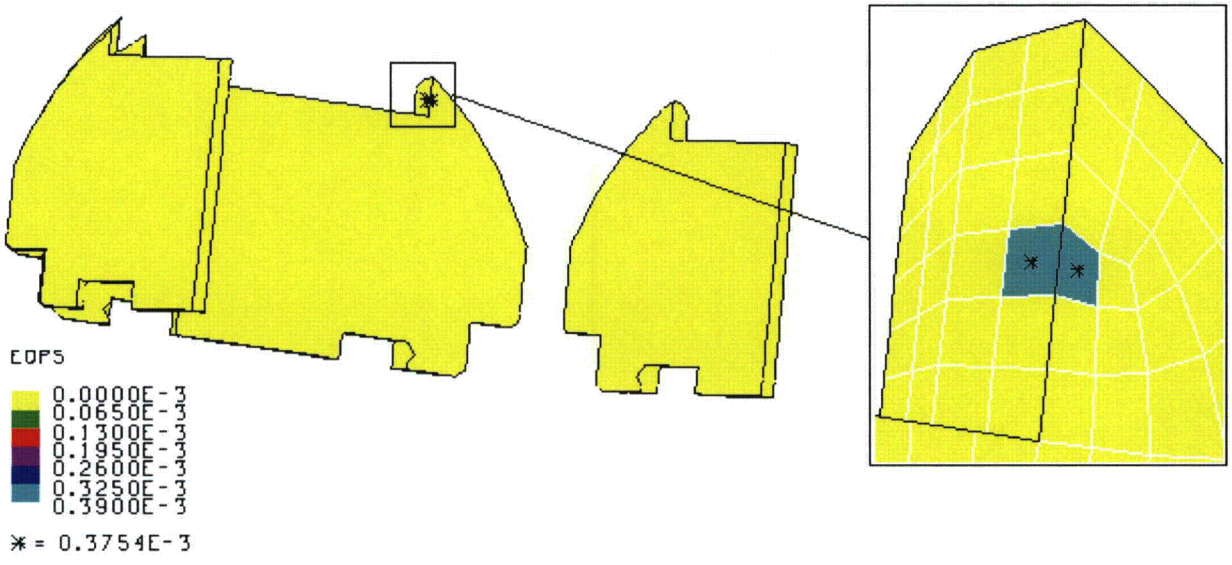

Figure 2-83. NCT SC-1 End Impact with Support Structure Rotated 0° - EQPS in Top Legs

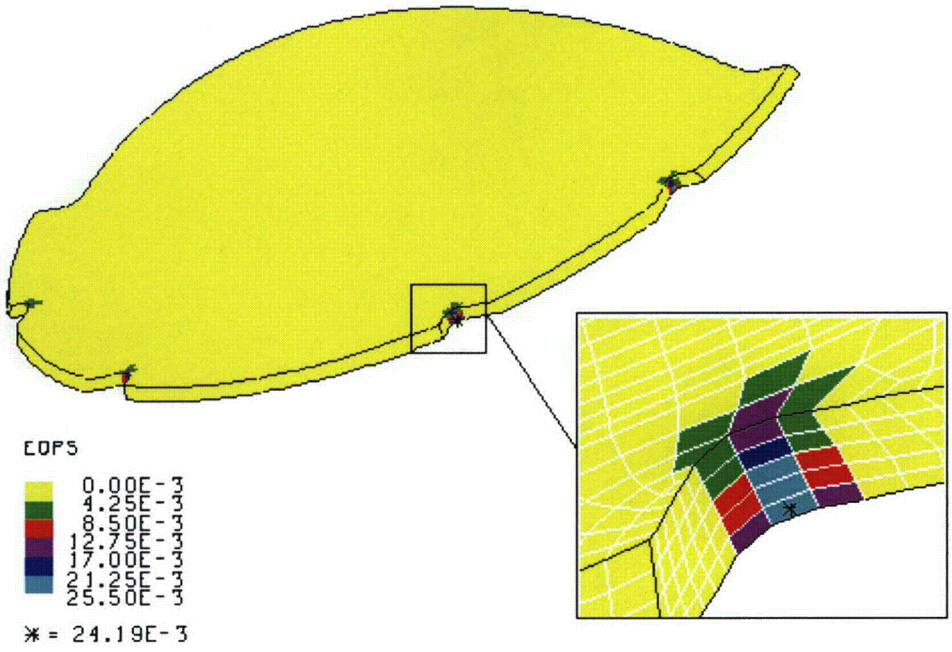

Figure 2-84. NCT SC-1 End Impact with Support Structure Rotated 0° – EQPS in Top Dish

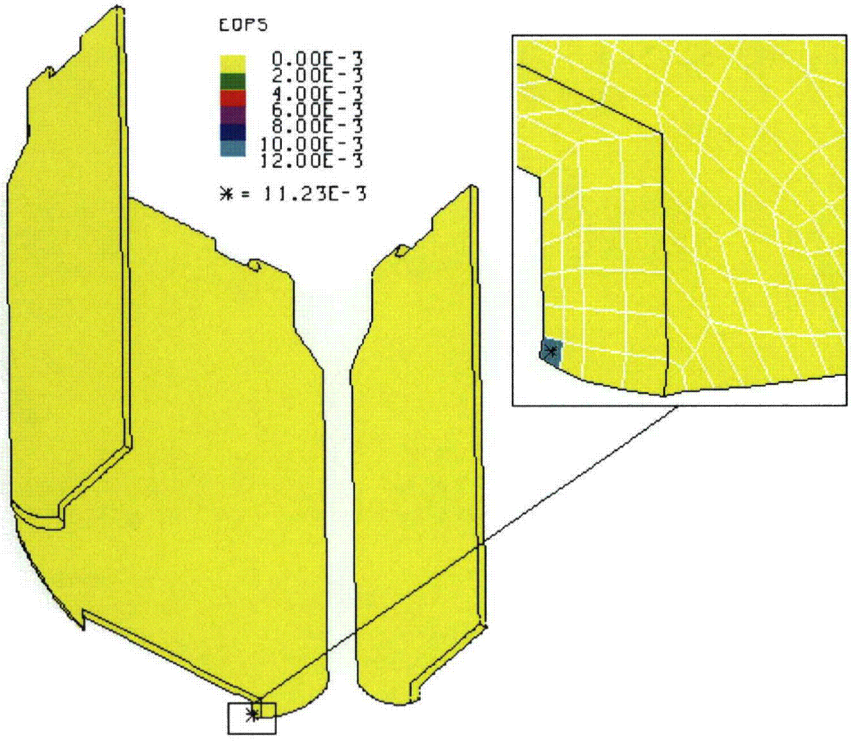

Figure 2-85. NCT SC-2 End Impact with Support Structure Rotated 0° – EQPS in Bottom Legs

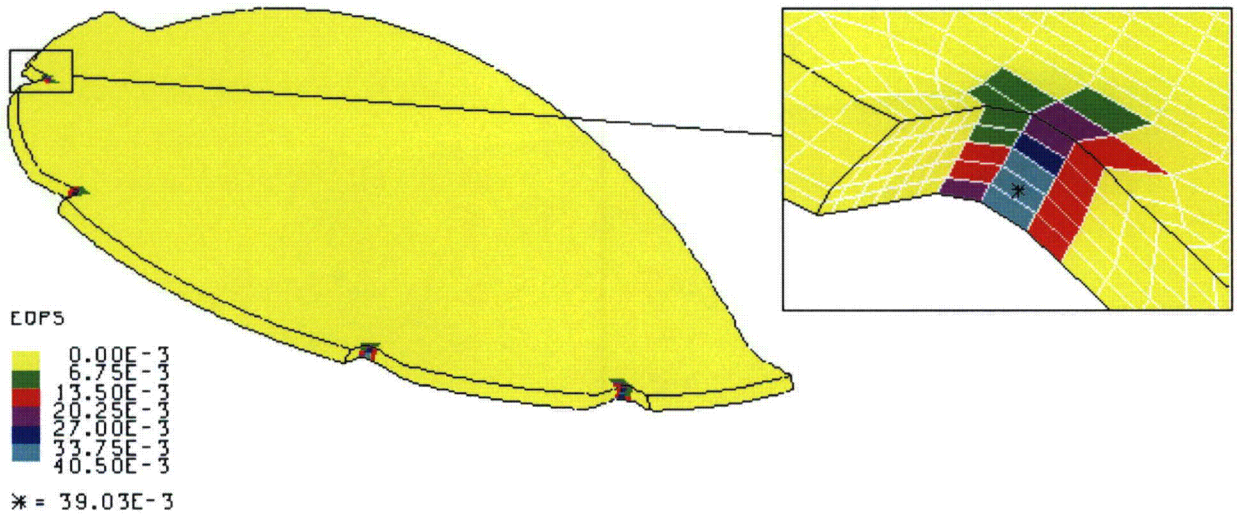

Figure 2-86. NCT SC-2 End Impact with Support Structure Rotated 0° – EQPS in Top Dish

Table 2-16. Maximum Strains in 4 ft End Drop Models

Model/Part	EQPS
SC-1 End Impact	
Bottom Legs	1.52e-2
Upper Legs	3.75e-4
Upper Dish	2.42e-2
SC-2 End Impact	
Bottom Legs	1.12e-2
Upper Dish	3.90e-2

2.12.5.3.2 NCT Side Drop Analysis

The models created for the 4-ft-drop side impact for the SC-1 AND SC-2 (0 and 45 degree rotated) at time 0 are shown in Figure 2-87 and Figure 2-88. The post-4-ft-drop models are shown in Figure 2-89 through Figure 2-92, and for these side impact cases more localized denting of the overpack lid rings is visible than for the end impact cases. The kinetic energy histories for these four impacts are shown in Figure 2-93 through Figure 2-96, indicating that sufficient analysis time transpired to capture the entire impact event, and the PAT-1 package actually bounced after impact. As shown in Figure 2-97 through Figure 2-105 and Table 2-17, the minimal plasticity (less than 7% and only in small localized areas of internal or external corners) observed in the titanium support structure, or inner cradle, verifies that the overall structure remained essentially elastic and the original position of the sample containers would remain unchanged. The zero plasticity post-drop condition of the T-Ampoule is shown in Figure 2-106, as well as zero plasticity in the TB-1 in Figure 2-107 and extremely low through-thickness stress intensities in Figure 2-108, below ASME limits shown in Table 2-4.

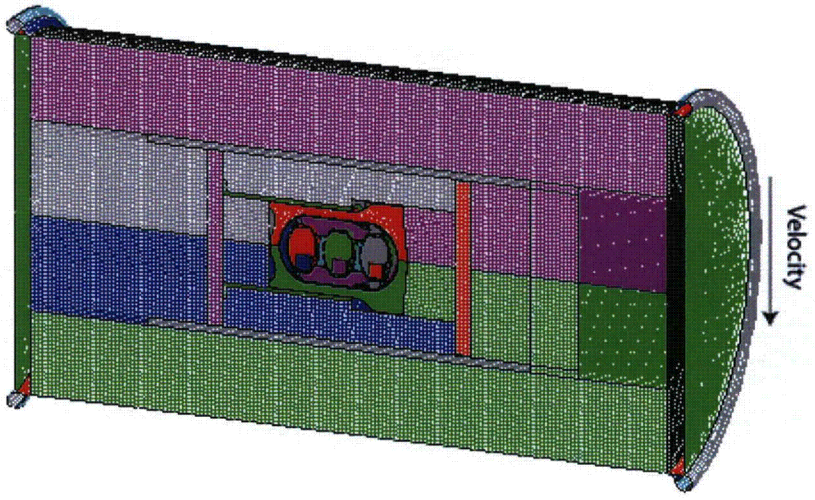

Figure 2-87. NCT SC-1 Side Impact with Support Structure Rotated 45°

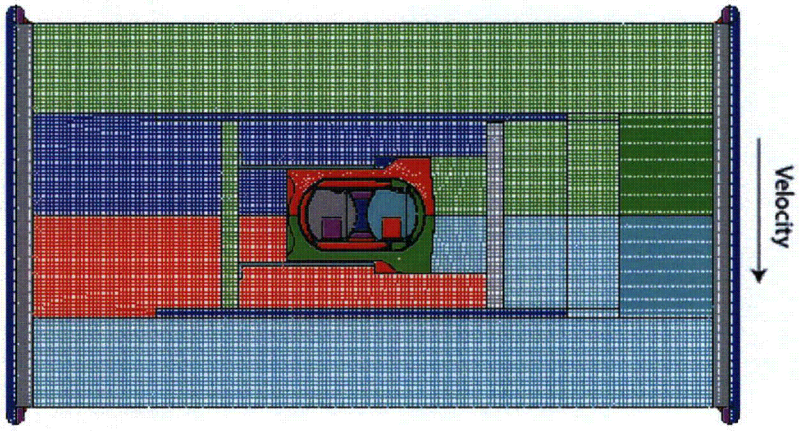

Figure 2-88. NCT SC-2 Side Impact with Support Structure Rotated 0°

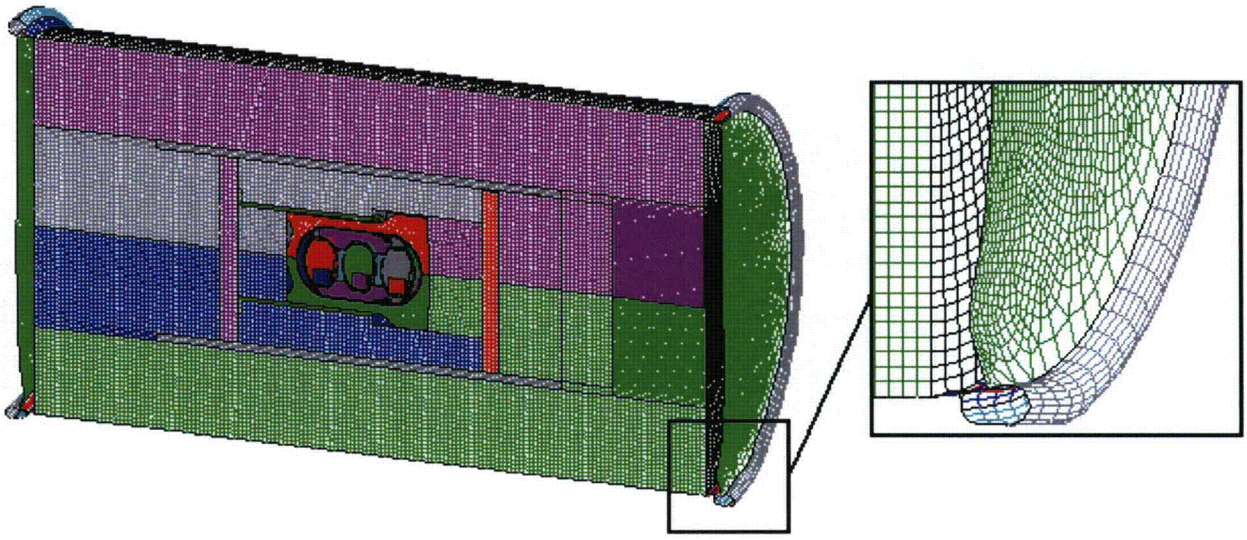

Figure 2-89. NCT SC-1 Side Impact with Support Structure Rotated 45° – Final Displacement

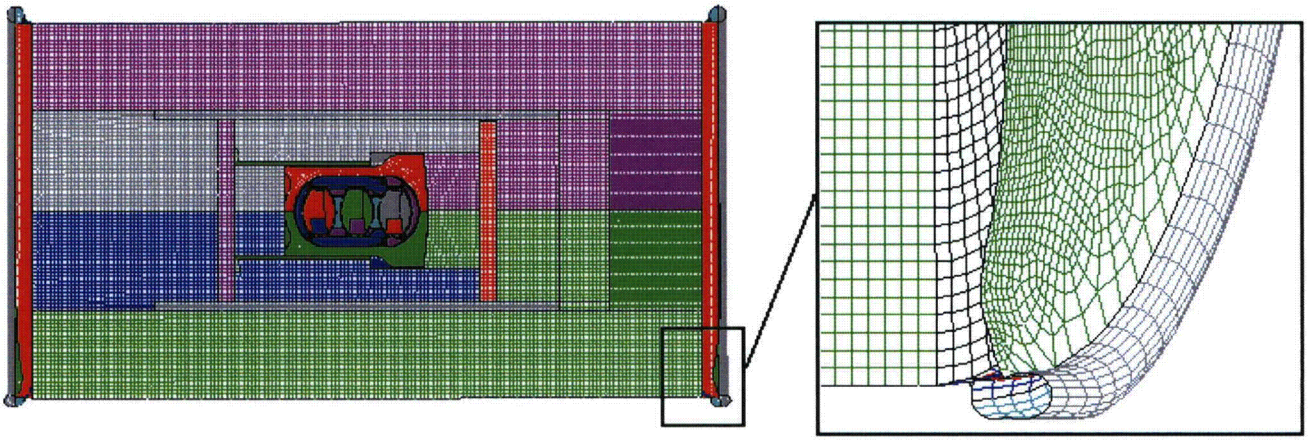

Figure 2-90. NCT SC-1 Side Impact with Support Structure Rotated 0° – Final Displacement

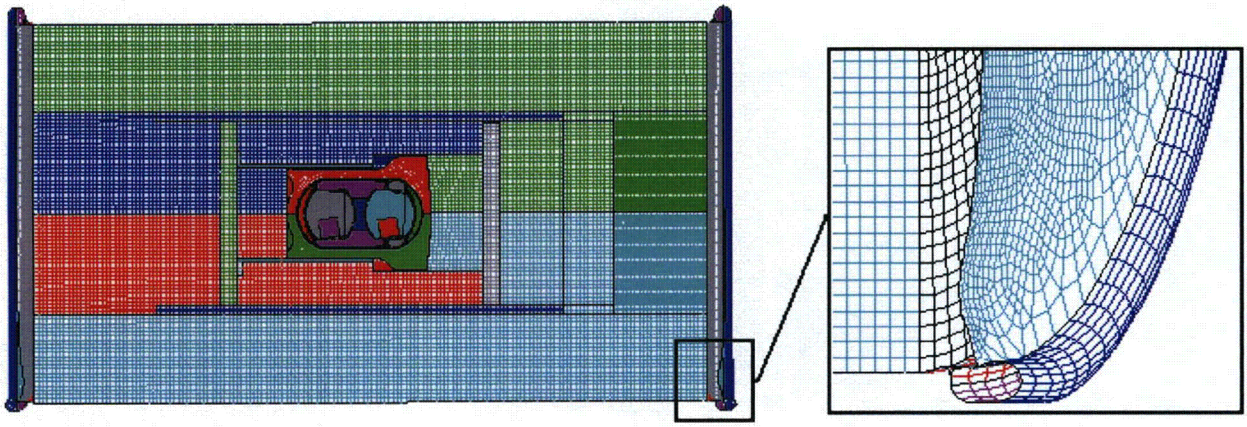

Figure 2-91. NCT SC-2 Side Impact with Support Structure Rotated 45° – Final Displacement

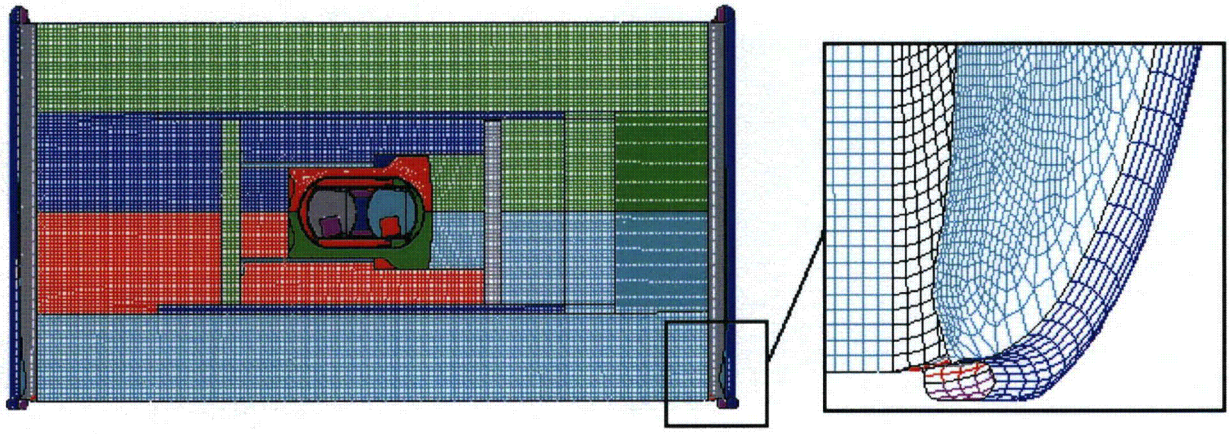

Figure 2-92. NCT SC-2 Side Impact with Support Structure Rotated 0° - Final Displacement

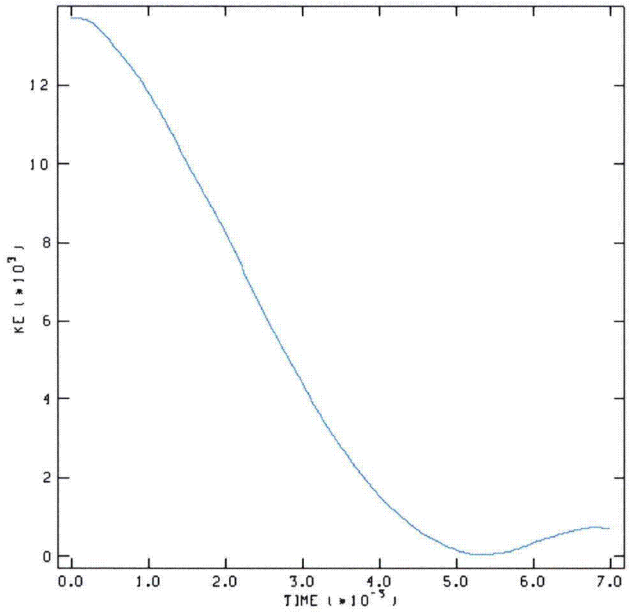

Figure 2-93. NCT SC-1 Side Impact with Support Structure Rotated 45° - Kinetic Energy Time History

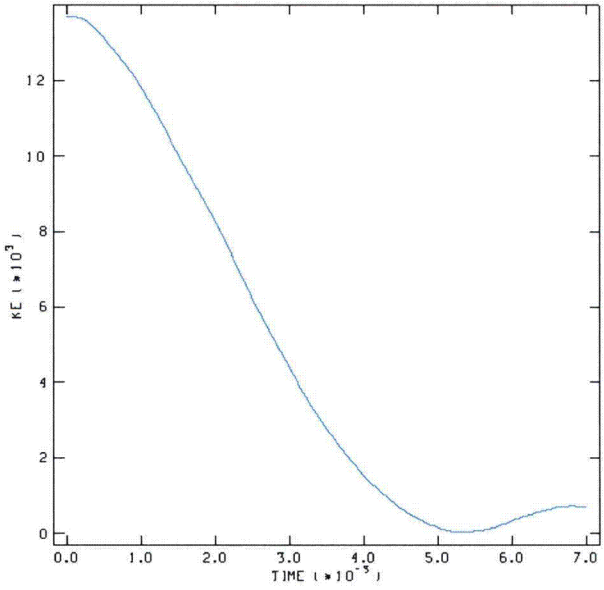

Figure 2-94. NCT SC-2 Side Impact with Support Structure Rotated 45° - Kinetic Energy Time History

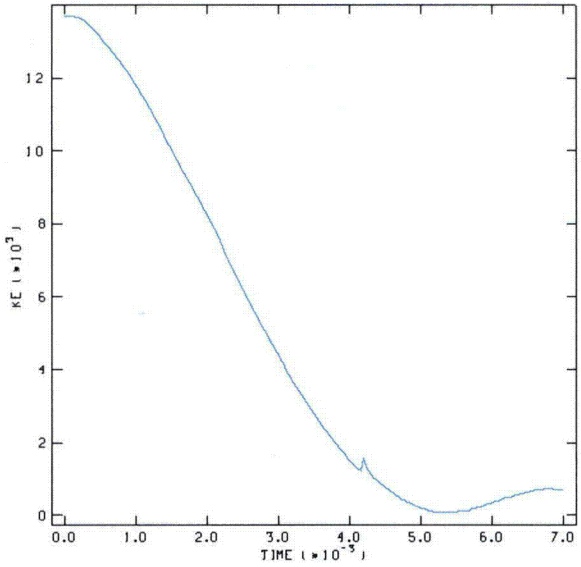

Figure 2-95. NCT SC-1 Side Impact with Support Structure Rotated 0° – Kinetic Energy Time History

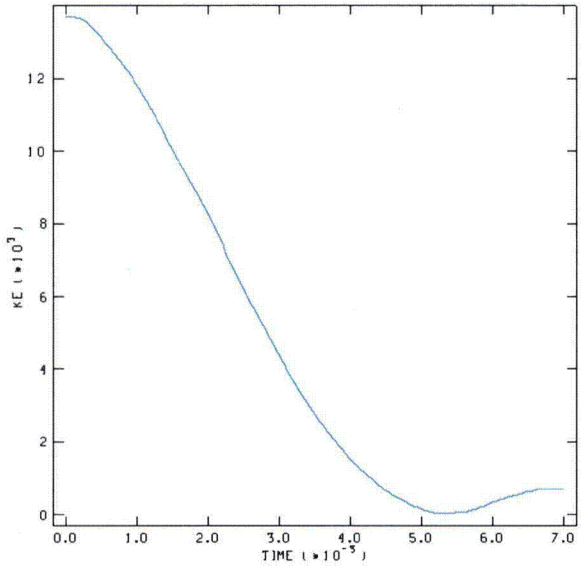

Figure 2-96. NCT SC-2 Side Impact with Support Structure Rotated 0° – Kinetic Energy Time History

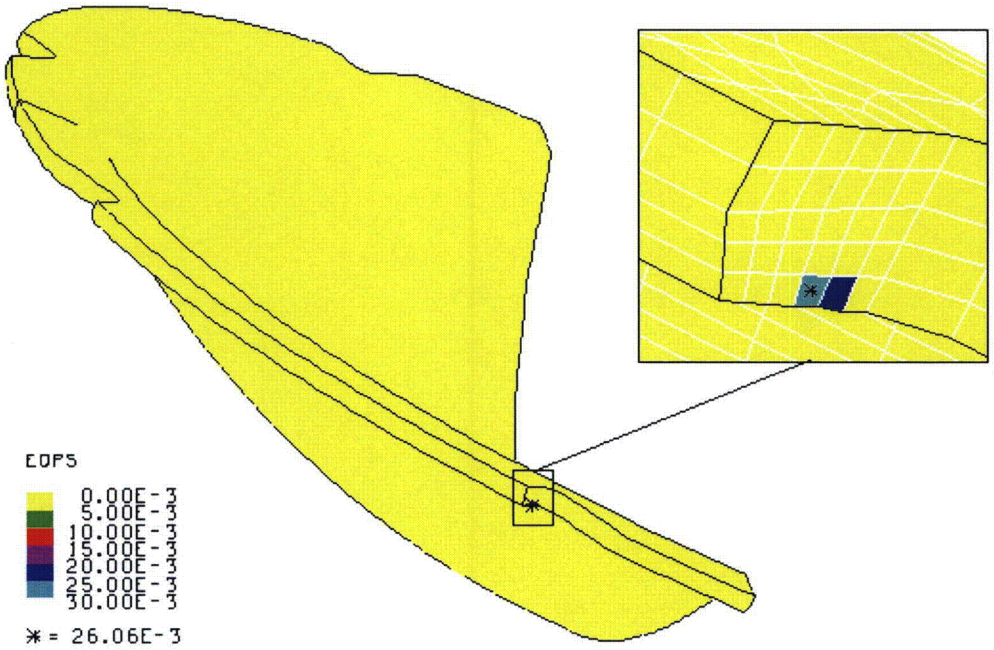

Figure 2-97. NCT SC-1 Side Impact with Support Structure Rotated 45° – EQPS in Bottom Dish

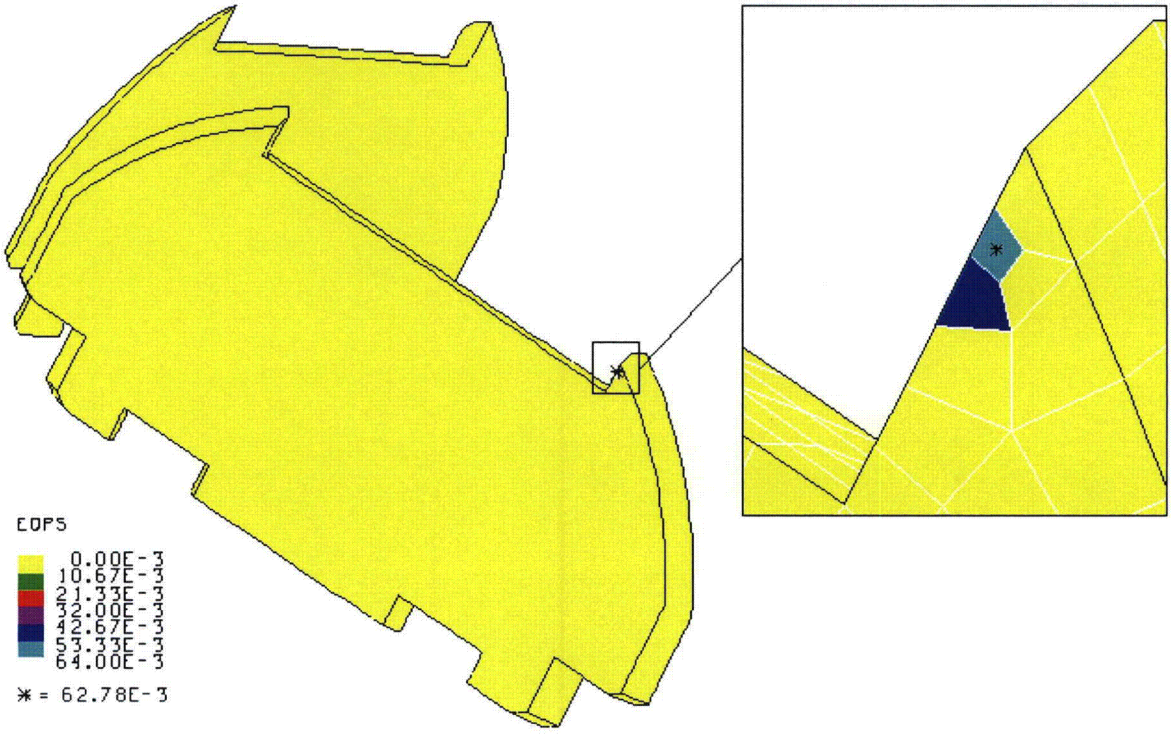

Figure 2-98. NCT SC-1 Side Impact with Support Structure Rotated 45° – EQPS in Top Legs

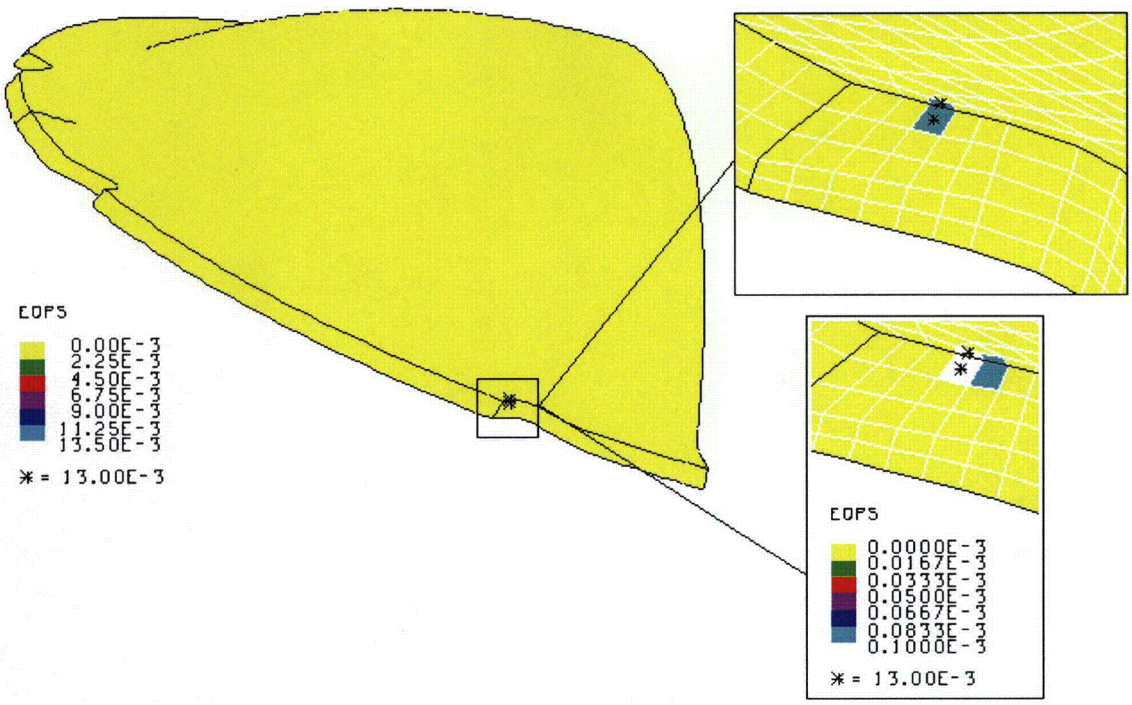

Figure 2-99. NCT SC-1 Side Impact with Support Structure Rotated 45° – EQPS in Top Dish

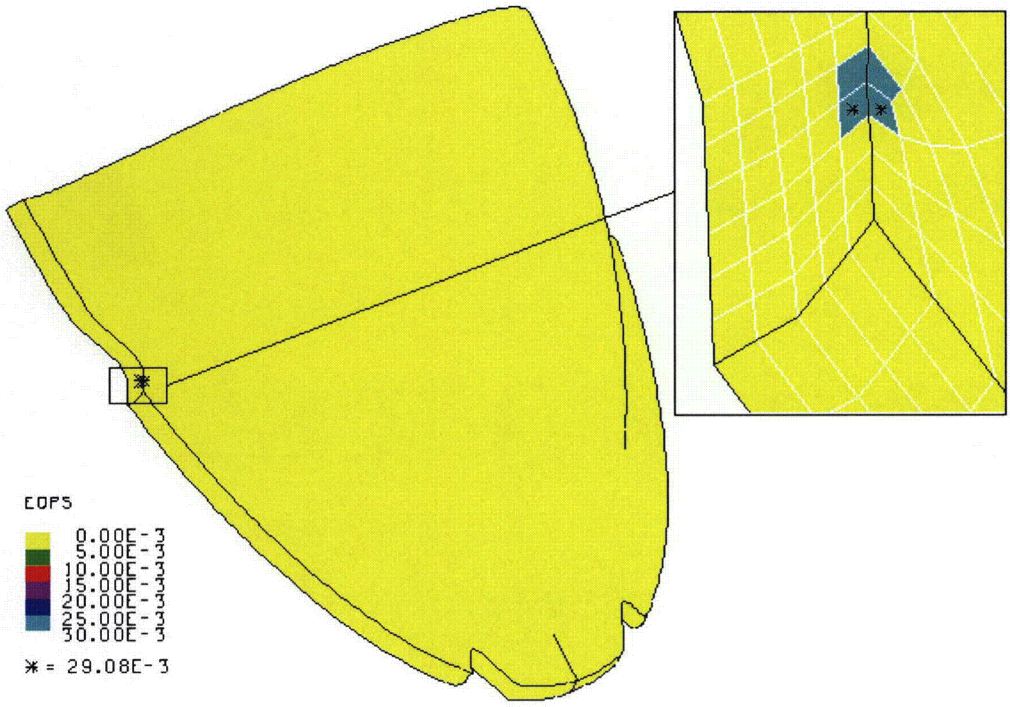

Figure 2-100. NCT SC-2 Side Impact with Support Structure Rotated 45° – EQPS in Bottom Dish

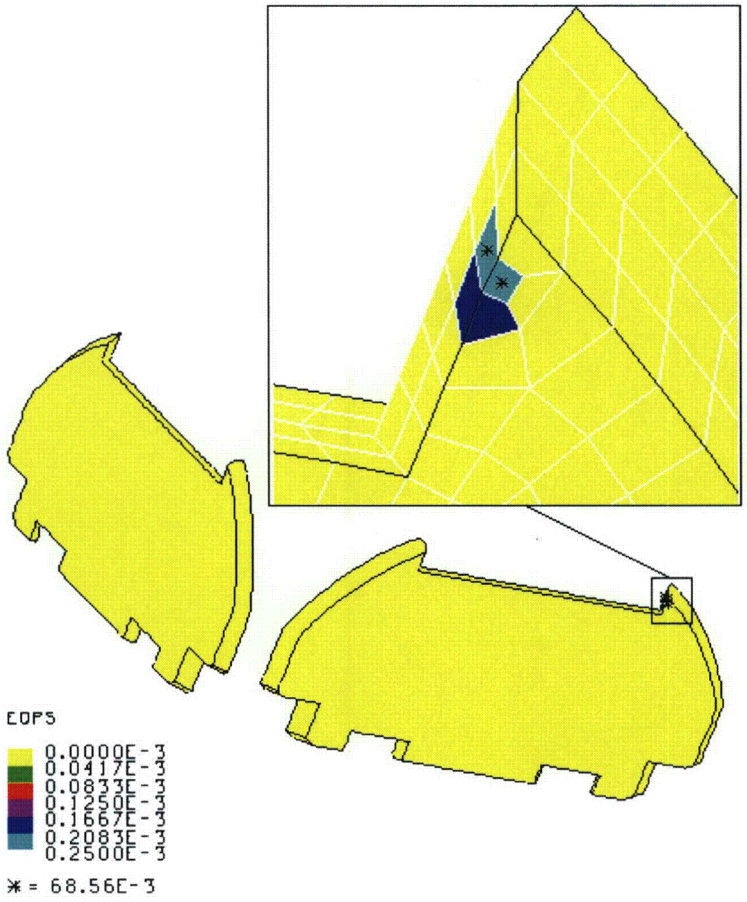

Figure 2-101. NCT SC-2 Side Impact with Support Structure Rotated 45° – EQPS in Top Legs

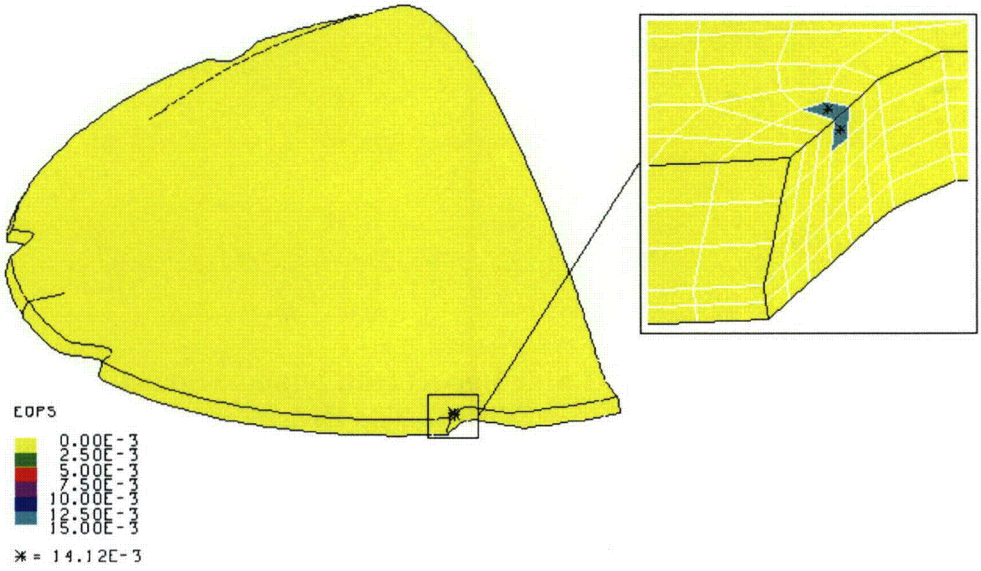

Figure 2-102. NCT SC-2 Side Impact with Support Structure Rotated 45° – EQPS in Top Dish

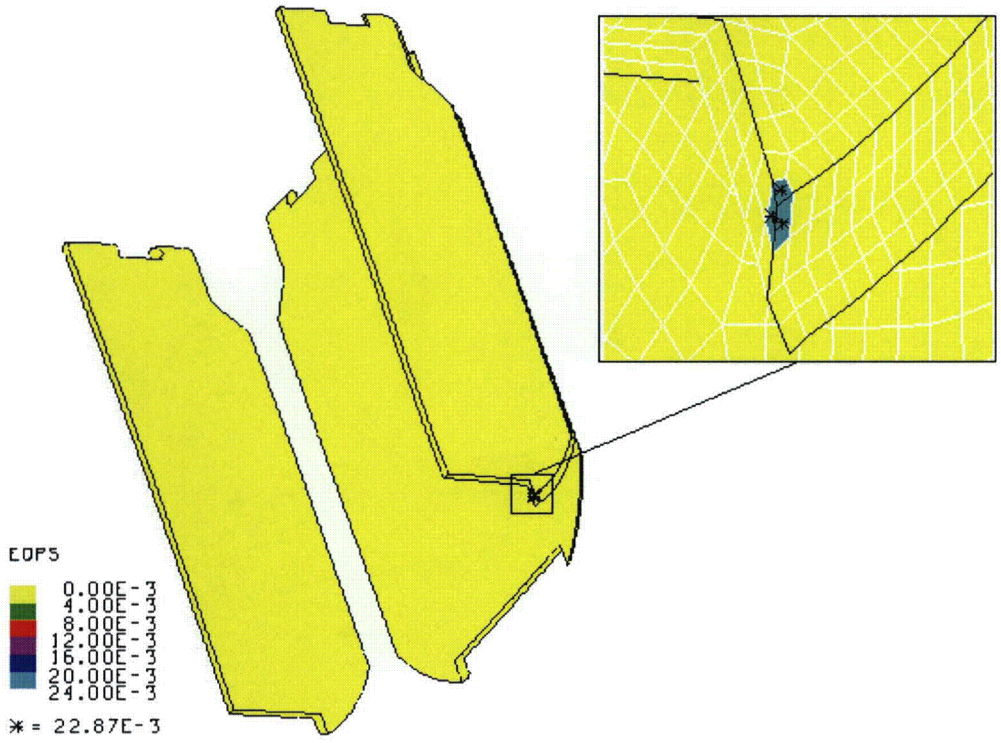

Figure 2-103. NCT SC-1 Side Impact with Support Structure Rotated 0° – EQPS in Bottom Legs

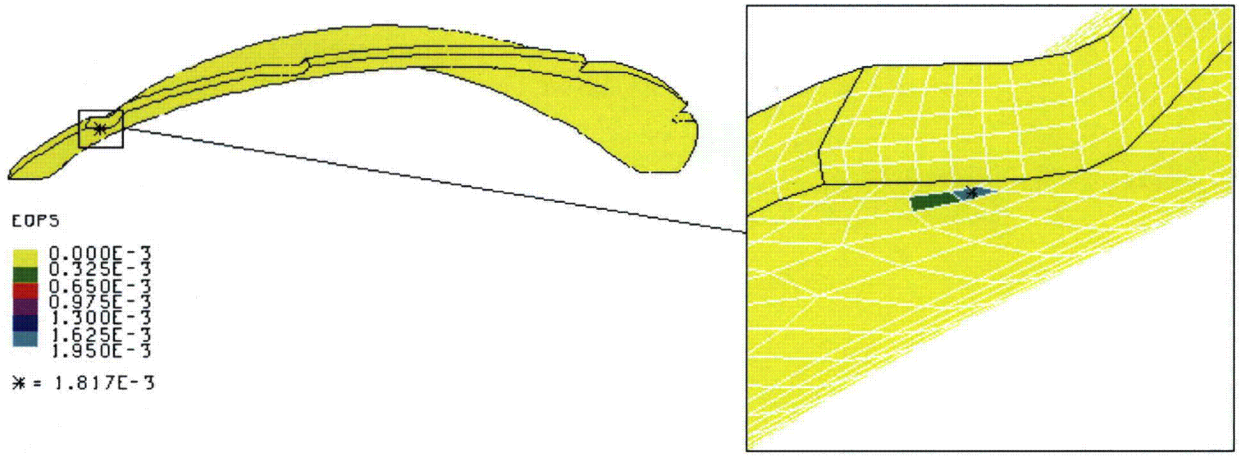

Figure 2-104. NCT SC-1 Side Impact with Support Structure Rotated 0° – EQPS in Top Dish

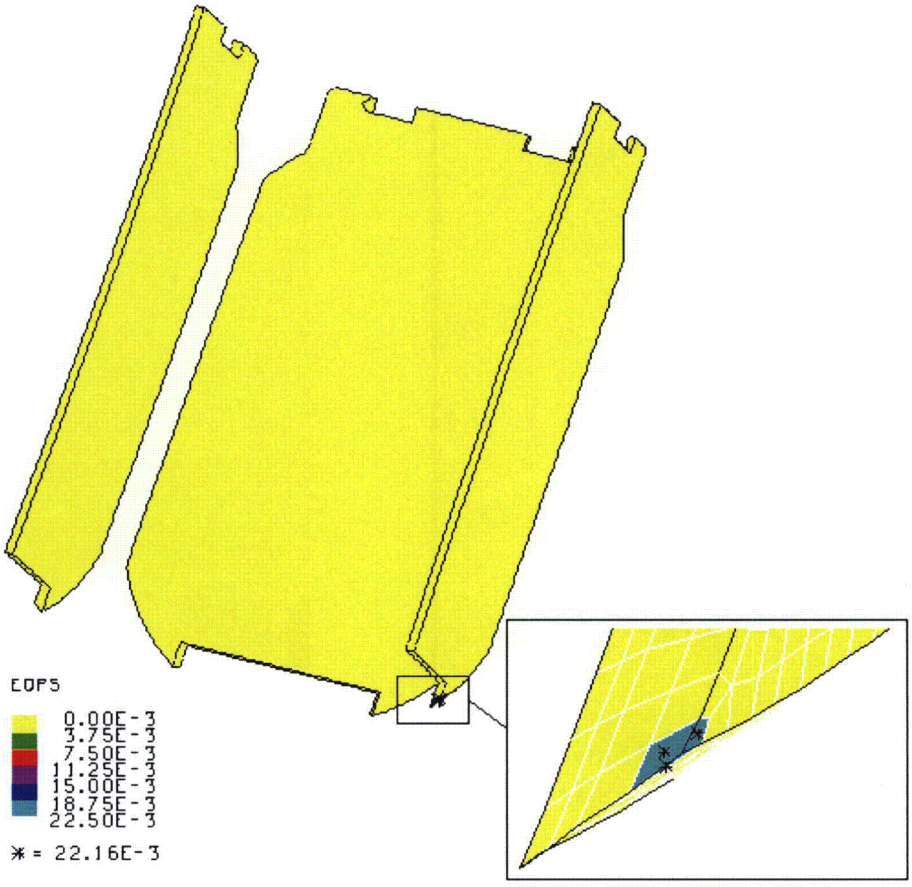

Figure 2-105. NCT SC-2 Side Impact with Support Structure Rotated 0° – EQPS in Bottom Legs

Table 2-17. Maximum Strains in 4 ft Side Drop Models

Model/Part	EQPS
SC-1 45° Side Impact	
Bottom Dish	2.61e-2
Upper Legs	6.28e-2
Upper Dish	1.30e-2
SC-2 45° Side Impact	
Bottom Dish	2.91e-2
Upper Legs	6.86e-2
Upper Dish	1.41e-2
SC-1 0° Side Impact	
Bottom Legs	2.29e-2
Upper Dish	1.82e-3
SC-2 0° Side Impact	
Bottom Legs	2.22e-2

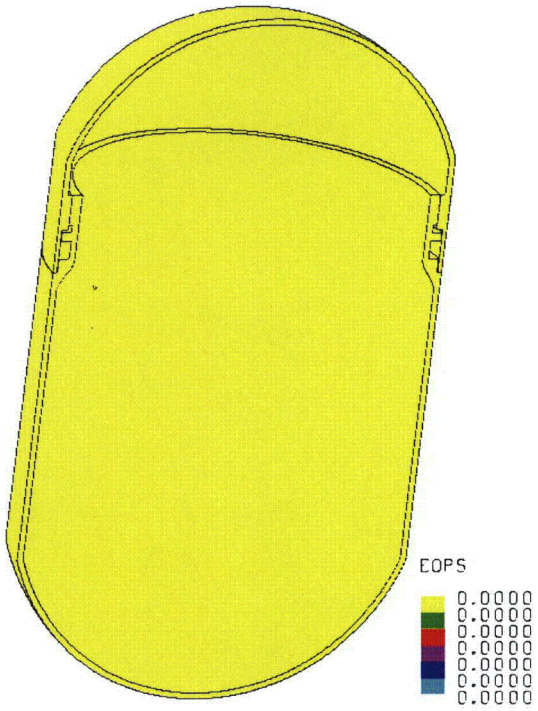

Figure 2-106. NCT SC-2 Side Impact with Support Structure Rotated 45° - EQPS in T-Ampoule

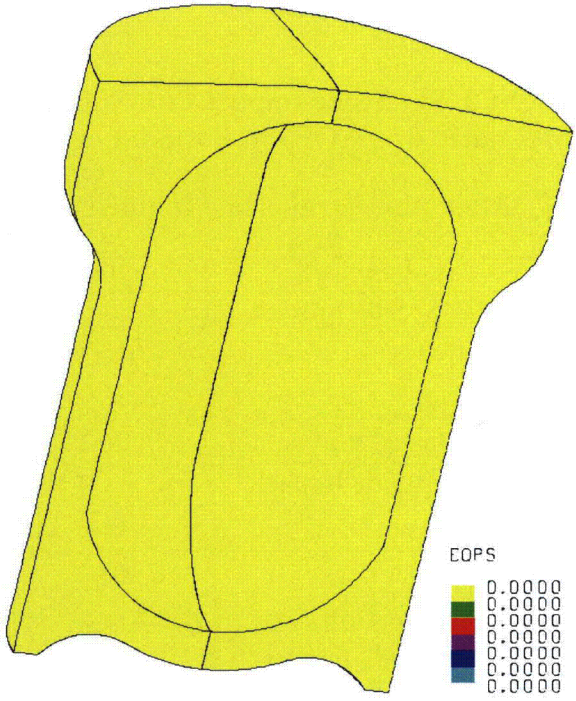

Figure 2-107. NCT SC-2 Side Impact with Support Structure Rotated 45° - EQPS in TB-1

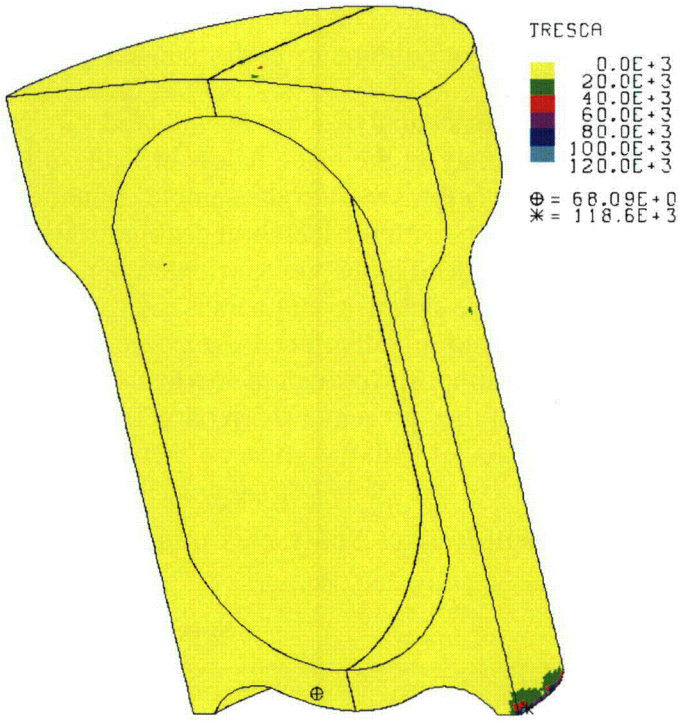

Figure 2-108. NCT SC-2 Side Impact with Support Structure Rotated 45° - Tresca Stress in TB-1

2.12.5.3.1 NCT End and Side Drop Analysis Summary

The two previous sections highlight the fact that the position of the contents within their sample containers and support cradle is essentially unchanged after 4-ft NCT drops. The titanium Inner Cradle remains essentially undeformed and the contents' positions no farther from the T-Ampoule than pre-drop, as well as no plasticity in the TB-1 and the T-Ampoule, all means that HAC and aircraft impact analyses are justified in assuming an undamaged PAT-1 package and contents before those events.

2.12.5.4 Aircraft Accident Impact Analyses

Detailed PAT-1 package models identical to those shown in the previous NCT section, except for neglecting the rolled ring lid ends, were analyzed to determine the response of the T-Ampoule and TB-1 when subjected to the loading of 10 CFR 71.74 (accident conditions for air transport of plutonium). Each combination of package orientation (lid end, side, and CG-over-corner) and contents was analyzed at an initial velocity of 422 ft/sec and each package impacts onto an analytically unyielding target.

The TB-1 was shown in the SAR[1] aircraft impact tests to remain elastic and maintain containment. With similar mass contents, similar TB-1 response would be expected, excepting the possibility of minor localized denting due to more dense contents (solid Pu vs. oxide powder). Effective or von Mises stresses (which capture three-dimensional stress states well and is more conservative than Tresca stress to show avoidance of yielding) were calculated and an acceptance criterion of "below through-thickness yielding" used to demonstrate similar TB-1

behavior as in the original regulatory testing. This also means zero plasticity in the seal area of the TB-1, ensuring similar containment requirements performance of the containment vessel.

A total of twenty-seven high speed impact analyses were conducted for the five potential contents in various orientations; the analyses are listed below in Table 2-18. In the hollow-cylinder (ER cylinder) component models, as well as the sample container models, no credit is taken for the positioning of the cylinders with the tantalum packing foil. Each form contents are assumed to be unconstrained and are placed in the worst orientation and most severe location for each impact. The delta-plutonium in the sample containers is relatively soft and has a greater degree of plasticity, so although its location will affect T-Ampoule loading, its local orientation would not. However, the beryllium composite cylinders are much harder and stronger, so their orientation is always rotated such that they present a sharp corner (CGOC, actually) towards the normal surface of the T-Ampoule, parallel with the impact direction.

Table 2-18. Aircraft Accident Impact Analyses, Components, and Orientations

Run No.	Component	Submodel Orientation
1	831 g Plutonium Metal Hollow Cylinder, alpha Pu	Bottom position, top impact
2	831 g Plutonium Metal Hollow Cylinder, alpha Pu	Bottom position (angled), top impact
3	831 g Plutonium Metal Hollow Cylinder, alpha Pu	Bottom position (angled), CGOC impact
4	831 g Plutonium Metal Hollow Cylinder, alpha Pu	Far side position, side impact
5	831 g Plutonium Metal Hollow Cylinder, alpha Pu	Far side position (angled), side impact
6	731 g Plutonium Metal Hollow Cylinder, alpha Pu	Bottom position, top impact
7	731 g Plutonium Metal Hollow Cylinder, alpha Pu	Bottom position (angled), top impact
8	731 g Plutonium Metal Hollow Cylinder, alpha Pu	Bottom position (angled), CGOC impact
9	731 g Plutonium Metal Hollow Cylinder, alpha Pu	Far side position, side impact
10	731 g Plutonium Metal Hollow Cylinder, alpha Pu	Far side position (angled), side impact
11	SC-1 – Pu	Bottom position, support structure 0°, top impact
12	SC-1 – Pu	Far side position, support structure 0°,side impact
13	SC-1 – Pu	Far side position, support structure 45°, side impact
14	SC-1 – Pu	Bottom position, support structure 0°, CGOC impact
15	SC-1 – Pu	Bottom position, support structure 45°, CGOC impact

Table 2-18. Aircraft Accident Impact Analyses, Components, and Orientations (Continued)

Run No.	Component	Submodel Orientation
16	SC-2 – Pu	Bottom position, support structure 0°, top impact
17	SC-2 – Pu	Far side position, support structure 0°,side impact
18	SC-2 – Pu	Far side position, support structure 45°, side impact
19	SC-2 – Pu	Bottom position, support structure 0°, CGOC impact
20	SC-2 – Pu	Bottom position, support structure 45°, CGOC impact
21	SC-1 – Be	Bottom position, angled Be, support structure 0°, top impact
22	SC-1 – Be	Far side position, angled Be, support structure 0°, side impact
23	SC-1 – Be	Far side position, angled Be, support structure 45°, side impact
24	SC-1 – Be	Bottom position, angled Be, support structure 0°, CGOC impact
25	SC-1 – Be	Bottom position, angled Be, support structure 45°, CGOC impact
26	SC-2 – Pu	Far side position, support structure 45°, side impact, friction 0.4
27	SC-2 – Pu	Far side position, support structure 45°, side impact, friction 0.2

2.12.5.4.1 ER Cylinder Analyses

Ten separate plutonium metal hollow cylinder, high-speed impact analyses were conducted. There are several inherent conservatisms in this model:

1. The tantalum foil used to package the plutonium metal hollow cylinders inside the T-Ampoule is not modeled. The small quantity of energy it would absorb, and load spreading it would provide, is conservatively ignored. In addition, any initial positioning that would be provided by the foil is also ignored. Each analysis is run with the plutonium metal hollow cylinder in a location farthest from the impact surface.

2. The Pu material is modeled using a power-law hardening constitutive model without fracture. Hecker and Stevens[3] present two curves for alpha-plutonium; one curve depicts a very brittle material, and the other represents a finer-grain material with more ductility. To maximize the energy and impulse load applied to the T-Ampoule wall, the plutonium metal was modeled as a continuously hardening material that does not fracture, which is extremely conservative in terms of the reaction loading of the T-Ampoule. This conservatism (stronger alpha material, continuously hardening) allows for the possibility that the cylinder could also consist of delta Pu, if transport of that material were desired instead.

3. The dimensions of the plutonium metal hollow cylinders are conservatively assumed to be the "strongest" possible. Within the bounds of LANL-defined tolerances of machining these cylinders, they are the most resistant to buckling (shortest, thickest wall,

maximum OD and minimum ID, see Figures 2-70and 2-71), which allows for the greatest loading of the T-Ampoule.

2.12.5.4.2 Run 1 - 831-g Plutonium Metal Hollow Cylinder with Bottom Initial Location and a Top Impact

The top end impact model for the plutonium metal hollow cylinder, oriented axially (with the impact direction, as opposed to angled) is shown in Figure 2-109. Note that the cylinder is located at the bottom of the T-Ampoule so that its net impact velocity with the top of the T-Ampoule is maximized. The post-impact deformation is shown in Figure 2-110 and its kinetic energy history in Figure 2-111. Note the similar degree of overpack crush up as compared to the certification test end impact analysis in Figure 2-12, despite the slightly reduced impact velocity of 422 ft/sec versus the tested 445 ft/sec. The plutonium metal hollow cylinder exhibits significant buckling, despite its conservatively "strongest shape" definition.

Equivalent Plastic Strain (EQPS) in the TB-1 vessel is shown in Figures 2-112 and 2-113 to be less than 2.3%, and only in some localized outer contact regions with the redwood overpack. This localized ring of plasticity in the top outer surface of the TB-1 lid is due to a minor contact over closure between the TB-1 and the redwood; it is only a minor modeling artifact. This minor modeling artifact is not a concern because even though it produces elevated localized stresses and even miniscule plasticity, it does not increase through-thickness stresses or in any way negatively affect the integrity of the containment vessel. The von Mises stresses (see Figures 2-114 and 2-115) peak at 147.5 ksi, just above the elevated-temperature minimum yield strength for the TB-1 of 141 ksi, but more importantly, through-thickness TB-1 stress values are in the less-than-50 ksi range, below yield. The time at which the peak value of the von Mises stress occurs coincides with the peak value of the contact force (summed over the lid area). A plot of this force as a function of time is shown in Figure 2-116. A maximum contact load of 66,000 lbs is applied to the inner surface of the TB-1 lid during the impact, which is below the 108,000 lb preload in the bolts. No T-Ampoule elements exceeded the tested B-W strain locus, and the peak Tearing Parameter value (see Table 2-11, High Velocity (Aircraft) Impact Analyses Peak Tearing Parameter Values, run #1) of 0.0528 was below the critical Tearing Parameter value of 1.012 for Ti-6Al-4V.

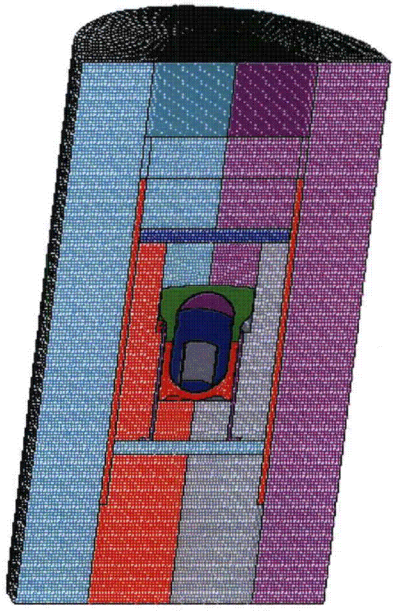

Figure 2-109. Finite Element Mesh for the 831-g, Plutonium Metal Hollow Cylinder, Bottom Position, End Impact

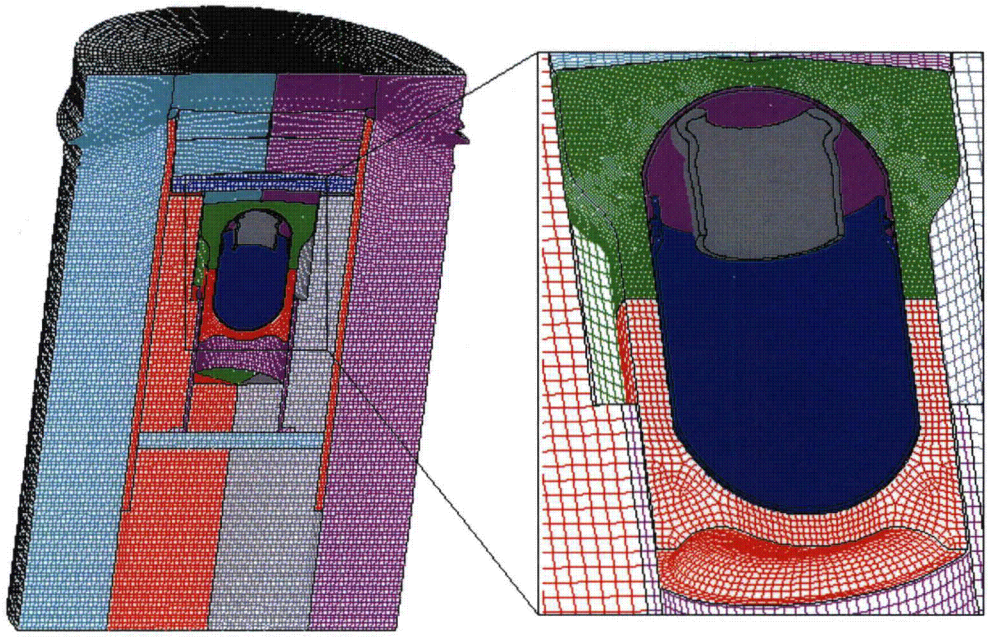

Figure 2-110. Finite Element Mesh for the 831-g, Plutonium Metal Hollow Cylinder, Bottom Position, End Impact – Final Displacement

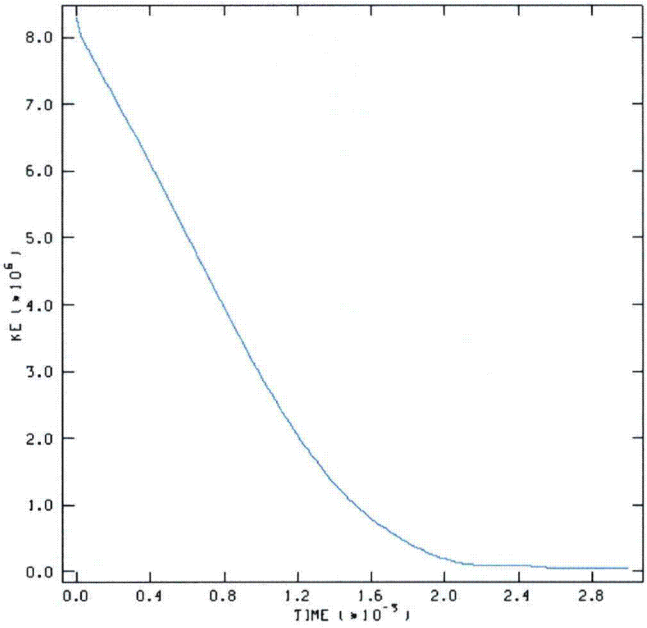

Figure 2-111. Kinetic Energy Time History for the 831-g, ER Cylinder, Bottom Position, End Impact

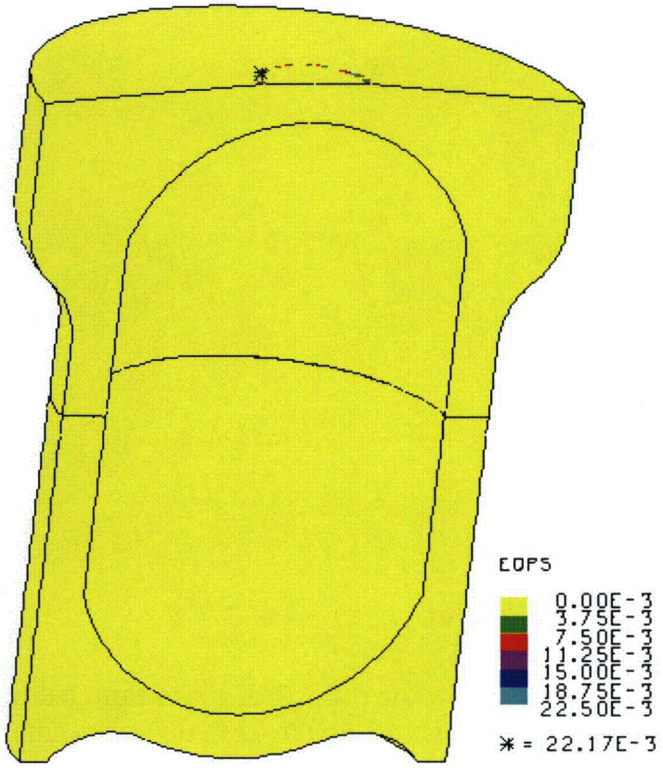

Figure 2-112. EQPS in the TB-1 for the 831-g, ER Cylinder, Bottom Position, End Impact

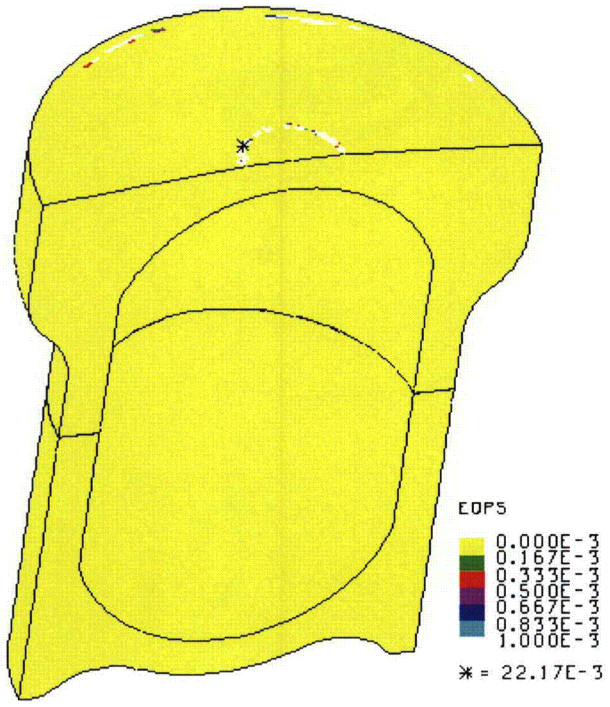

Figure 2-113. EQPS in TB-1 (Range Zoomed in to Show All Elements with non-zero EQPS) for the 831-g, Hollow Cylinder, Bottom Position, End Impact

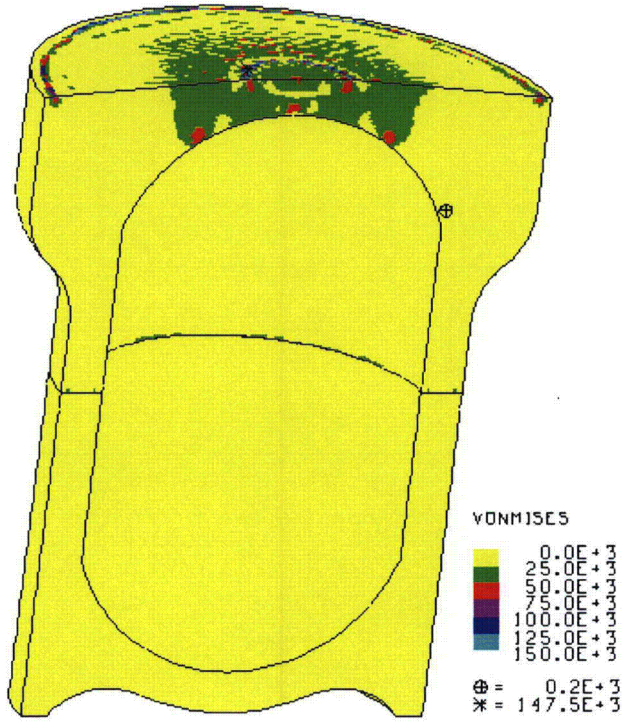

Figure 2-114. von Mises Stress in the TB-1 for the 831-g Plutonium Metal Hollow Cylinder, Bottom Position, End Impact (Rotated Forward for Ease of Viewing)

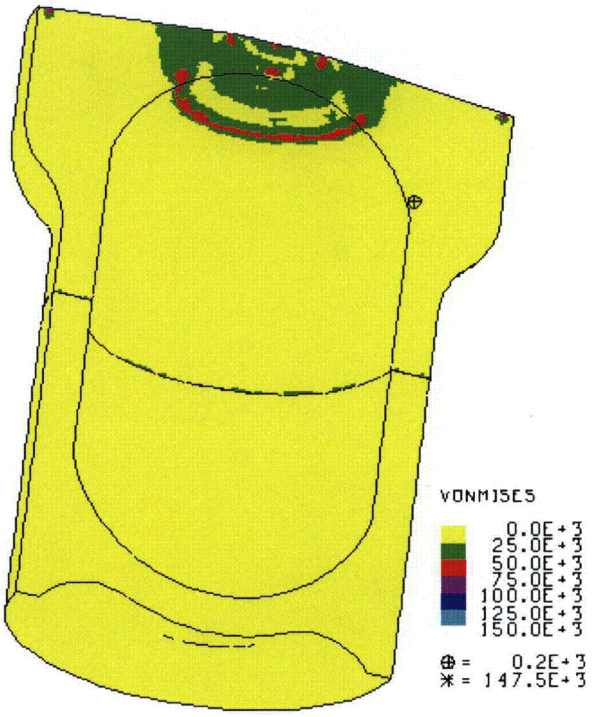

Figure 2-115. von Mises Stress in the TB-1 for the 831-g, Plutonium Metal Hollow Cylinder, Bottom Position, End Impact (Rotated Backward for Ease of Viewing)

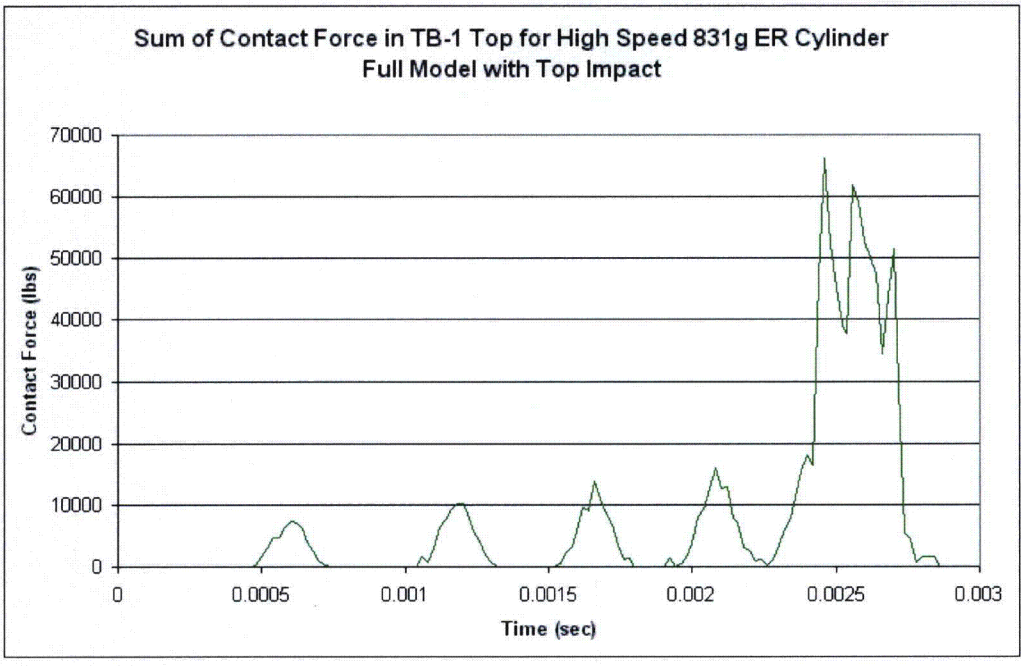

Figure 2-116. Summed Contact Force on the TB-1 Top for a 831-g, Plutonium Metal Hollow Cylinder, Top Impact